Phase-Sensitive Parametric Signal Processing in Optical Communications

Abel Lorences-Riesgo

Phase-Sensitive Parametric Signal Processing in Optical Communications

Abel Lorences-Riesgo

Göteborg, December 2016

Photonics Laboratory
Department of Microtechnology and Nanoscience (MC2)
Chalmers University of Technology, SE-412 96 Göteborg, Sweden
Phone: +46 (0) 31 772 1000

Front cover illustration: Measured constellation diagrams in the x- and y-polarizations for a self-homodyne detected DP-32-QAM signal.

Phase-Sensitive Parametric Signal Processing in Optical Communications

Abel Lorences-Riesgo

Photonics Laboratory

Department of Microtechnology and Nanoscience (MC2)

Chalmers University of Technology, SE-412 96 Göteborg, Sweden

Abstract

This thesis covers the analysis of several schemes for parametric processing in fiber-optic communication systems, focusing mainly on phase-sensitive processing. Vector phase-sensitive amplifiers are characterized and phase regeneration of a dual-polarization (DP)-binary phase-shift keying signal (BPSK) signal is experimentally demonstrated. Theoretically, the requirements for achieving polarization-independent phase-sensitive amplification of both single and dual polarization signals in a general scenario are also analyzed in this work. This part of the thesis is concluded by experimentally demonstrating mitigation of fiber nonlinearities in an installed link by performing mid-span spectral inversion with a vector parametric amplifier.

This thesis also covers the analysis of polarization-assisted phase-sensitive processors to achieve quadrature decomposition. Using a vector amplifier, decomposition of a quadrature phase-shift keying (QPSK) signal into two BPSK signals is experimentally demonstrated. A polarization-assisted phase-sensitive processor based on a polarization-diverse implementation is used for achieving quadrature decomposition of a 16 quadrature-amplitude modulation (16-QAM) into two 4 pulse-amplitude modulation (4-PAM) signals .

The final part of this thesis proposes and demonstrates the concept of self-homodyne superchannel by comb regeneration. By transmitting two unmodulated carriers, self-homodyne detection of 24×DP-32-QAM signals is demonstrated by all-optical comb regeneration based on Brillouin amplification and a parametric comb in a proof-of-principle experiment. Compared to conventional self-homodyne schemes, comb regeneration reduces the complexity and limits the spectral overhead in self-homodyne receivers.

Keywords: Fiber nonlinearities, four-wave mixing, parametric amplification, phase-sensitive amplification, all-optical processing, mid-span spectral inversion, self-homodyne, parametric comb, comb regeneration.

List of Papers

This thesis is based on the following appended papers:

[A] **A. Lorences-Riesgo**, F. Chiarello, C. Lundström, M. Karlsson, and P. A. Andrekson, "Experimental analysis of degenerate vector phase-sensitive amplification," *Opt. Exp.*, vol. 22, no. 18, pp. 21889–21902, Sep. 2014.

[B] **A. Lorences-Riesgo**, C. Lundström, F. Chiarello, M. Karlsson, and P. A. Andrekson, "Phase-sensitive amplification and regeneration of dual-polarization BPSK without polarization diversity," *in European Conference on Optical Communication (ECOC)*, Sept. 2014, paper Tu.1.4.3.

[C] **A. Lorences-Riesgo**, P. A. Andrekson, and M. Karlsson, "Polarization-insensitive phase-sensitive amplification," *J. Lightwave Technol.*, vol. 34, no. 13, pp. 3171–3180, Jul. 2016.

[D] J. Sun, **A. Lorences-Riesgo**, F. Parmigiani, K R. H. Bottrill, S. Yoshima, G. D. Hesketh, M. Karlsson, P. A. Andrekson, D. J. Richardson, and P. Petropoulos, "Optical nonlinearity mitigation of 6×10 GBd polarization-division multiplexing 16QAM signals in a field-installed transmission link," *accepted to Optical Fiber Communication Conference (OFC)*, Mar. 2017, paper Th3J.2.

[E] **A. Lorences-Riesgo**, L. Liu, S. L. I. Olsson, R. Malik, A. Kumpera, C. Lundström, S. Radic, M. Karlsson, and P. A. Andrekson, "Quadrature demultiplexing using a degenerate vector parametric amplifier," *Opt. Exp.*, vol. 22, no. 24, pp. 29424–29434, Nov. 2014.

[F] **A. Lorences-Riesgo**, T. A. Eriksson, M. Mazur, P. A. Andrekson, and M. Karlsson, "Quadrature decomposition of a 20 Gbaud 16-QAM signal into 2×4-PAM signals," *in European Conference on Optical Communication (ECOC)*, Sept. 2016, paper Tu.1.E.3.

[G] **A. Lorences-Riesgo**, T. A. Eriksson, A. Fülöp, P. A. Andrekson and M. Karlsson, "Frequency-comb regeneration for self-homodyne superchannels," *J. Lightwave Technol.*, vol. 34, no. 8, pp. 1800-1806, Apr. 2016. (Top Scored).

[H] **A. Lorences-Riesgo**, M. Mazur, T. A. Eriksson, P. A. Andrekson and M. Karlsson, "Self-homodyne 24×32-QAM superchannel receiver enabled by all-optical comb regeneration using Brillouin amplification," *Opt. Exp.*, vol. 24, no. 26, pp. 29714-29723, Dec. 2016.

Related papers by the author not included in the thesis:

[I] C. Lundström, R. Malik, **A. Lorences-Riesgo**, S. L. I. Olsson, B. Corcoran, M. Karlsson, and P. A. Andrekson, "Fiber-optic parametric amplifiers without pump dithering," *in Workshop on Specialty Optical Fibers and their Applications*, Aug. 2013, paper W3.12.

[J] **A. Lorences-Riesgo**, C. Lundström, M. Karlsson, and P. A. Andrekson, "Demonstration of degenerate vector phase-sensitive amplification," *in European Conference on Optical Communication (ECOC)*, Sept. 2013, paper We.3.A.3.

[K] R. Malik, A. Kumpera, **A. Lorences-Riesgo**, P. A. Andrekson, and M. Karlsson, "Frequency-resolved noise figure measurements of phase (in) sensitive fiber optical parametric amplifiers," *Opt. Exp.*, vol. 22, no. 23, pp. 27821–27832, Nov. 2014.

[L] **A. Lorences-Riesgo**, T. A. Eriksson, C. Lundström, M. Karlsson, and P. A. Andrekson, "Phase-sensitive amplification of 28 GBaud DP-QPSK signal," *in Optical Fiber Communications Conference (OFC)*, Mar. 2015, paper W4C.4.

[M] A. Kumpera, R. Malik, **A. Lorences-Riesgo**, and P. Andrekson, "Parametric coherent receiver," *Opt. Exp.*, vol. 23, no. 10, pp. 12952-12964, May 2015.

[N] **A. Lorences-Riesgo**, T. A, Eriksson, A. Fülöp, M. Karlsson, and P. A. Andrekson, "Frequency-comb regeneration for self-homodyne superchannels," *in European Conference on Optical Communication (ECOC)*, Sept. 2015, paper We.3.6.2.

[O] T. A. Eriksson, **A. Lorences-Riesgo**, P. Johannisson, T. Fehenberger, P. A. Andrekson, and M. Karlsson, "Achievable rates comparison for phase-conjugated twin-waves and PM-QPSK," *in OptoElectronics and Communications Conference (OECC)*, Jul. 2016, paper TuB3-3.

[P] E. Nazemosadat, **A. Lorences-Riesgo**, M. Karlsson, and P. A. Andrekson, "Highly nonlinear few-mode fiber for optical parametric amplification," *in European Conference on Optical Communication (ECOC)*, Sep. 2016, paper W.4.P1.SC1.7

[Q] Y, Ding, H. Ou, J. Xu, M. Xiong, Y. An, H. Hu, M. Galili, **A. Lorences-Riesgo**, J. Seoane, K. Yvind, L. K. Oxenløwe, X. Zhang, D. Huang, and C. Peucheret, "Linear all-optical signal processing using silicon micro-ring resonators," *Frontiers of Optoelectronis*, vol. 9, no. 3, pp. 362-376, Sep. 2016.

[R] M. Mazur, **A. Lorences-Riesgo**, M. Karlsson, and P. A. Andrekson, "10 Tb/s self-homodyne 64-QAM superchannel transmission with 4% spectral overhead," *accepted to Optical Fiber Communication Conference (OFC)*, Mar. 2017, paper Th3F.4.

[S] A. Fülöp, M. Mazur, **A. Lorences-Riesgo**, P.-H. Wang, Y. Xuan, D. E. Leaird, M. Qi, P. A. Andrekson, A. M. Weiner, and V. Torres-Company "Frequency noise of a normal dispersion microresonator-based frequency comb," *accepted to Optical Fiber Communication Conference (OFC)*, Mar. 2017, paper W2A.6.

Acknowledgment

Several people deserve my gratitude for their support, help and collaboration. First, I would like to thank my supervisors Prof. Magnus Karlsson and Prof. Peter Andrekson for accepting me as a Ph. D. student. Their guidance and support have been fundamental in order to complete this work.

I would like to thank Prof. Periklis Petropoulos and Dr. Francesca Parmigiani for accepting me as Ph.D. visitor at the University of Southampton. I should also thank the time they devoted to me during my visit. Yujia Sun also deserves my gratitude for his hard work in our joint project.

Many thanks also go to two guest researches, Dr. Fabrizio Chiarello and Dr. Lan Liu, with whom I was fortunate to collaborate.

Tobias Eriksson deserves special thanks for all his collaboration and help as well as all ping-pong games and football talks. I am also very grateful to Mikael Mazur for all his collaboration and discussions as well as being willing to talk to our angry neighbor in Düsseldorf. I have been fortunate to share PSA discussions with Dr. Bill Corcoran, Dr. Carl Lundström, Dr. Samuel Olsson, Dr. Rohit Malik and Dr. Aleš Kumpera. I should also thank Dr. Elham Nazemosadat for fruitful discussions and sharing her knowledge about nonlinearities in multimode fiber.

Thanks in general to all members of the Photonics Laboratory and the FORCE group. I should specially mention Henrik Eliasson for his collaboration in supervising students, and Dr. Pontus Johannisson and Prof. Víctor Torres-Company for sharing their expertise. Jeanette Träff deserves a deep thank you for solving every administrative issue I have had.

I also want to thank Prof. Christophe Peucheret who made me feel interested about fiber-optic communication in general.

Last but not least, I would like to express my deepest thanks to my wife Lara, whose support through these years has been essential. Thanks also to my parents, sister and friends.

Abel Lorences-Riesgo

Göteborg
December 2016

List of Acronyms

ASE amplified spontaneous emission

BPSK binary phase-shift keying

CW continuous wave

DP dual-polarization
DSP digital signal processing

EDFA erbium-doped fiber amplifier

FOPA fiber-optic parametric amplifier
FWM four-wave mixing

HNLF highly-nonlinear fiber

LO local oscillator

NF noise figure

OIL optical-injection locking
OSNR optical signal-to-noise ratio

PAM pulse-amplitude modulation
PBS polarization-beam splitter
PC polarization controller
PI phase-insensitive
PIA phase-insensitive amplifier
PLL phase-locked loop
PMD polarization-mode dispersion

PMF polarization-maintaining fiber

PPLN periodically-poled lithium niobate

PRBS pseudo-random bit sequence

PS phase-sensitive

PSA phase-sensitive amplifier

PSK phase-shift keying

PTN pump-transferred noise

QAM quadrature-amplitude modulation

QPSK quadrature phase-shift keying

RF radio frequency

SBS stimulated Brillouin scattering

SH self-homodyne

SNR signal-to-noise ratio

SOP state of polarization

SPM self-phase modulation

SRS stimulated Raman scattering

SSMF standard single-mode fiber

WDM wavelength-division multiplexing

XPM cross-phase modulation

ZDW zero-dispersion wavelength

Table of Contents

Chapter 1

Introduction

One of the events characterizing the 20th century was the development of a global network, called the Internet. Thanks to this global network, we have access to many different services such as video streaming, online gaming, video calls, and so on. Nowadays, the backbone of this global network consists of fiber optical links and therefore the evolution of this global network is directly linked to advances in the field of fiber-optic communications.

The proposal of the optical fiber in 1966 [1] in combination with the semiconductor laser in 1962 [2, 3] can be considered as the main events which started the field of optical communications. Since then, advances in both optical and electrical subsystems have enabled a continuous increase of the transmission capacity. One of the main events enabling the transmission capacity increase is the demonstration of the erbium-doped fiber amplifier (EDFA) in 1987 [4]. In the last years, the demonstration of digital coherent receivers should be highlighted [5]. Despite all these historical advances, technology should continue evolving in order to cope with future demands [6].

During the last decades, much research has investigated the use of parametric effects for providing different functionalities within the context of fiber-optic communications. Parametric effects are very attractive due to their fast response as well as capability for wide bandwidth operation. Applications such as demultiplexing [7], optical sampling [8], low-noise amplification [9], dispersion compensation [10] and mitigation of fiber nonlinearities [11–13] by phase conjugation were demonstrated already during the 90s. Advances in both χ^2 [14] and χ^3[15] nonlinear platforms in recent years have extended the numbers of applications in which parametric processing can be used. Functionalities such as wideband comb regeneration [16], multicasting [17], signal phase regeneration [18, 19], low noise amplification of wavelength-division multiplexing (WDM) signals [20] and WDM to optical time-division multiplexing [21] have been demonstrated using parametric effects.

All-optical parametric signal processing has thus been proven to provide different functionalities within the field of fiber-optic communications. However, in today's fiber-optic communciations, digital coherent receivers have enabled the use of advanced modulation formats as well as the use of both polarizations for encoding of data. It is then necessary to investigate whether parametric processing can be adapted to this context and whether new functionalities can be provided.

1.1 This Thesis

The motivation of this thesis has been to develop and understand new functionalities provided by parametric processing in optical communications using highly-nonlinear fiber (HNLF) as the nonlinear medium, focusing mainly on phase-sensitive (PS) processes. With the development of coherent receivers, the use of modulation formats utilizing both amplitude and phase, e.g. quadrature-amplitude modulation (QAM), has become standard in optical communications. The capability of optical processing these signals is thus of great interest. This thesis covers multiple ways of all-optical processing, focusing mainly on those that are PS, i.e., where the output depends on the input signal phase. Among the different functionalities that PS processing can provide are phase regeneration and low noise amplification. Around 2010, the demonstration of phase-regeneration of binary phase-shift keying (BPSK) [18] and quadrature phase-shift keying (QPSK) [19] signals in a black-box implementation showed the potential of PS regenerators for improving the signal quality. In addition, WDM-compatible low-noise amplification (below the quantum limited noise figure (NF) of phase-insensitive amplifiers (PIAs)), showed the potential of replacing conventional EDFAs by phase-sensitive amplifiers (PSAs) as inline amplifiers [20]. However, thanks the development of the coherent receivers, the use of dual-polarization (DP) signals is ubiquitous when coherent receivers are used. This contrasts with the mentioned demonstrations which were limited to signals that only transmit information in one polarization. The first part of this thesis, [Paper A-C], has been devoted to PS processing in scenarios in which DP signals are used, focusing on vector PSAs. In addition, in [Paper D], we assess the capabilities of mid-span spectral inversion for mitigation of fiber nonlinearities in an installed link when also using DP signals. Using a single nonlinear medium, we demonstrate phase-conjugation of six WDM signals without any spectral efficiency loss due to the conjugation process.

Another functionality provided by PS processors is quadrature demultiplexing, in which an incoming signal is decomposed into its inphase and quadrature components. Quadradure decomposition can be of interest for data demultiplexing, simplifying the digital signal processing (DSP) receiver at the expense of more complex optics [22] or as a first stage of a signal regenerator [23]. Prior to this work, experimental demonstrations of quadrature demultiplexing had showed decomposition of a QPSK signal into 2×BPSK signals at two different wavelengths [24]. The scheme used in these demonstrations requires four phase-locked pumps and therefore there was need need for a simpler scheme. Another demonstration showed the ability to extract one quadrature by using the phase-squeezing capabilities of a signal-degenerate PSA [25]. In [Papers E, F] we demonstrate the extraction of both quadrature components at the

same wavelength as that of the input signal. In [Paper E], a QPSK signal to $2\times$BPSK demultiplexing is demonstrated using a degenerate vector parametric amplifier. In [Paper F], 16-QAM to 2×4 pulse-amplitude modulation (PAM) demultiplexing is demonstrated using a degenerate polarization-diverse PS parametric processor.

This thesis is concluded by proposing, analyzing and demonstrating the novel concept of comb regeneration for self-homodyne (SH) superchannels. This technique enables a multi-channel SH receiver by transmitting only two unmodulated lines, and therefore it can enable SH detection with low spectral overhead. Compared to conventional SH schemes, in which a pilot tone is usually transmitted in an orthogonal polarization [26, 27] or at another frequency [28], SH superchannels reduces the complexity since often polarization tracking and narrow filtering are required for each pilot tone. Thus, an SH superchannel only requires two polarization trackers and two narrow filters whereas conventional SH requires as many polarization tracking schemes and narrow filters as WDM channels. Whereas the concept of an SH superchannel had been proposed [29], comb regeneration had not been demonstrated prior to this work. In [Paper G], we propose comb regeneration by transmitting two unmodulated carriers and analyze the quality of the regenerated comb. In [Paper H], we perform the first demonstration of SH data transmission enabled by comb regeneration.

1.2 Thesis Outline

This thesis is organized as follows. In Chapter 2, we describe the main propagation effects in a silica-based single-mode HNLF, focusing on those which are relevant within in the context of parametric processing. In Chapter 3, we explain the basics for parametric amplifiers and processors. We discuss the polarization properties of polarization-diverse and vector PSAs, and applications such as phase conjugation, phase regeneration and quadrature decomposition. In Chapter 4, we discuss frequency combs, focusing on the basics of parametric combs and their implementation. We also introduce the technique of SH superchannels based on comb regeneration. A future outlook is provided in Chapter 5. Finally, in Chapter 6 we summarize the papers appended in this thesis.

Chapter 2

Wave Propagation Effects

In this chapter, we describe the main propagation effects in a silica-based HNLF, which is the nonlinear platform used in the experimental works included in this thesis. We should however mention that parametric processing has also been demonstrated in many other platforms. Examples of $\chi^{(2)}$ platforms are bulk crystals [30, 31] and periodically-poled lithium niobate (PPLN) waveguides [14]. Silicon waveguides [32], chalcogenide waveguides [33], silicon-germaniun waveguides [34], silicon-nitride waveguides [35], and bismuth-oxide-based HNLF [36] are some examples of $\chi^{(3)}$ platforms. Some advantages of silica-based HNLF are compatibility with standard single-mode fibers (SSMFs) (splicing loss can be below 0.5 dB), flexibility for dispersion engineering, and (relative) high nonlinear coefficient while still having low attenuation and dispersion [15]. Nevertheless, integrated platforms are getting more mature and they can already outperform HNLFs in some applications. For example, wavelength conversion over 750 nm has been demonstrated using an AlGaAs waveguide [37].

This chapter is organized as follows. First, we discuss the linear effects, i.e. fiber attenuation, chromatic dispersion and polarization-mode dispersion (PMD). Then, we describe the main nonlinear effects which are the Kerr effect, stimulated Brillouin scattering (SBS) and stimulated Raman scattering (SRS). Parametric processing in silica-based HNLFs has its origin in the Kerr effect, but as will be explained in this chapter, the remaining propagation effects should also be taken into account when analyzing parametric processing.

2.1 Linear Propagation Effects

In a parametric processor, the linear propagations effects to be considered are the loss, the chromatic dispersion and the fiber birefringence.

2.1.1 Fiber Attenuation

In silica fiber, the attenuation in the communication window is mainly caused by material absorption and Rayleigh scattering. At 1550 nm, a record-low loss of 0.147 dB/km has been reported [38] whereas typical attenuation for SSMF is about 0.2 dB/km. In the silica-based HNLFs used in this work, the loss coefficient is around 0.6-1.2 dB/km. The attenuation dependance on the wavelength can be neglected when operating in the communication bands.

In the context of fiber nonlinearities, the nonlinear effective length [39, Ch. 4]

$$L_{\text{eff}} = \frac{1 - e^{-\alpha L}}{\alpha} \tag{2.1}$$

is often defined in order to account for the fiber attenuation when calculating the strength of a nonlinear effect. In this equation, L is the physical length and α is the attenuation in m^{-1}. In nonlinear platforms with high loss, the physical length should be limited to the order of the nonlinear length since large physical length only increases the accumulated attenuation without further increasing the nonlinear interaction. When using short and low-loss fibers, the effective length and the physical length are approximately the same, which means that the attenuation can be neglected. This is the typical case of parametric processing in silica HNLFs, where the typical lengths used in experiments are from 50 m to 500 m.

2.1.2 Chromatic Dispersion

The chromatic dispersion, which is a wavelength dependence of the refractive index, is an effect of great importance for parametric processing. This effect is often accounted by describing the propagation constant, $\beta = n(\omega)\omega/c$ where $n(\omega)$ and c are the refractive index and speed of light in vacuum, in a Taylor series around the carrier frequency ω_0 we are operating,

$$\beta = \beta_0 + \beta_1(\omega - \omega_0) + \frac{\beta_2}{2!}(\omega - \omega_0)^2 + \frac{\beta_3}{3!}(\omega - \omega_0)^3 + ..., \tag{2.2}$$

where $\beta_i = \frac{d^i \beta}{d\omega^i}\Big|_{\omega_0}$.

The parameter β_0 is related to the phase velocity by $v_{\text{p}} = \omega_0/\beta_0$. The group velocity, v_{g}, is directly related to β_1 by $v_{\text{g}} = 1/\beta_1$. The dispersion parameter β_2 and third-order dispersion β_3, determine the group-velocity dependence on the frequency. Higher-order terms are usually neglected, although they should be taken into account in cases of wide bandwidth operation. The more commonly used dispersion parameter, D, and the dispersion-slope parameter, S, quantifying the group-velocity dependence on the wavelength, λ, as $D = \frac{dv_{\text{g}}}{d\lambda}$ and $S = \frac{dD}{d\lambda}$ are related to the above Taylor expansion coefficients by

$$D = -\frac{2\pi c}{\lambda^2}\beta_2, \tag{2.3}$$

$$S = \left(\frac{2\pi c}{\lambda^2}\right)^2 \beta_3 + \frac{4\pi c}{\lambda^3}\beta_2. \tag{2.4}$$

The dispersion is responsible for changes in the temporal shape of a pulse when it propagates through the fiber. In SSMF, the dispersion is about $D =17$ ps/(nm km) at 1550 nm. HNLFs are usually designed such that the dispersion is low in the operation wavelength with common values of $|D|<0.5$ ps/(nm km). In this case the dispersion slope is a parameter which needs to be considered and higher-order terms should also be considered in the case of large bandwidth devices. The capability for dispersion tailoring is one of the main advantages of silica-based HNLFs [15]. It is also important to realize that not only the global fiber dispersion parameters are important but also how the dispersion properties vary along the fiber since this can limit the bandwidth [40, 41] and also have an impact on the noise properties of parametric amplifiers [42].

2.1.3 Polarization-Mode Dispersion

Due to the fiber rotational symmetry, two orthogonal polarization modes are guided in an single-mode optical fiber. In an ideal fiber, these two orthogonal modes have the same propagation constant when neglecting nonlinear effects, i.e. they are degenerate. However, PMD is caused by fiber birefringence, i.e., waves with different polarizations do not experience the same refractive index due to fiber asymmetry caused by e.g., variation in the core shape, internal stress and external effects such as bends or lateral stress. Depending on the fiber design, fiber birefringence can be random or deterministic.

Polarization-maintaining fibers (PMFs) are fibers in which a deterministic birefringence is induced in the manufacturing process. Usually, a longitudinal stress is applied in the fiber, which causes a strong linear birefringence. By launching the input wave in one of the main axes (fast or slow axes), PMFs preserve the polarization of this wave through (ideally) infinite distances.

In optical fibers with random birefringence, the orientation of the main axes (locally defined fast and slow axes) changes randomly along the fiber. The length in which the main axes can be considered constant is only on the order of several meters. Moreover, the fiber birefringence changes with time due to environmental changes on the fiber such as vibrations, temperature and external stress. In these situations, the fiber PMD is a stochastic effect and it is usually analyzed in statistical terms. When a polarized continuous wave (CW) signal is launched into an optical fiber with random birefringence, its polarization will therefore change along the fiber. Moreover, the output polarization also depends on the signal wavelength. The two launched polarization states in which the output polarization is frequency independent to first-order approximation are the so-called principal states of polarization (SOPs) [43]. The difference in propagation time between a wave launched in one of the principal states of polarization compared to the wave launched in the other principal state of polarization is the differential-group delay.

HNLFs can be either PMFs or fibers with random birefringence. Since polarization determines the strength of the nonlinearities, polarization-maintaining HNLFs would, in principle, be better than HNLF with random birefringence. However, manufacturing a polarization-maintaining-HNLFs with adequate values of dispersion and nonlinearities is challenging and expensive. Thus, and since lab-environments can be

controlled, HNLFs with random birefringence are employed in most experiments. In scalar fiber-optic parametric amplifiers (FOPAs), influence from fiber birefringence can be mitigated by launching the involved waves into the main SOPs. However, PMD affects severely the performance of vector FOPAs [44–46], and more so when operating in PS mode [Paper A].

2.2 Kerr Effect

Apart from being wavelength-dependent, the refractive index, n, also depends on the instantaneous intensity of the light, I propagating through the fiber. The effect of the refractive index dependence on the optical intensity is named the Kerr effect. When accounting for the Kerr effect, the refractive index is usually expressed as [47, Ch. 4]

$$n(\omega, I) = n_0(\omega) + n_2 I, \tag{2.5}$$

where $n_0(\omega)$ is the linear part and n_2 is the nonlinear refractive index. The nonlinear refractive index is related to the third order susceptibility, $\chi^{(3)}$, by [47, Ch. 4]

$$n_2 = \frac{3}{4n_0^2\epsilon_0 c}\chi^{(3)}, \tag{2.6}$$

where ϵ_0 is the vacuum permittivity. Here, we have assumed that the light is linearly polarized, and $\chi^{(3)}$, which in general is a fourth-rank tensor, is expressed as a scalar. It is important to realize that the second-order susceptibility, $\chi^{(2)}$, vanishes in silica fibers due to molecular symmetry. Materials in which $\chi^{(2)}$ does not vanish can be used to achieve parametric amplification as well.

In the analysis of wave propagation in fibers, the nonlinear coefficient, γ, is often used to incorporate the field distribution into the analysis since the intensity is determined by the field distribution. The nonlinear coefficient, γ, is defined as [39, Ch. 2]

$$\gamma = \frac{2\pi n_2}{\lambda A_{\text{eff}}}, \tag{2.7}$$

where A_{eff} is the effective mode area, and thus it determines the confinement of the mode. The nonlinear coefficient takes value of about 1.3 (W m)$^{-1}$ in SSMF. In our experiments, we have used HNLFs with nonlinear coefficient of around 10 (W m)$^{-1}$ but silica-based HNLF can have nonlinear coefficients up to 30 (W m)$^{-1}$ [15].

2.2.1 Coupled-Mode Equations

In order to analyze the nonlinear refraction with arbitrary SOPs, the 81 elements of the third order susceptibility tensor, $\chi^{(3)}$, should be considered. However, many of these elements vanishes due to symmetries and in the case of silica-based fibers there are only three independent terms [39, Ch. 6]. In an ideal fiber, the propagation of the two polarization modes can be described by [39, Ch. 6]

$$\frac{\partial A_{\text{r}}}{\partial z} + \frac{\alpha}{2}A_{\text{r}} + i\frac{\beta_2}{2!}\frac{\partial^2 A_{\text{r}}}{\partial t^2} - \frac{\beta_3}{3!}\frac{\partial^3 A_{\text{r}}}{\partial t^3} - i\frac{2}{3}\gamma\left(|A_{\text{r}}|^2 + 2|A_{\text{l}}|^2\right)A_{\text{r}} = 0, \tag{2.8}$$

$$\frac{\partial A_l}{\partial z} + \underbrace{\frac{\alpha}{2} A_l}_{\text{Loss}} + \underbrace{i \frac{\beta_2}{2!} \frac{\partial^2 A_l}{\partial t^2} - \frac{\beta_3}{3!} \frac{\partial^3 A_l}{\partial t^3}}_{\text{Disperion}} - \underbrace{i \frac{2}{3} \gamma \left(|A_l|^2 + 2|A_r|^2 \right) A_l}_{\text{Kerr nonlinearities}} = 0, \qquad (2.9)$$

where $A_{r,l}$ are the electric field in the right and left hand circular polarizations. The fields are normalized such that $|A_{r,l}|^2$ corresponds to the optical power. These equations are written in a reference frame moving at the group velocity. This model however is only valid in the case of short fibers or rapidly spun fibers [48, 49] since the fiber birefringence should be taken into account. In addition, in the case of a random birefringent fiber, the analysis should ideally be performed in statistical terms. The analysis can be simplified by assuming that fiber birefringence does not change the relative polarization between the waves and that the SOP of the wave travelling through the fiber lies anywhere in the Poincaré sphere with equal probability. With these assumptions, the averaged coupled equations describing the field propagation are [50, 51]

$$\frac{\partial A_u}{\partial z} + \frac{\alpha}{2} A_u + i \frac{\beta_2}{2!} \frac{\partial^2 A_u}{\partial t^2} - \frac{\beta_3}{3!} \frac{\partial^3 A_u}{\partial t^3} - i \frac{8}{9} \gamma \left(|A_u|^2 + |A_v|^2 \right) A_u = 0, \qquad (2.10)$$

$$\frac{\partial A_v}{\partial z} + \underbrace{\frac{\alpha}{2} A_v}_{\text{Loss}} + \underbrace{i \frac{\beta_2}{2!} \frac{\partial^2 A_v}{\partial t^2} - \frac{\beta_3}{3!} \frac{\partial^3 A_v}{\partial t^3}}_{\text{Disperion}} - \underbrace{i \frac{8}{9} \gamma \left(|A_v|^2 + |A_u|^2 \right) A_v}_{\text{Kerr nonlinearities}} = 0, \qquad (2.11)$$

where A_u and A_v are the wave components in two orthogonal polarizations.

The validity of the Manakov model depends on the considered bandwidth, fiber length and fiber birefringence. In cases where PMD is not negligible and changes the relative polarization between the waves, this model should be further modified. This model does not apply to the case of PMFs. Considering the lengths of HNLFs employed in parametric amplification, the Manakov model is a reasonable assumption [39, Ch. 10],[52] that significantly simplifies the analysis.

From the Manakov model, two important consequences are derived compared to the ideal fiber model. First, the absolute polarization does not determine the strength of the nonlinearities. Second, the power in each polarization is conserved when neglecting the fiber loss.

Henceforth, the factor $\frac{8}{9}$ will be included in γ, and the Manakov model will be assumed unless otherwise stated.

2.2.2 Self-Phase Modulation

Self-phase modulation (SPM) is a process in which a wave propagating through the fiber phase modulates itself by inducing changes in the fiber refractive index. In the case of a CW, the nonlinear phase shift is described by

$$\Phi_{\text{NL,SPM}} = \gamma P L_{\text{eff}}, \qquad (2.12)$$

where P is the power of the propagating wave. Here, we can see how the effective length is an useful parameter to define the strength of the nonlinearity. This equation is only valid in cases in which we can neglect the dispersion, as e.g. slow-varying input signal or operating at the zero-dispersion wavelength (ZDW). However, in

most cases, the interplay between dispersion and SPM should be considered, which often requires a numerical solution. An interesting effect of the interaction between SPM and dispersion is the generation of optical solitons in which dispersion and nonlinearities cancel out [53, 54].

2.2.3 Cross-Phase Modulation

Cross-phase modulation (XPM) is a process in which the phase of a wave travelling through the fiber is modulated by a co-propagating wave. The induced nonlinear phase shift on a CW by a second CW with power P_2 is

$$\Phi_{\text{NL,XPM12}} = 2\gamma P_2 L_{\text{eff}} \tag{2.13}$$

if we assume that both waves are co-polarized. We can see here that the nonlinear phase shift induced by XPM is twice the nonlinear phase shift induced by SPM.

If the two waves are cross-polarized, we then have

$$\Phi_{\text{NL,XPM12}} = \gamma P_2 L_{\text{eff}} \tag{2.14}$$

where we have assumed the Manakov model. We can see here that the strength of XPM can vary by a factor of two when varying the relative polarization between the two waves. Such difference between the nonlinear phase shift induced by XPM, gives raise to an effect called cross-polarization modulation, an effect in which the polarization of a wave is modulated by another wave. Similar to the case of SPM, dispersion should also be considered when accounting for the strength of XPM.

2.2.4 Four-Wave Mixing

Scalar Four-Wave Mixing

Four-wave mixing (FWM), also named as four-photon mixing, is a process which involves the interaction between four photons and energy exchange between them. In a classical interpretation, FWM can be qualitatively explained by moving gratings. When two co-polarized waves, E_1 and E_2, with frequencies ω_1, ω_2 are co-propagating through the fiber, they generate an intensity beat tone with frequency $\omega_1 - \omega_2$. Thus, the fiber refractive index is modulated at this frequency in accordance with the Kerr effect and the grating propagation is determined by $\beta_1 - \beta_2$ where $\beta_{1,2}$ are the propagation constants for each wave. When a third co-polarized wave, E_3 with frequency ω_3, also propagates together with the two previous waves, power from this third wave is scattered at frequencies $\omega_4 = \omega_3 \pm (\omega_1 - \omega_2)$. The Bragg grating condition $\beta_4 - \beta_3 = \pm(\beta_1 - \beta_2)$ determines the strength of the process [55]. In the same way, E_2 is scattered by the beating between E_1 and E_3, and E_1 is scattered by the beating between E_2 and E_3. If all the waves have different frequencies, the FWM process is said to be non-degenerate. As shown in Fig. 2.1, the non-degenerate FWM creates three new wavelengths at frequencies $\omega_{\text{kmn}} = \omega_{\text{k}} + \omega_{\text{m}} - \omega_{\text{n}}$ where $k, m, n \in \{1, 2, 3\}$, $k \neq m$, $k \neq n$ and $m \neq n$. Note that two terms are created at the same frequency. The degenerate processes include E_1 being scattered by the beating between itself and E_2 and the beating between between itself and E_3; and similarly
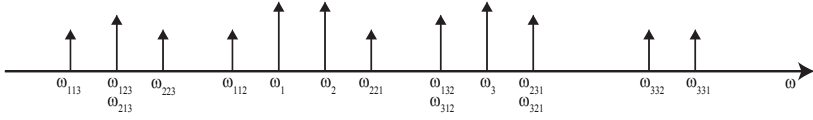
Fig. 2.1: Schematic of waves generated by FWM processes when three input co-polarized waves are considered. The frequencies of the input waves are ω_1, ω_2 and ω_3.
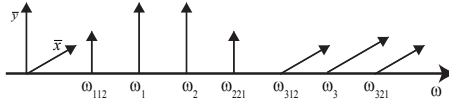
Fig. 2.2: Schematic of waves generated by FWM processes when three input are considered, with two co-polarized waves and the third wave cross-polarized to them. The frequencies of the input waves are ω_1, ω_2 and ω_3.

to the cases in which E_2 and E_3 are scattered. The new frequencies created by degenerate processes are $\omega_{kmn} = \omega_k + \omega_k - \omega_m$ with $k, m \in \{1, 2, 3\}$, $k \neq m$. Six new frequency components are created when considering degenerate FWM. Taking into account degenerate and non-degenerate FWM, the total number of new frequency components is nine.

Vector Four-Wave Mixing

The previous explanation is valid for scalar FWM in which all waves are co-polarized. Vector FWM, in which waves have different polarizations can also occur. We now assume that two waves, E_1 and E_2, are co-polarized and a third wave, E_3, is cross-polarized with respect to them. In this case, the two co-propagating and co-polarized waves, E_1 and E_2, set the beat tone; and power from E_3 will be scattered to waves at frequencies $\omega_3 \pm (\omega_1 - \omega_2)$ as shown in Fig. 2.2. These generated waves are co-polarized with E_3. An special case is that in which $\omega_1 + \omega_3 = 2\omega_2$, and a new wave at the same frequency as E_2 but cross-polarized to E_2 is created. Combinations of E_1 -E_3 and E_2 -E_3 do not establish an intensity beat tone as they are cross-polarized pair of waves. The degenerate process involving E_1 and E_2 also generates new waves as explained previously with co-polarized waves. Here, we should remark that this interpretation is only valid for the Manakov model. Vector FWM requires the knowledge of the absolute polarization and not only the relative polarization in an ideal fiber.

Quantum-Mechanical Interpretion

From a quantum mechanical point of view, the FWM process is interpreted as follows: two photons at frequencies ω_1, ω_2 are annihilated, and two photons at frequencies

ω_3 and ω_4 are created. FWM is a process in which energy is conserved, thus we have $\omega_1 + \omega_2 = \omega_3 + \omega_4$. Momentum is also conserved and similar to the Bragg condition determines the strength of the process.

In an ideal fiber without birefringence, Eqs. (2.8), (2.9), spin angular momentum is also conserved, determining the possible combinations of the spin of the annihilated photons and created photons. When the two annihilated photons have the same spin, the created photons also have the same spin as the annihilated photons. When the two annihilated photons have opposite spin, the two created photons also have opposite spin. As a consequence, power from two waves with right-hand circular polarization cannot scatter to two waves with right-hand circular polarization. However, power from two co-polarized waves with linear polarization can scatter to two waves with orthogonal polarization to the original waves.

In Chapter 3 we will provide more insight about FWM and its use to achieve parametric amplification. We will also discuss the interplay between dispersion, SPM, XPM and FWM.

2.3 Brillouin Scattering

Brillouin scattering is an inelastic nonlinear process, caused by the electrostriction effect: the medium is compressed in presence of an optical field. Brillouin scattering involves energy transfer to the medium in the form of an acoustic vibration. Contrary to SRS, the created downshifted wave only propagates backwards. The gain peak, dictated by the speed of the acoustic wave, is about 10 GHz in silica fibers, and the gain bandwidth is on the order of tens of MHz [39, Ch. 9].

For narrow-band waves, SBS imposes a limitation on the maximum power that can be launched into the fiber [56]. This effect is then detrimental in parametric processing using HNLF since high-power CWs are often needed. In order to overcome SBS limitations, different techniques have been developed. The fiber can be doped with a material which lowers the SBS gain such as Al_2O_3 [57]. The use of these dopants to increase the SBS threshold do however increase fiber loss. Since the amplified wave travels backwards, the use of isolators is another way to mitigate SBS [58]. This technique cannot however be implemented in bidirectional FOPAs. Furthermore, it also introduces additional losses. SBS is also reduced when the wave spectrum is broadened beyond the bandwidth of SBS [59]. In parametric amplification, the pump spectrum is usually broadened by phase modulation with radio frequency (RF) tones [60], white noise [61] or pseudo-random bit sequence (PRBS) [62]. However, the pump-phase modulation is transferred to the idler which is undesired when performing wavelength conversion. In PSAs, pump-phase modulation degrades the performance of the amplifier. In two-pump amplifiers, counter-phase modulation of the pumps can alleviate the penalty due to pump phase modulation [62]. Applying a temperature gradient [63, 64] or a strain gradient [65–67] in the fiber also decrease the SBS. As a drawback, both temperature and strain gradient causes ZDW fluctuations which might degrade the performance of FOPAs [40]. The solution is applying the strain such that it mitigates inherent ZDW fluctuations of the HNLF as well as SBS [68]. Fiber straining also enhances the fiber PMD which is unde-

sired in FOPAs [69]. Fibers more tolerant towards straining have therefore been designed [70]. These techniques can also be combined in order to achieve larger SBS suppression. For example, the combination of fiber straining and isolators has allowed the design of FOPAs with large net gain without pump spectral broadening [71].

SBS is often considered a detrimental effects on parametric amplification. However, it can also be used to enhance some FOPA properties. Using SBS to perform a phase shift on the signal can enhance FOPA bandwidth and gain [72–74]. In addition, such a method has also been shown to control the saturation characteristics in FOPAs [75].

SBS has also gained attention recently to be used as a narrow-band amplifier. It has been demonstrated that Brillouin amplification can be utilized to achieved phase regeneration of BPSK [76] and QPSK [77] signals without the need of a phase-locked loop (PLL). It has also been demonstrated that Brillouin amplification can also be used as a technique for performing narrow filtering of a pilot tone in SH detection [78] and [Paper H].

2.4   Raman Scattering

Raman scattering is an inelastic nonlinear process, commonly interpreted as the delayed response of the Kerr effect. From a quantum mechanical point of view, a photon is annihilated, and a photon at lower frequency is created together with an optical phonon (vibration). The created downshifted photons can travel in either forward direction or backward directions. In silica fibers, SRS gain has a large bandwidth with its peak being downshifted about 13.2 THz from the scattered wave [39, Ch. 8]. Amplifiers using SRS are quite attractive since they can perform distributed amplification without the practical challenges of parametric amplifiers.

The effect of Raman scattering in parametric processing can be either beneficial or detrimental. The SRS can be used to increase the FOPA gain and/or bandwidth [79]. A hybrid Raman-parametric amplifier can be used for mitigating the crosstalk when using parametric amplification in a WDM scenario [80]. However, Raman scattering affects the noise properties of parametric amplifiers, mainly in broadband parametric amplifiers [81, 82]. The NF degradation due to Raman scattering will be discussed in Section 3.7.

Chapter 3

Fiber-Optical Parametric Processing

This chapter focuses on the use of FWM for parametric amplification and processing with special attention to those processes which are PS. In this chapter, we only consider one FWM process, meaning that only four waves (three waves when the process is degenerate) interact. Thus, we first describe the basics of the four wave model which gives raise to parametric amplification and phase conjugation, discussing how the efficiency of these processes depends on the fiber characteristics and pump power. Using the relation derived in the four-wave model, different PSA schemes and PS processors are discussed[1]. We first describe the conventional PSAs schemes. Afterward, different practical schemes for implementation of PSA are described. Then, we discuss both PS processors based on polarization-diverse as well as vector implementations. We briefly discuss the noise properties of PSAs. We describe possible applications for which parametric processing can be utilized. The chapter is concluded by discussing the main challenges in parametric processing.

3.1   Four-Wave Model

Parametric amplification can be achieved by means of both degenerate and non-degenerate FWM, and using either vector or scalar FWM. When using degenerate FWM in scalar phase-insensitive (PI)-FOPAs, the input waves consists of a strong wave, known as pump, and a weak signal to be amplified. In this case, the most efficient process is the one in which power from the pump scatters due to the grating set by the pump and the signal. The pump power is indeed scattered to the signal wave and to a new wave, known as idler, at frequency $\omega_I = 2\omega_P - \omega_S$ where ω_P and ω_S are the pump and the signal frequencies. The process in which power from

---

[1]Here, we refer to a PS processors as a processor in which the output signal depends on the input signal phase, without the need for amplification.

the signal scatters can usually be neglected due to its lower strength. When using non-degenerate FWM in scalar PI-FOPAs, the input waves usually consists of two strong waves, pump waves, and the weak signal to be amplified. In vector PI-FOPAs, the input consists of two cross-polarized pumps and a signal. In both non-degenerate cases, the amplifier is often designed such that only one idler at frequency $\omega_I = \omega_{P1} + \omega_{P2} - \omega_S$ needs to be considered and other created waves can be neglected due to their lower strength. Here, ω_{P1} and ω_{P2} denote each pump frequency.

The evolution of the pumps, A_{P1} and A_{P2}, the signal A_S and idler, A_I, fields can be described by a set of four coupled equations in both scalar and vector non-degenerate FWM processes. This set of four equations is obtained from applying Eqs. (2.10), (2.11) to this situation. In scalar FWM, four co-polarized waves are considered. In the case of vector FWM, for simplicity, we assume that the signal field, A_S, is co-polarized with one pump, A_{P1}, and the idler field, A_I, is then co-polarized with the other pump, A_{P2}. Then, we have [83]

$$
\begin{aligned}
\frac{\partial A_{P1}}{\partial z} =& i\gamma \left(|A_{P1}|^2 + \epsilon|A_{P2}|^2 + \epsilon|A_I|^2 + 2|A_S|^2 \right) A_{P1} \\
&+ i\epsilon\gamma A_S A_I A_{P2}^* \exp(i\Delta\beta z),
\end{aligned}
\tag{3.1}
$$

$$
\begin{aligned}
\frac{\partial A_{S}}{\partial z} =& i\gamma \left(|A_{S}|^2 + \epsilon|A_{P2}|^2 + \epsilon|A_I|^2 + 2|A_{P1}|^2 \right) A_{S} \\
&+ i\epsilon\gamma A_{P1} A_{P2} A_I^* \exp(-i\Delta\beta z),
\end{aligned}
\tag{3.2}
$$

$$
\begin{aligned}
\frac{\partial A_{I}}{\partial z} =& i\gamma \left(|A_{I}|^2 + \epsilon|A_{P1}|^2 + \epsilon|A_S|^2 + 2|A_{P2}|^2 \right) A_{I} \\
&+ i\epsilon\gamma A_{P1} A_{P2} A_S^* \exp(-i\Delta\beta z),
\end{aligned}
\tag{3.3}
$$

$$
\begin{aligned}
\frac{\partial A_{P2}}{\partial z} =& i\gamma \left(\underbrace{|A_{P2}|^2}_{\text{SPM}} + \underbrace{\epsilon|A_{P1}|^2 + \epsilon|A_S|^2 + 2|A_I|^2}_{\text{XPM}} \right) A_{P2} \\
&+ i\epsilon\gamma \underbrace{A_S A_I A_{P1}^* \exp(i\Delta\beta z)}_{\text{FWM}},
\end{aligned}
\tag{3.4}
$$

where the parameter $\epsilon = 2$ in the scalar case and $\epsilon = 1$ in the vector case which allows the use of the same set of equations in both cases [83, 84]. The parameter $\Delta\beta = \beta_S + \beta_I - \beta_{P1} - \beta_{P2}$ is the linear phase mismatch due to the difference of the pump, the signal and the idler propagation constants. These equations assume that the pumps, the signal and the idler are CWs or negligible dispersion over the bandwidth of the signal, the idler and the pumps; and also negligible fiber loss. On the right-hand side, the different terms corresponding to SPM, XPM and FWM can be observed. The strength of XPM and FWM is halved when considering vector amplification. Here, we have used a set of four scalar equations, but a more general description in which the pumps can have any relative SOP is also possible when

using Jones vectors [39, Ch. 10]. By using the set of four scalar equations, we can gain much insight into the two most common cases of parametric amplification.

Equations (3.1), (3.4) can be solved when the pump waves remain undepleted. The pump fields are then given by [83]

$$A_{\mathrm{P1}} = A_{\mathrm{P1}}(0) \exp[i\gamma(P_{\mathrm{P1}} + \epsilon P_{\mathrm{P2}})L], \tag{3.5}$$

$$A_{\mathrm{P2}} = A_{\mathrm{P2}}(0) \exp[i\gamma(\epsilon P_{\mathrm{P1}} + P_{\mathrm{P2}})L], \tag{3.6}$$

where L is the fiber length, and the pump powers are denoted by $P_{\mathrm{P1}} = |A_{\mathrm{P1}}|^2$ and $P_{\mathrm{P2}} = |A_{\mathrm{P2}}|^2$. The input pump fields are denoted by $A_{\mathrm{P1,P2}}(0)$. In the small-signal regime, the pumps are only affected by SPM and XPM between them. The solutions for the signal and the idler fields are then given by

$$\begin{aligned} A_{\mathrm{S}} = &[\mu A_{\mathrm{S}}(0) + \nu A_{\mathrm{I}}^*(0)] \\ &\cdot \exp(-i\beta L/2 + i\gamma \frac{3}{2} P_{\mathrm{P1}} L + i\gamma(\epsilon - 1/2) P_{\mathrm{P2}} L) \end{aligned} \tag{3.7}$$

$$\begin{aligned} A_{\mathrm{I}} = &[\mu A_{\mathrm{I}}(0) + \nu A_{\mathrm{S}}^*(0)] \\ &\cdot \exp(-i\beta L/2 + i\gamma \frac{3}{2} P_{\mathrm{P2}} L + i\gamma(\epsilon - 1/2) P_{\mathrm{P1}} L). \end{aligned} \tag{3.8}$$

In Eqs. (3.7), (3.8), the phase term is often neglected for simplicity. The coefficients μ and ν defining the input-output relations are given by [83]

$$\mu = \cosh(gL) + i(\kappa/g)\sinh(gL), \tag{3.9}$$

$$\nu = i\epsilon\gamma(A_{\mathrm{P1}}(0)A_{\mathrm{P2}}(0)/g)\sinh(gL), \tag{3.10}$$

where $g = \sqrt{\epsilon^2\gamma^2 P_{\mathrm{P1}} P_{\mathrm{P2}} - (\kappa/2)^2}$ with $\kappa = \Delta\beta + \gamma(P_{\mathrm{P1}} + P_{\mathrm{P2}})$. The relation $|\mu|^2 - |\nu|^2 = 1$ is always fulfilled.

Here, our analysis has been limited to four-wave interaction. However, it is worth realizing that there are scenarios in which more waves needs to be considered. For instance, six waves should be considered in four-mode amplifiers in which there are three idlers to be considered [85]. We have also assumed that the pumps remain undepleted and thus, we are operating in the small-signal regime. The solution in the case of large signal power requires the use of elliptical functions [86]. The FWM between the pumps can also generate additional waves that deplete the pumps, invalidating this model.

The previous analysis is valid for non-degenerate FWM but similar solutions have been demonstrated for the cases of pump degenerate and signal degenerate FWM. In the case of scalar pump degenerate FWM, the analysis can be found in [87]. For the purpose of this thesis, it is sufficient to mention that similar equations as Eqs. (3.7), (3.8) can be used to calculate the output signal and idler fields[2]. In this case, we have $g = \sqrt{\gamma^2 P_{\mathrm{P}}^2 - (\kappa/2)^2}$ with $\kappa = \Delta\beta + 2\gamma P_{\mathrm{P}}$, and $\Delta\beta = \beta_{\mathrm{S}} + \beta_{\mathrm{I}} - 2\beta_{\mathrm{P}}$.

---

[2]In the case of scalar single pump FWM, the phase term in Eqs. (3.7), (3.8) can be found in [87].

Here, P_P denotes the pump power and β_P indicates the propagation constant of the pump. For the single pump case, the parameter ν can be calculated as

$$\nu = i\gamma(A_P^2(0)/g)\sinh(gL), \tag{3.11}$$

where $A_P(0)$ is the input pump.

The scalar signal-degenerate FWM can be calculated by replacing $A_I = A_S$ in Eq. (3.7) and not considering Eq. (3.8). In the vector FWM case, the signal-degenerate FWM can still be analyzed with the previous Eqs. (3.7), (3.8) since signal and idler are two cross-polarized waves.

3.2 Phase-Insensitive Amplification

When there is no input idler, the output signal and idler, Eqs. (3.7), (3.8), are independent of the phase relation of the input waves. The processor is then operating in the PI regime. The signal gain is in this case determined by

$$G = |\mu|^2 = 1 + \left(\frac{\epsilon\,\gamma P_{P1}P_{P2}}{g}\sinh(gL)\right)^2. \tag{3.12}$$

In this case, the idler is internally generated with a wavelength-conversion efficiency given by

$$|\nu|^2 = \left(\frac{\epsilon\,\gamma P_{P1}P_{P2}}{g}\sinh(gL)\right)^2. \tag{3.13}$$

Using Eq. (3.10) and assuming parametric gain, the phase of the generated idler, ϕ_I, is given by $\phi_I = \pi/2 + \phi_{P1} + \phi_{P2} - \phi_S$, where ϕ_{P1}, ϕ_{P2} and ϕ_S are the pump and signal phases respectively. As can be seen, the idler is a conjugated copy of the signal with an additional phase-shift when considering CW pumps. As will be discussed in Section 3.8.3, the creation of a phase conjugated copy of the signal can be exploited for dispersion compensation as well as mitigation of fiber nonlinearities in transmission links.

The maximum gain and conversion efficiency will occur when g is maximized, i.e., $\kappa = 0$. This condition is known as the phase-matching condition. It states that the parametric gain is maximized when the linear phase shift and nonlinear phase shift cancel out. We can also observe that phase-matching is obtained for both scalar and vector FWM with the same conditions. In other words, maximum parametric gain occurs for the same pump, signal and idler wavelength locations in both vector or scalar amplifiers. Assuming high gain, the gain when fulfilling phase-matching is given by

$$G = |\mu|^2 \approx \exp[2L\epsilon\gamma\sqrt{(P_{P1}P_{P2})}]/4. \tag{3.14}$$

The gain has an exponential dependence on the pump power, the fiber length and the fiber nonlinear coefficient. For this reason, we commonly refer to this case as the exponential gain regime. Equation (3.14) also states that the scalar scheme has twice the gain in dB than the vector scheme when assuming large gain and phase matching in both schemes. However, in the scalar case, only the signal component

parallel to the pump is amplified when assuming the Manakov model. In the vector scheme, both components are amplified. If the input signal is co-polarized to P_2, the same gain is easily obtained by exchanging the idler and signal in our previous analysis.

To study the gain bandwidth, we describe the linear phase mismatch [39, Ch. 10]

$$\Delta\beta = \beta_2 \left[(\omega_S - \omega_c)^2 - \omega_d^2 \right] + \frac{\beta_4}{6} \left[(\omega_S - \omega_c)^4 - \omega_d^4 \right], \qquad (3.15)$$

where β is expanded around the center frequency $\omega_c = \frac{\omega_{P1}+\omega_{P2}}{2}$ and we have defined $\omega_d = \frac{\omega_{P1}-\omega_{P2}}{2}$. The dispersion parameters beyond β_4 have been neglected. The third-order dispersion β_3 is considered but it does not affect $\Delta\beta$. If the pumps are far apart, the term given by ω_d in Eq. (3.15) dominates over a large bandwidth. We desire $\beta_2\omega_d^2 + \beta_4\omega_d^4/6 \approx \gamma(P_{P1} + P_{P2})$ to achieve phase-matching over the bandwidth in which $w_d^2 \gg (\omega_s - \omega_c)^2$. For this reason, dual-pump parametric amplifiers are often operated with two pumps far apart, but the center wavelength close to the ZDW, such that a flat gain spectrum is achieved over a large bandwidth. If the center wavelength is not close to the ZDW, the pump separation is limited by the value of β_2.

By noting that $\omega_d = 0$ and $\omega_c = \omega_P$ in the pump-degenerate scheme, we can realize that achieving flat and large bandwidth is not as simple as with dual-pump schemes. When neglecting β_4, a flat gain spectrum can be obtained by placing the pump at the ZDW, but the gain depends in this case quadratically on the pump power, fiber length and fiber nonlinearity [88]. The exponential gain regime can be achieved by placing the pump on the anomalous dispersion, but the exponential gain is only achieved for a certain signal-pump separation. If the signal is close to the pump, the gain has a quadratic dependence on the pump power. The exponential gain regime over a certain bandwidth can be achieved by placing the pump in the anomalous regime and having positive β_4, although such scheme is very sensitive to ZDW fluctuations [89, Ch. 5], which makes it challenging from an experimental perspective.

3.3 Scalar Phase-Sensitive Amplification

In the previous section, we have assumed that the idler wave is not present at the fiber input. When both the signal and the idler waves are present at the fiber input, the process is said to be PS since, as we can see from Eqs. (3.7), (3.8), the output signal and idler depends on the phase relation of the input waves. In this section, we introduce the four most common scalar PSA schemes. These scheme are shown in Fig. 3.1. When the signal and the idler are located at two different frequencies, Fig. 3.1 (top row), the amplifier is a two-mode amplifier. If the signal and the idler are located at the same frequency, Fig. 3.1 (bottom row), the amplifier is said to be an one-mode amplifier. The cases of scalar one-mode and two-mode PSAs will be considered separately below.

(a)

(b)

(c)

(d)
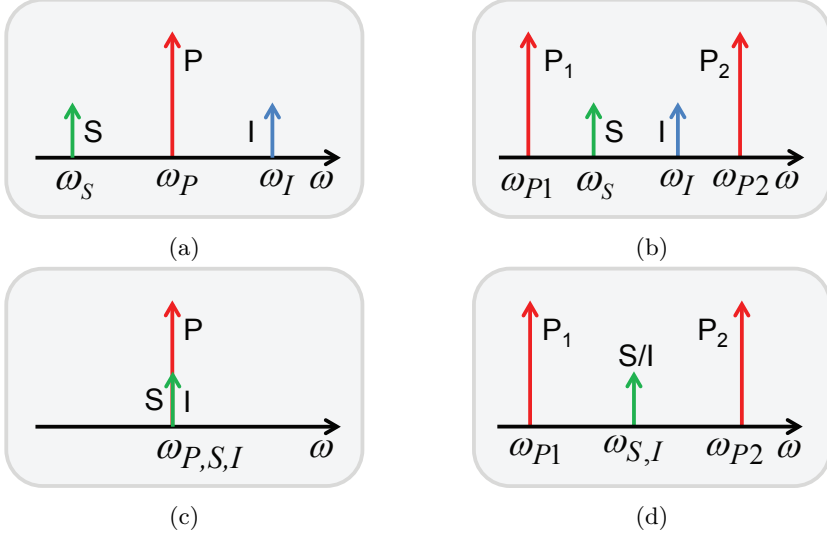
Fig. 3.1: Scalar PSA schemes based on (a) pump-degenerate FWM, (b) non-degenerate FWM, (c) fully-degenerate FWM and (b) signal-degenerate FWM.

3.3.1 Scalar Two-Mode Phase-Sensitive Amplification

The pump-degenerate, Fig. 3.1(a), and the non-degenerate, Fig. 3.1(b), PSAs are two-mode amplifiers since the interaction occurs between the signal and one idler which are located at different frequencies. In the pump-degenerate PSA, the signal, the idler and the pump frequencies are related by $2\omega_P = \omega_S + \omega_I$. In the non-degenerate PSA, we have $\omega_{P1} + \omega_{P2} = \omega_S + \omega_I$. The output signal, S_{out}, and idler, I_{out} are given by [90, 91]

$$\begin{bmatrix} S_{\text{out}} \\ I_{\text{out}}^* \end{bmatrix} = \begin{bmatrix} \mu & \nu \\ \nu^* & \mu^* \end{bmatrix} \begin{bmatrix} S_{\text{in}} \\ I_{\text{in}}^* \end{bmatrix}, \tag{3.16}$$

where S_{in} and I_{in} are the input signal and idler waves. The parameters μ and ν coefficients can be found from Eqs. (3.9), (3.10) by adapting the g and k for the cases of non-degenerate and degenerate pumps. In Eq. (3.16), we can observe that the process of a two-mode PSA can be described as the coherent superposition of two PI process, one with only the signal at the input and the other one with the only idler at the input. The signal gain can be expressed as

$$G = \frac{|S_{\text{out}}|^2}{|S_{\text{in}}|^2} = |\mu|^2 + |\nu|^2 + 2|\mu||\nu|\cos(\phi) \tag{3.17}$$

where $\phi = \phi_S + \phi_I + \phi_\mu - \phi_\nu$. We have have assumed that the input signal and the input idler powers are equal, which translates into maximum PS interaction between both waves in the limit of large gain[3].

The maximum gain is

$$G_{\text{max}} = \frac{|S_{\text{out}}|^2}{|S_{\text{in}}|^2} = |\mu|^2 + |\nu|^2 + 2|\mu||\nu| = (|\mu| + |\nu|)^2, \qquad (3.18)$$

which corresponds to an idler which is a conjugated copy of the signal and an additional phase shift, $\phi_I = -\phi_S - \phi_\mu + \phi_\nu$.

The minimum gain or maximum attenuation is

$$G_{\text{min}} = \frac{|S_{\text{out}}|^2}{|S_{\text{in}}|^2} = |\mu|^2 + |\nu|^2 - 2|\mu||\nu| = (|\mu| - |\nu|)^2, \qquad (3.19)$$

corresponding to an idler with phase $\phi_I = \pm\pi - \phi_S - \phi_\mu + \phi_\nu$. Obviously, $G_{\text{min}}G_{\text{max}} = 1$, which establishes that the maximum attenuation equals the maximum gain. We can also observe that the maximum gain corresponds to four times higher than the gain in PI mode, Eq. (3.12), when assuming the high-gain regime ($\mu \approx \nu$).

3.3.2   Scalar One-Mode Phase-Sensitive Amplification

The two most basic scalar one-mode PSA schemes are the fully-degenerate PSA and the signal-degenerate PSA. In the fully-degenerate PSA, Fig. 3.1(c), the pump, the signal and the idler are located at the same frequency. In order to differentiate the signal from the pump, this scheme is implemented in an interferometer structure, either a Mach-Zehnder interferometer [92] or a Sagnac loop [93]. In the signal-degenerate PSA, Fig. 3.1(d), the amplifier input waves are formed by the two pump waves, and the signal/idler wave. The frequencies of these waves are related by $2\omega_S = \omega_{P1} + \omega_{P2}$.

In one-mode PSAs, the input-output relation is given by [83, 92]

$$S_{\text{out}} = \mu S_{\text{in}} + \nu S_{\text{in}}^*, \qquad (3.20)$$

where S_{in}, and S_{out} are the input and output signals. The parameters μ and ν are different in each case but they fulfill $|\mu|^2 - |\nu|^2 = 1$ regardless of the scheme. In the case of fully degenerate PSA, their values can be found by analyzing the nonlinear phase-shift from SPM [94]. For the signal-degenerate PSA, we can calculate their values from Eqs. (3.9), (3.10). The signal gain can be expressed as

$$G = \frac{|S_{\text{out}}|^2}{|S_{\text{in}}|^2} = |\mu|^2 + |\nu|^2 + 2|\mu||\nu|\cos(\phi), \qquad (3.21)$$

with the relative phase defined as

$$\phi = 2\phi_S + \phi_\mu - \phi_\nu. \qquad (3.22)$$

---

[3]At low gain, the signal and idler power can be adjusted to achieve maximum PS interaction in either the signal or the idler wave.

(a)   (b)
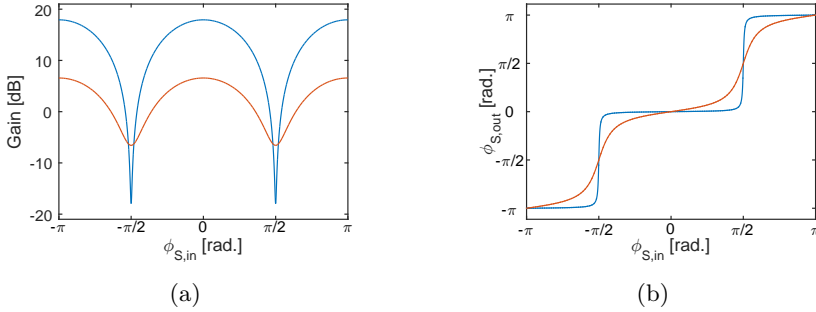
Fig. 3.2: a) Gain vs. signal phase, ϕ, when the maximum PS gain is 18 dB (blue), and 6.5 dB (red) for a one-mode PSA. b) Output signal phase vs. input signal phase for the same cases. The parameters μ and ν have been considered to take real values for simplicity.

Here, ϕ_S, ϕ_μ, and ϕ_ν denote the signal phase and the phases of the parameters μ and ν.

The gain dependence on the signal phase is shown in Fig. 3.2(a). The maximum gain is given by Eq. (3.18) and it corresponds to a signal with phase $\phi_S = \phi_\nu/2 - \phi_\mu/2$ or $\phi_S = \pi + \phi_\nu/2 - \phi_\mu/2$. The minimum gain, given by Eq. (3.19), is also the inverse of the maximum gain in this case.

As can been seen in Fig. 3.2(b), the output signal phase is squeezed at large gain. Phase squeezed output is achieve since, as can be seen from Eq. (3.21), one-mode PSAs amplify one signal quadrature whereas the other quadrature component is attenuated, which means that the output signal phase is squeezed. In addition, the quadrature that is amplified can be selected by controlling the pump phases, i.e. by varying the phase of the ν parameter. This effect has been utilized to achieve phase regeneration as will be discussed in Section 3.8.2.

Comparing the fully-degenerate PSA and the signal-degenerate PSA, the former one has several drawbacks. The gain dependence on the pump power is quadratic, contrary to all-other schemes here that under the phase-matched assumption have exponential dependence on the pump power and fiber length. The Mach-Zehnder interferometer is penalized by any mismatch between the two arms of the interferometer or between the couplers. The Sagnac loop nonlinear interferometer is degraded by guided acoustic-wave Brillouin scattering. Though 1.8 dB NF was demonstrated with such a PSA, it was measured at 16 GHz [93] and at lower frequencies the performance was degraded by guided acoustic-wave Brillouin scattering.

The main difference of two-mode amplifiers with respect to one-mode amplifiers is that the former one can PS amplify any signal regardless of the modulation format as long as the idler is a conjugated copy of the signal. In the degenerate case, only PAM signals can be amplified.
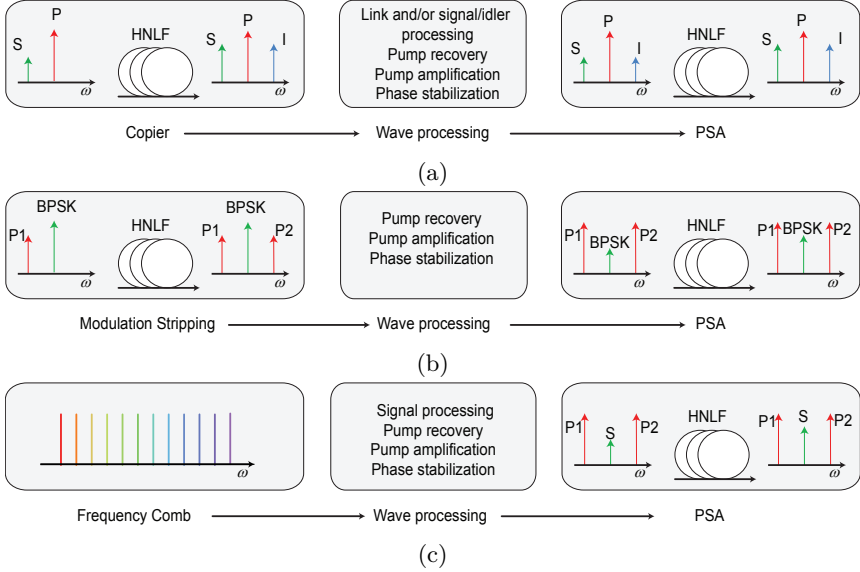
Fig. 3.3: Schematic of three different PS processor implementation. (a) Copier-PSA scheme (b) modulation stripping scheme and (c) comb-based scheme.

3.4 Implementations of Phase-Sensitive Processing

In all PS processor configurations, the input phase relation among all waves, pump(s), signal and idler, needs to be adjusted to obtain the desired output. Thus, pump, signal, and idler waves must be frequency and phase locked. In this section, we discuss three different methods for generation these four (or three) frequency and phase-locked waves.

3.4.1 Copier-PSA

The generation of four (or three) phase and frequency locked waves can be implemented using a parametric amplifier operating in PI mode [95, 96], the so-called copier-PSA scheme. The illustration for the copier-PSA scheme is shown in Fig. 3.3(a). The copier generates the idler as a conjugated copy of the signal located at frequency $\omega_{P1} + \omega_{P2} - \omega_s$. Then, at the copier output, signal, idler and pump(s) are frequency and phase locked. In Fig. 3.3, we show the copier-PSA implementation for a degenerate-pump case, but the scheme can also be used with non-degenerate schemes [96]. As will be discussed in Sections 3.5.2 and 3.6.1, the copier-PSA can also be implemented with polarization-diverse [97] and vector PSAs [98] in order to perform amplification of DP-modulated signals.

In between the copier and the PSA, the wave processing can vary depending with the application. The mid-stage consisting of a filter with programable phase-response

was used to characterize the PSA using CWs in [99]. The dynamic response of the PSA can be measured by phase modulating some of the waves. For example, in experiments characterizing the pump-degenerate scalar PSA the pump(s), the signal and the idler were divided into two branches and only the pump was phase modulated [100, 101]. Note that modulating the three waves simultaneously would give an invariant relative phase. An important drawback when any of the waves travels through a different path is the need for a PLL which compensates for environmental drifts. Using signals modulated with data, differential PSA-based receivers have been demonstrated using a dispersive element as the mid-stage [102, 103]. The idler is delayed by one symbol period with respect to the signal in the dispersive element and in the PSA demodulation is achieved by the superposition of the idler and the signal. The mid-stage can also consist of a fiber link [104, 105] such that the PSA is placed at the receiver end to exploit the low-noise amplification provided by the PSA. The copier-PSA scheme is the preferred option in transmission experiments since it is WDM-compatible and modulation format independent [20, 106].

3.4.2 Modulation Stripping

Modulation stripping has been proposed and demonstrated to operate as a pre-stage before the PSA [18, 107]. In its basic configuration, a CW and BPSK signal are combined in a parametric amplifier. The generated wave is located at the frequency $2\omega_s - \omega_{P1}$ and its phase is $\pi/2 + 2\phi_s - \phi_{P1}$. In other words, the second order harmonic of the BPSK signal has been generated. This harmonic corresponds to a CW since the binary phase modulation of the signal is erased. After the modulation stripping stage, this generated pump is often filtered and amplified by means of optical-injection locking (OIL). Both pumps are further amplified by an EDFA before being combined with the signal. As will be discussed in Section 3.8.2, this scheme is utilized for achieving signal regeneration. A similar scheme has also been demonstrated with DP-BPSK signals [108].

3.4.3 Frequency Combs

The use of frequency combs have also been successfully proven in order to generate the corresponding phase and frequency locked waves before the PSA. In this case, by selecting four (three) carriers from a comb source we already have three frequency and phase-locked carriers. Thus, by using frequency comb sources, there is no need for a PI parametric processor before the PSA. The use of electro-optic combs is of special interest when characterizing the PSA NF [109] since no excess noise is added to the signal and idler as in the copier approach. However, when requiring data-modulated signal and idler, with the idler being a conjugated copier of the signal, this scheme requires independent modulation of the signal and idler. For applications such as quadrature demultiplexing [110], [Paper E, F], frequency combs have also been used since a scheme for achieving black-box quadrature demultiplexing without pilot tones is challenging.
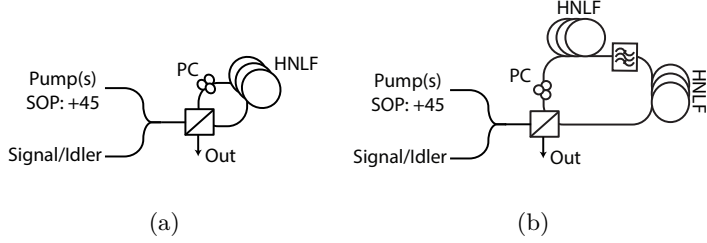
Fig. 3.4: Polarization-diversity FOPAs implemented in a loop with (a) one nonlinear medium (b) two nonlinear media and filter removing the pumps.

3.5 Polarization-Diverse Phase-Sensitive Amplification

When using scalar PSAs, the use of a polarization-diverse scheme, a separate PSA for each signal and idler polarization, is necessary when aiming amplification and processing of data encoded in both polarizations, which is becoming ubiquitous in optical networks. In this section, we thus discuss the use of polarization diverse PSAs, their possible implementation schemes and the conditions for achieving PS amplification of DP-modulated signals. We also describe the use of polarization-diverse schemes for achieving PS processing without the need for large gain.

3.5.1 Implementations

In scalar PSAs, only the signal component on the pump polarization is amplified and polarization diversity is then needed to amplify both polarizations. Such a polarization-diverse PSA [97, 111] is usually implemented in a loop similar to polarization-diverse PI-FOPAs [112–115]. In Fig. 3.4, two possible implementations of polarization-diverse FOPAs are shown. The pumps, or pump in case of pump degenerate FWM, polarization is aligned such that their power is equally divided after the polarization-beam splitter (PBS), e.g. linear polarized at 45°. In the case of signal-degenerate FWM, the input waves are the pumps and the signal. In this scheme, a polarization controller (PC) is used to direct the output to the other port by making the clockwise and counterclockwise waves cross-polarized within the loop. Another option would be directing the waves to the same port as the input port and the use of a circulator to separate the input and output waves, as performed in [Paper F]. By using a loop, both signal components are combined coherently after being amplified as shown in Fig. 3.4(a). When using the loop implementation, the same nonlinear medium can be used to amplify both signal components. However, degradation of the amplifier performance has already been reported in bidirectional PI-FOPAs [115, 116], caused by Rayleigh and Brillouin scattering. This degradation is expected to be detrimental when requiring low-noise PS amplification. It can be mitigated by implementing a loop with two different nonlinear media, as shown in Fig. 3.4(b). A similar scheme has already been experimentally demonstrated using $\chi^{(2)}$-material-based PSAs [97]. In PI amplification, this scheme has also been demon-

strated using HNLFs [117]. As can be seen, the pumps are attenuated by e.g. an optical filter in between the two FOPAs. Then, the amplification of each polarization component occurs in each HNLF.

3.5.2 Polarization-Diverse Two-Mode Phase-Sensitive Amplification

When implementing a polarization-diversity scheme, the output signal and idler (non-degenerate signal) are determined by [118],[Paper C]

$$J_{\text{S,out}} = \mu J_{\text{S,in}} + \nu A J_{\text{I,in}}^{*}, \tag{3.23}$$

$$J_{\text{I,out}} = \mu J_{\text{S,in}} + \nu A J_{\text{S,in}}^{*}, \tag{3.24}$$

where J_{S} and J_{I} correspond to the signal and the idler Jones vectors. The operator * denotes conjugation in each vector component. The coefficients μ and ν were defined in Eqs. (3.9), (3.10) for the non-degenerate and the pump-degenerate FOPAs. Here, the matrix

$$A = \begin{bmatrix} 1 & 0 \\ 0 & \exp(i2\psi) \end{bmatrix} \tag{3.25}$$

models the case of different pump phases in the anticlockwise and clockwise direction [Paper C]. Since the phase of the ν parameter depends on the phase of the pumps, we can use a common ν parameter by making use of the matrix A. The parameter ψ is the relative phase between the pumps in each direction. For example, the pumps could be right circularly polarized ($\psi = \pi/2$) before the PBS since the only condition is that equal power travels in each direction. In some experiments, the pumps are combined with the signal after the PBS, which can also be modeled by the matrix A. We have also assumed that the FOPAs in each direction perform equally. Neglecting fiber attenuation, the same PI gain is achieved by using the same HNLF in bidirectional implementation [119] when clockwise and anticlockwise propagating waves are aligned to be co-polarized or we assume a fiber with similar fiber properties in both polarization modes. The matrix A can model the difference in the phase of the ν parameter in each direction caused by different dispersion properties along the fiber. When using two nonlinear media, the gain must be equalized for both FOPAs, which can be challenging in the case of broadband amplification since it requires identical HNLFs.

Maximum PS gain occurs when the $\mu J_{\text{S,in}}$ and $\nu A J_{\text{I,in}}^{*}$ are aligned, i.e.

$$\mu J_{\text{S,in}} = k \nu A J_{\text{I,in}}^{*}, \tag{3.26}$$

with k being a positive scalar constant. In this case, the maximum PS gain is four times larger than the PI (no input idler) gain as in any PSA when assuming large gain ($\mu \approx \nu$) and equal input signal and idler powers, i.e. $k \approx 1$. Additionally, when having maximum PS interaction, the output signal SOP is the same as in the case of no input idler. In [Paper C], we have shown that the relation in Eq. (3.26) between the signal and idler SOPs to achieve maximum PS amplification can be described by the means of a mirror plane when using Stokes vectors. The idler needs to be mirrored around the planed normal to the vector $S_{\text{mirror}} = [0 \ -\sin(\psi) \ \cos(\psi)]^{T}$. In

the case of $\psi = 0$, this plane corresponds to $S_3 = 0$, and maximum gain can then be obtained for e.g. when the signal and the idler are both co-polarized with linear polarization or both waves are cross-polarized with circular SOPs.

An idler which fulfills the conditions to achieve maximum amplification can be generated by a polarization-diverse PI-FOPA, without any constraint on the input signal to the copier. In fact, the condition for obtaining maximum PS amplification is the same as the output signal and idler relation in a PI polarization-diverse amplifier. Thus, PS amplification of DP-modulated signals can be achieved by the means of a copier-PSA when both are implemented with polarization diversity. However, the implementation of the copier-PSA with polarization-diversity will be affected by any absolute change of polarization in either the signal, the idler or both during the mid-stage. In other words, any rotation on the signal and the idler SOPs will affect the performance of the scheme [118], [Paper C].

Another interesting case is when the input signal and idler SOPs fulfill

$$J_{S,in}^{H} A J_{I,in}^{*} = 0. \tag{3.27}$$

Here, the operator ^{H} denotes conjugate transpose. This case corresponds to an input idler SOP orthogonal to the state of maximum PS interaction. It can be shown than in this case, the output signal and the idler powers are independent of the input phase relation. However, the output signal and the idler SOPs depend on their input phase relation. This phase to polarization dependance could be exploited by using a polarizer, similarly to the polarization-assisted PS processor explained in the next section.

3.5.3 Polarization-Diverse One-Mode Phase-Sensitive Amplification

The signal-degenerate case can be analyzed by substituting $J_{I,in}$ by $J_{S,in}$ in Eq. (3.23) which gives

$$J_{S,out} = \mu J_{S,in} + \nu A J_{S,in}^{*}. \tag{3.28}$$

Using the signal definition introduced in Appendix A, the gain can be described by

$$G = \frac{|J_{S,out}|^2}{|J_{S,in}|^2} = |\mu|^2 + |\nu|^2 + 2|\mu||\nu|\sin(\alpha)\cos(\phi), \tag{3.29}$$

where α is polarization angle in Stokes space between the signal and the axis $S_{mirror} = [0 \ -\sin(\psi) \ \cos(\psi)]^T$, which is the vector normal to the mirror plane in the case of polarization-diverse two-mode PSA. The parameter ϕ is related to the input phase relation between the pumps and the signal, similar to the case of scalar PSAs, Eq. (3.22).

When the input signal SOP is normal to the mirror plane (defined as in the case of non-degenerate polarization-diverse PSA), the output signal power does not depend on the input signal phase. In this case, the input signal can be expressed as

$$J_{S,in} = \frac{S'_{in}}{\sqrt{2}} \begin{bmatrix} 1 \\ i\exp(i\psi) \end{bmatrix}, \tag{3.30}$$
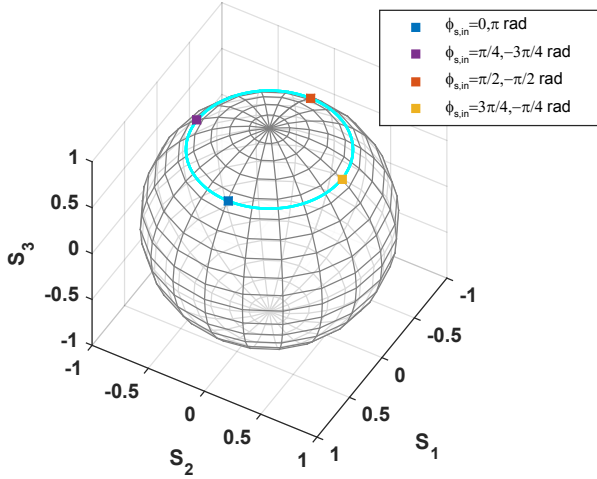
Fig. 3.5: Output signal SOP in a polarization-diverse PSA when the input signal SOP is circular and $\psi = 0$, based on Eq. (3.31). The output signal SOP (cyan line) vs. input signal phase forms a circle on the Poincaré sphere. For simplicity, μ and ν are assumed to have the same phase, and $|\mu|^2 = 1.1528$.

where S'_{in} represents an scalar field. The output signal is then

$$
\begin{aligned}
J_{\text{S,out}} = & \frac{1}{\sqrt{2}} \, \mathfrak{Re}[S'_{\text{in}}]((\mu + \nu)\hat{x} + i \exp(i\psi)(\mu - \nu)\hat{y}) \\
& + \frac{i}{\sqrt{2}} \, \mathfrak{Im}[S'_{\text{in}}]((\mu - \nu)\hat{x} + i \exp(i\psi)(\mu + \nu)\hat{y}),
\end{aligned}
\tag{3.31}
$$

where $\mathfrak{Re}$ and $\mathfrak{Im}$ stand for the real and imaginary operators.

Thus, the output signal can be expressed as the combination of the input real and imaginary component on two different polarizations. The polarization dependence on the input phase relation is the effect exploited in the polarization-assisted PS processor [Paper F]. As shown in Fig. 3.5, the signal output SOP forms a circle on the Poincaré sphere when the input signal phase is varied. This circle approximate the $S_3 = 0$ plane at high gain ($\psi = 0$), and the point $S_3 = 1$ at low gain. By placing a polarizer that blocks the imaginary (real) component, the output signal is proportional to the real (imaginary) part of the input signal, resembling the effect of a large gain degenerate PSA showed in Fig. 3.2. In this case, there is not any constrain on the gain or conversion efficiency. However, the power of the signal after the polarizer depends on the conversion efficiency. It can be shown that at low conversion efficiency ($|\mu| \approx 1$, $|\nu| \ll 1$), the power of the signal after a polarizer obtaining the in-phase component is about $4|\nu|^2$ times the power corresponding to the input in-phase component. Thus, the loss and consequently signal-to-noise ratio (SNR) degradation that the signal suffers should be taken into account.
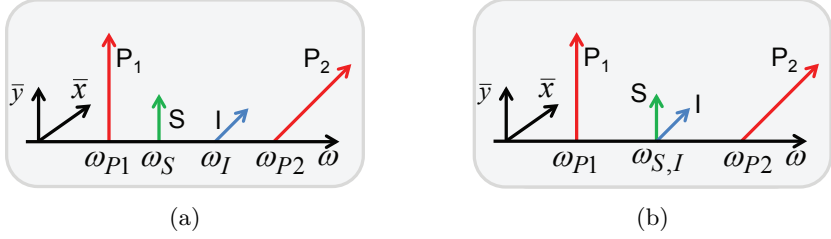
Fig. 3.6: Vector PSA schemes based on (a) non-degenerate FWM and (b) signal-degenerate FWM

Looking at Eq. (3.28) and assuming $\psi = 0$, we can observe that maximum PS amplification occurs for any input signal which is linearly polarized for the same relation, which agrees with Eq. (3.29). If we have a DP-PAM signal with linearly polarized data channels, i.e. $S_{\mathrm{PAM}} = \exp(i\phi_{\mathrm{s}})(D_1[\cos(\theta)\sin(\theta)]^T + D_2[\sin(\theta)\cos(\theta)]^T)$, where θ defines the linear SOP of the data channels, ϕ_{s} is the signal phase and $D_{1,2}$ are real value since it is a PAM signal; it is simple to observe that maximum PS amplification will occur regardless the value of θ when assuming $\psi = 0$. Therefore, amplification of DP-PAM signals can be achieved in a polarization-diverse PSA. However, the scheme is polarization dependent [118], [Paper C]. To simplify the analysis we have assumed $\psi = 0$, but a more complete analysis of the requirements on the polarization for PS amplification of DP-PAM signals with this scheme can be found in [Paper C].

3.6 Vector Phase-Sensitive Amplification

In this section, we discuss PS processing using vector amplifiers, i.e. having two cross-polarized pumps. The two most basic schemes are the signal-degenerate vector PSA and the non-degenerate vector PSA, shown in Fig. 3.6. As in vector PI-FOPAs, two orthogonal pumps are required and it is not possible to achieve vector PSA with a single-mode pump. It is worth realizing that we show the pump with linear SOPs, but this is not a requirement of vector schemes, when assuming the Manakov model.

3.6.1 Non-Degenerate Vector Phase-Sensitive Amplification

Taking into account Eqs. (3.7), (3.8) and assuming that the same power in each pump, when having a non-degenerate vector PSA, the output signal, $J_{\mathrm{S,out}}$, and the output idler $J_{\mathrm{I,out}}$ are given by

$$J_{\mathrm{S,out}} = \mu J_{\mathrm{S,in}} + \nu B J_{\mathrm{I,in}}^* \tag{3.32}$$

$$J_{\mathrm{I,out}} = \mu I_{\mathrm{in}} + \nu B J_{\mathrm{S,in}}^*, \tag{3.33}$$

where $J_{\mathrm{S,in}}$ and $J_{\mathrm{I,in}}$ are the input signal and idler Jones vectors, $B = J_{\mathrm{P1}}J_{\mathrm{P2}}^T + J_{\mathrm{P2}}J_{\mathrm{P1}}^T$, with $J_{\mathrm{P1,2}}$ being the unit vectors which determine the pump SOPs. The coefficients μ and ν have been defined in Eqs. (3.9), (3.10). The definition of the

phase of the ν parameter must be done accordingly with the definition of B. Though we have mainly limited the description of vector amplifiers to the case of random birefringent fibers, these equations are also valid for the case of an isotropic fiber with linearly cross-polarized pumps or circularly polarized fibers [118]. This model is also valid for the case of a strong birefringent, PMF, fiber with two-cross polarized pumps [120]. In these cases, the parameters μ and ν will take different value while still maintaining the relation $|\mu|^2 - |\nu|^2 = 1$.

Similar to the polarization-diverse case, maximum PS gain occurs when μS_{in} and $\nu B I_{\text{in}}^*$ are aligned. Assuming $\mu, \nu \gg 1$, the maximum PS gain is four times larger than when there is not input idler or PI gain. In [Paper C] we have shown that the signal input Stokes vector needs should be mirrored in the plane normal to the pump SOPs to achieve maximum PS amplification. Thus, the gain of the amplifier is determined by the relative polarization between signal and idler as well as the absolute polarization. In the same way as in the polarization-diverse two-mode PSA, an idler fulfilling those conditions can be created by a vector PI-FOPA regardless the signal input polarization and phase. This would lead to a scheme capable of PS amplification of DP-modulated signals. However, such a scheme requires control of the relative signal and idler SOPs with regard to the pump SOPs between the copier and the PSA.

The output power will be independent of the input phase relation, when the input idler is orthogonally polarized to the case of maximum gain,

$$J_{\text{S,in}}^H B J_{\text{I,in}}^* = 0. \tag{3.34}$$

In this case, the output polarization depends on the input phase relation between pump, signal and idler.

Comparing with the polarization-diverse PSA, both schemes provide the same gain for the same pump powers assuming phase-matching in both cases. Two scalar PI-FOPAs sharing pump power (as in the case of polarization diversity) have the same gain as a single vector PI-FOPA using all the pump power when assuming exponential gain regime.

3.6.2 Degenerate Vector Phase-Sensitive Amplification

In the case of degenerate vector PSAs, the output signal Jones vector, S_{out} is given by

$$J_{\text{S,out}} = \mu J_{\text{S,in}} + \nu B J_{\text{S,in}}^*, \tag{3.35}$$

where $J_{\text{S,in}}$ is the input signal. The matrix B has been defined for the case of non-degenerate vector PSA.

Similar to the polarization-diverse one mode PSA, we can gain much insight by describing the gain as the function of the input phase relation and input signal polarization. Using the signal definition presented in Appendix A, the gain is given by

$$G = \frac{|J_{\text{S,out}}|^2}{|J_{\text{S,in}}|^2} =$$
$$|\mu|^2 + |\nu|^2 + 2|\mu||\nu|[\sin(\alpha)\cos(\phi)]. \tag{3.36}$$

where α is the polarization angle (Stokes space) among the signal and the pumps, and ϕ denotes the phase relation as presented in Eq. (3.22). This equation has been validated experimentally in [Paper A].

When the signal is co-polarized with either of the pumps, $\alpha = 0, 180°$, the output signal power does not depend on the phase relation. A conjugated copy of the signal is generated in the orthogonal polarization. The generation of such shift-free phase conjugated copy can be very interesting for dispersion compensation [121] and mitigation of fiber nonlinearities. In this case of PI signal output power, the output signal can be expressed

$$S_{\text{out}} = \mathfrak{Re}[S'_{\text{in}}](\mu J_{\text{P1}} + \nu J_{\text{P2}}) + i \, \mathfrak{Im}[S'_{\text{in}}](\mu J_{\text{P1}} - \nu J_{\text{P2}}), \qquad (3.37)$$

where we have defined the input signal as $J_{\text{S,in}} = S'_{\text{in}} J_{\text{P1}}$, with S'_{in} being a scalar value. The output signal is then given as the summation of the input real and imaginary components on two different polarizations. These two different polarizations are only orthogonal in the case of high gain. The fact that the output polarization depends on the input phase relation can be utilized to achieve a signal squeezed in phase by adding a polarizer after the parametric amplifier. This scheme is the polarization-assisted PS processor with a vector implementation [110, 122]. The polarizer should be aligned such that it blocks the imaginary part of the signal, and therefore the output after the polarizer is proportional to the input inphase component of the signal. Similar to the polarization-assisted PS processor with polarization-diverse implementation, this scheme can ideally operate at any nonlinear phase shift at the expense of signal SNR degradation. Using the Poincaré sphere representation, the output signal SOP forms a circle when its input phase is varied as shown in Fig. 3.7.

Since this scheme can be described by scalar equations in which the signal and the idler are the signal components on each pump polarization [83], we can easily realize that maximum PS interaction corresponds to the case of the degenerate wave SOP lying in the plane normal to pump SOPs, since this conditions is equivalent to have similar signal and idler input power. Moreover, the signal components on the pump SOPs need to be conjugated copies of each other, as in a general PSA. For instance, if the signal components on the P_1 polarization is a QPSK signal, the signal component on the on the P_2 polarization component should be its conjugated copy. Such pair of conjugated and cross-polarized waves at the same wavelength can be achieved by means of a degenerate vector FOPA operating in PI mode. A copier is not required to generate such a pair of waves since any pair of two data signals which are cross-polarized and conjugated can be defined as a DP-PAM signal.

3.7 Noise in Phase-Sensitive Amplification

In our previous analysis, we have neglected the noise generated during the amplification process. The main contribution of noise in a parametric amplifier is the amplified quantum noise [82, 123]. In a semi-classical analysis, we can calculate the output of a two-mode scalar parametric amplifier as [124]

$$\begin{bmatrix} S_{\text{out}} \\ I^*_{\text{out}} \end{bmatrix} = \begin{bmatrix} \mu & \nu \\ \nu^* & \mu^* \end{bmatrix} \begin{bmatrix} S_{\text{in}} + n_{\text{S}} \\ I^*_{\text{in}} + n^*_{\text{I}} \end{bmatrix}, \qquad (3.38)$$
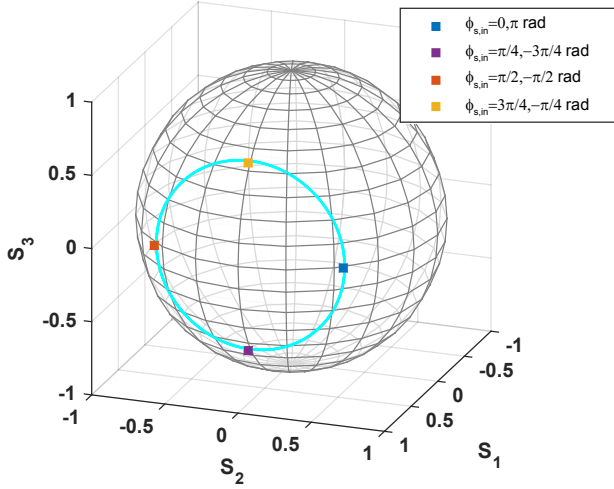
Fig. 3.7: Output signal SOP in a vector amplifier when the input signal SOP is aligned to $P1$, and the S_1 axis. The output signal SOP (cyan line) vs. input signal phase forms a circle on the Poincaré sphere. For simplicity, μ and ν are assumed to have the same phase, and $|\mu|^2 = 1.1528$.

where n_s and n_i represent the vacuum noise. They can be modeled as complex Gaussian distributions with $< n_{S,I} >= 0$, $< n_{S,I}^2 >= 0$ and $< |n_{S,I}|^2 >= h f_{S,I}/2$ where h is the Planck constant and f the optical frequency. Equation (3.38) is valid for both the non-degenerate and the pump-degenerate scalar PSAs.

In PI operation, assuming high gain and shot-noise limited input signal, the quantum-noise limited NF of a PI-FOPA is 3 dB [123]. Furthermore, the idler output noise is practically equal to the conjugated signal noise. From this fact, we know that detecting both signal and idler directly after the amplifier does not improve the SNR unless the detector is limited by thermal noise. We can also deduce that the quantum-limited NF of the wavelength conversion process is 3 dB.

When both the signal and the idler waves are present at the input, we can also observe that the output noise does not vary. If the PSA is operating so that maximum gain is obtained and assuming large gain, the output signal and idler powers are 6 dB higher than in the PI case, whereas the noise powers are the same. Therefore, the signal NF is -3 dB, 6 dB lower than the quantum-limited NF of a PI-FOPA. For the same reason, the quantum-limited idler NF is also -3 dB. The NF of the amplifier needs to take into account that both waves are present at the input, and it has been shown that it can be calculated as the sum of the idler and the signal NFs [20, 125]. Therefore, the quantum limited NF of PSAs is 0 dB which means that SNR is not degraded by the amplifier when assuming a shot-noise limited input. A similar reasoning can be done for the NF of both polarization-diverse and vector PSAs, in which the maximum PS gain is 6 dB larger than their counterpart PI amplifier.

The previous analysis regarding NF is valid for both scalar and vector PSAs as long as they can be defined as two-mode amplifiers. It has also been demonstrated that signal-degenerate PSAs also have a quantum-limited NF of 0 dB [126]. The unique property of performing amplification without degrading the SNR is only possible in PSAs, i.e., amplifiers in which the gain depends on the phase of the input waves [127].

Here, it is important to realize that the NF is defined for a quantum-noise limited input, and therefore signal and idler noises are not correlated. If the idler is generated by the copier with high gain, directly after the copier the signal and idler noises are correlated. For that reason, a lossy element in between the copier and the PSA is necessary in order to decorralate the signal and the idler noises and benefit from the low NF of PSAs.

In the case of 4-mode PSAs, the quantum-limited NF is also 0 dB when four modes are present at the input. If in a 4-mode PSA, only two modes are present at the input, the NF will be degraded in accordance with the strength of the modes which are not present at the input [84, 90]. For this reason, dual-pump parametric amplifiers are commonly designed such that only one idler is strong, so that the signal NF is not degraded.

Apart from amplified quantum noise, there are different noise contributions which degrade the performance of parametric amplifiers. These contributions are mainly the pump-transferred noise (PTN) [123] and Raman scattering [81]. PTN has its origin in the pump-power fluctuations. Since pumps are amplified by EDFAs before being launched into the HNLF, the launched pumps have in-band amplified spontaneous emission (ASE) noise which cannot be filtered and cause power fluctuations. Since the gain depends on the pump powers, these power fluctuations are transferred as in-band noise to the signal and idlers. The performance degradation due to PTN has been analyzed both in PI-FOPAs [82, 123] and in PS-FOPAs [109]. Spontaneous Raman scattering also degrades the NF of FOPAs [81, 82]. Raman-induced NF degradation impose an ultimate limit in order to experimentally achieve quantum-limited NF. For instance, it imposes a limit of 0.4 dB NF on the scalar pump-degenerate PSA [81]. However, despite the additional NF degradation effects, NF as low as 1.1 dB have been demonstrated in pump-degenerate PSA [20].

3.8 Applications

In this section, we discuss several applications of parametric processing.

3.8.1 Low-Noise Amplification

The capability of low-noise amplification makes PS-FOPA very promising as inline amplifiers and preamplifiers. In the back-to-back case or single-span links, 6 dB better sensitivity (3 dB when accounting for signal and idler power) is expected when using a PSA-base preamplifier compared to a PIA-based preamplifier due to the difference in the quantum-limited NF. This better sensitivity has been demonstrated using the copier-PSA scheme, with the copier at the transmitter and the PSA at

the receiver in both back-to-back [128] and transmission implementations [104, 105]. In the latter case, the pump is attenuated before the link to avoid nonlinear effects within the link. At the receiver end, the pump is separated from the signal and idler. At the PSA end, the pump needs to be recovered with fidelity such that PTN does not degrade the NF. In order to achieve such a pump recovery, the use of an OIL scheme has been proposed and demonstrated successfully [129]. In multi-span links, a scheme using the copier-PSA provides four times larger transmission distance (6 dB link NF improvement) when transmitting in the linear regime [91]. The 6 dB NF improvement comes from the 3 dB NF improvement of the PSA and from the fact that idler is considered as an internal mode. Such increase in transmission distance has experimentally been demonstrated in multi-span transmission with in-line PS amplification [130]. In all these demonstrations of PSA-amplified links, the PSA configuration was the scalar pump-degenerate PSA which simplifies the pump recovery. The use of two-mode PSA in combination with the copier-PSA scheme translates into a scheme that is modulation format independent and WDM compatible [20, 106]. For instance, demonstrations have been performed with QPSK [131] and 16-QAM [105] signals. Low-noise PS amplification of WDM signals has been demonstrated in a back-to-back scenario [128]. Using PPLN as nonlinear medium, PS amplification of three WDM DP-QPSK signals after 80 km link has also been demonstrated though low-noise amplification was not demonstrated [132].

3.8.2 Phase Squeezing and Regeneration

PSAs have attracted much attention not only due to their low-noise amplification capabilities but also because the output phase is squeezed. Using the signal-degenerate scalar scheme, the output phase is squeezed to the real axis by adjusting the pump phases. When operating in the linear regime, phase noise is converted into amplitude noise. If PSAs are operated in saturation, both amplitude and phase noise can be regenerated. Therefore, the scheme is suitable in order to achieve simultaneous phase and amplitude regeneration of BPSK signals [18]. A requirement in order to have such a scheme is the presence of two pumps located symmetrically around the signal. Furthermore, the generation of these pumps must ideally be performed in a black-box implementation, meaning that the input consists of only the modulated signal. In order to achieve such a black-box implementation, modulation stripping and the use of an OIL laser has been proposed and successfully demonstrated [18, 107, 133, 134]. Modulation stripping is achieved by combining a pump wave with the signal and mixing in a parametric amplifier as shown in Fig. 3.3(b). In order to simultaneously amplify and filter the second-harmonic of the signal, an injection-locked laser is used. The use of Brillouin for amplifying the second pump has been recently demonstrated [76], which avoids the need for an active PLL. After this process, the two pumps (symmetrically located around the signal) and the signal are input into the degenerate-signal PSA. After the PSA, the signal phase and amplitude are regenerated when operating in saturation.

The concept has also been extended to perform regeneration of general phase-shift keying (PSK) signals [19, 135]. In order to regenerate an M-PSK signal, the signal must be coherently added with its (M-1)$^{\text{th}}$ conjugated harmonic. The black-

box regenerator consists of two stages, a first PI stage in which the (M-1)th and the Mth harmonics are generated by cascaded FWM. Note that modulation stripping is achieved in the Mth conjugated harmonic. In second stage, the harmonic wave and the signal are combined by means of a non-degenerate scalar PSA. It has also been demonstrated that the presence of (M-1)th conjugated harmonic wave at the input of the second stage is not necessary because it is internally generated as the PSA is operated in saturation [136]. Moreover, operation in saturation also provides amplitude regeneration.

Beyond M-PSK signals, experimental demonstrations of regenerating M-QAM signals still remain challenging. Phase regeneration of an 8-QAM signal has been demonstrated but the modulation format was limited to a star 8-QAM [137]. Regeneration of 16-QAM signals can be achieved by the regeneration of inner and outer QPSK signals into which the 16-QAM signal can be divided [138]. Numerically, it has also been demonstrated that the use of quadrature decomposition followed by a two-level amplitude regeneration can be used to regenerate a 16-QAM signal [139]. This scheme is quite promising since quadrature demultiplexing of 16-QAM signal has experimentally been demonstrated [Paper F] and 2-level amplitude regenerator [140] as well. Another method for regeneration of M-QAM signals is the regenerative Fourier transform [141]. However, many practical challenges need to be overcome to implement this scheme.

Recently, regeneration of 16 ×BPSK WDM channels has been accomplished by using WDM to optical-time domain multiplexing conversion, phase regenerating the optical-time domain multiplexing signal, and converting the regenerated signal to a WDM signal again [142]. Regarding DP-modulated signals, the use of polarization diverse PSAs has been demonstrated for regeneration of DP-BPSK signals [143], and DP-QPSK [108]. Using a degenerate vector amplifier, phase-regeneration of DP-BPSK has also been demonstrated [Paper B]. In the vector amplifier, operation in saturation will lead to crosstalk between the polarization channels. This would not be the case with a polarization-diverse scheme if each polarization channel is inputted into each PSA.

3.8.3 Mitigation of Fiber Nonlinearities

Parametric processing can be utilized for mitigating the effects of fiber nonlinearities during transmission. Two different techniques have been demonstrated in which parametric processing can be utilized to achieve mitigation of fiber nonlinearities. The most common one is mid-span spectral inversion or optical phase conjugation. This technique consists of creating a conjugated copy of the signal at the middle point of the transmission link. It can easily be shown that by transmitting the conjugated copy of the signal in the second part of the span, dispersion and fiber nonlinearities can be compensated when assuming a symmetric power map and neglecting PMD and even terms of the dispersion [144]. However, there are different challenges for an ideal compensation. One challenge is that the power map is not ideally symmetric unless Raman amplification is used. Second, often the generated idler is shifted to another frequency and therefore cancellation of nonlinearities and dispersion is impaired. PMD can also limit the performance of this scheme.

Mid-span spectral inversion has been investigated for decades [11–13]. Due to the use of advanced modulation formats enabled by digital coherent receivers, research on mid-span spectral efficiency has gained attention in recent years. These modulation formats are less tolerant towards noise, making mitigation of fiber nonlinearities necessary for transmitting over long distance. However, the use of advanced modulation formats imposes higher demands on the phase-conjugation process, since they require optical phase conjugators which do not degrade the signal phase.

Recently, it has been shown that implementing several phase conjugators along the link can further improve the mitigation of fiber nonlinearities [145]. This technique requires Raman amplification, but by implementing several phase conjugators the tolerance towards signal to noise interaction [146] and PMD [147] can be improved. A challenge which has been overcome recently is the spectral utilization. By implementing either two polarization-diverse PI parametric amplifiers [148, 149] or two vector parametric amplifiers [150, 151], [Paper D], it has been shown that the full spectrum can be conjugated even when using DP-modulated signals.

The second method for mitigation of fiber nonlinearities consist of transmitting two conjugated copies through the link with coherent superposition in a PSA [105]. Known as the twin-wave method, this method does not require a PSA and coherent superposition can be performed in DSP as originally suggested [152]. In both cases, the power and dispersion maps are important for achieving optimum mitigation. In the case of symmetric power map and anti-symmetric dispersion map, these two conjugated copies will experience autocorrelated distortions. Using perturbation analysis, the signal and idler fields after the link, S_{L} and I_{L}, can be expressed as [152]

$$S_{\mathrm{L}} = S_0 + \delta E \tag{3.39}$$

$$I_{\mathrm{L}} = I_0 - \delta E^* \tag{3.40}$$

where symmetric power map and antisymmetric dispersion map with respect to the half of the link is considered. Here, we have used the notation S and I to denote the signal and conjugated copy (idler). The subscripts $0, \mathrm{L}$ indicate the fiber input and end points. The distortions introduced by the nonlinearities during transmission denoted by δE. It is clear from Eqs. (3.39), (3.40) and the input-output relations, Eq. (3.16), that PSAs cancel the distortions due to fiber nonlinearities when assuming large gain in the PSA. Numerically, it has been shown that using an ideal flat dispersion map, the use of PSA after each span can efficiently mitigate fiber nonlinearities for WDM signals [153].

3.8.4 Modulation Format Conversion

The utilization of parametric processing for data demultiplexing has been studied for several years. The first experiments made use of phase erasure to achieve conversion from QPSK to BPSK and 8-PSK to either QPSK [154]. Phase erasure is however limited to M-PSK signals and does not allow the extraction of all bit streams. Another option for achieving data demultiplexing is quadrature decomposition, in which the inphase and quadrature components of an incoming signal are demultiplexed. Quadrature demultiplexing cannot be achieved by the means of passive optics and it requires a nonlinear operation [155, 156]. There have been many

schemes proposed for performing quadrature demultiplexing. One scheme requires four phase-locked pump and in the incoming signal into a nonlinear medium [22, 24]. Another option is utilizing the phase squeezing properties of degenerate PSAs [25]. In this case, only two phase-locked pumps are required but two PSAs are required for demultiplexing both quadrature components. The input and the output signals are located at the same wavelength which is usually desired. Quadrature demultiplexing has also been demonstrated by using polarization-assisted PS processors [110, 157], [Paper E, F]. Using the vector implementation described in Section 3.6.2, both quadrature components can be obtained by operating in the high gain regime and using a PBS [Paper E], since the polarization components with the information of the input in-phase and quadrature signal components in Eq. (3.37) become orthogonal when $|\mu| \approx |\nu|$. When operating in the low gain regime, the use of two polarizers would be necessary to obtain both quadratures. The use of polarization-assisted PS processing with polarization-diverse implementation (described in Section 3.5.3) has also been demonstrated [Paper F], when operating with low nonlinear phase shifts. Operating a polarization-assisted PS with large nonlinear phase shift would be equivalent to having two independent PSAs. However, by making use of the polarization-assisted implementation, the requirements for a high nonlinear phase-shift can be reduced. Moreover, the scheme could be implemented in any integrated nonlinear-optical waveguide without any constraints on the polarization properties of the waveguide.

Although in this thesis we have focused on data demultiplexing by quadrature decomposition, parametric processing can also be utilized to multiplex or two independent streams of data into a single one. For example, combining two BPSK into a QPSK signal [158] and three QPSK signals into a 64-QAM signal [159] have been demonstrated.

3.9 Discussion

In this chapter, we have introduced a 4-wave model for analyzing parametric processing. It is worth to mention that in the case of parametric amplifiers driven by two pumps, the pump wavelength selection determines whether this model can be applied. For example, in [Paper A] the predictions of the 4-wave model are not valid and numerical simulations of the Manakov equation were needed to model the fiber. A 6-wave model [84, 85] can instead be used for modeling this cases. However, solutions of the 6-wave have only been found for specific cases. Here, we have also assumed that the Manakov equation can be used for modeling vector amplifiers. However, PMD, which we did not account for, usually affects vector amplifiers [45, 160], [Paper A].

Based on the 4-wave model, we have described different PS processors schemes, focused in those processors implemented with polarization-diverse or vector schemes. Then we have discussed the noise properties of PSAs and possible implementation schemes. At the end of this chapter, we have discussed different applications of parametric processing, focusing on those applications which have been covered in this thesis. Apart from the applications discussed in this thesis, there are multiple

application in which parametric processing has been proposed, such as add/drop operation in routed networks [161], and multicasting [17].

One of the main applications for PSAs is as inline amplifiers to provide low-noise amplification and/or mitigation of fiber nonlinearities by coherent superposition. However, bandwidth constrains should be taken into account when comparing conventional the performance of PIA-based links and PSA-based links. A PSA-amplified link halves the bandwidth since both signal and idler need to be transmitted. We should note that the trends in today's fiber-optic communication is towards dense WDM, with low spacing between WDM channels. Therefore, such halving the bandwidth can be detrimental to achieve the largest possible data rate. In this case, a fair comparison should then be done in terms of information theory concepts such as mutual information. In most low-noise PSA-based transmission experiments [105, 130], the input signal into the PSA was low due to high span loss. However, this would not be the case in the case of conventional span losses of about 15-25 dB, in which the optimum input power per WDM signal is around 0 dBm; and, therefore, the signal input into the PSA is about -20 dBm. However, the NF of a parametric amplifier both in PI and PS mode, degrades at high input signals due to PTN [20, 109]. Therefore, for conventional link losses, to exploit the low-noise amplification provided by PSA, the pump optical signal-to-noise ratio (OSNR) should be large. In addition, when having multiple WDM channels, pump depletion should be avoided by either using quite large pump power and a short nonlinear medium, or by more advanced parametric amplifiers such as Raman-assisted FOPAs [80]. Another major drawback of PSAs is that they are polarization dependent, although the use of polarization trackers could overcome the polarization dependance [Paper C]. The use of distributed Raman amplification can be used for improving the span NF, beyond the improvement provided by a lumped PSA. Distributed PSAs have theoretically been proposed [87], but several practical challenges should be overcome for this to be realized. However, distributed PI parametric amplification has been demonstrated in dispersion-shifted fibers [162, 163]. Regarding the capabilities for mitigation of fiber nonlinearities provides by PSAs, two major drawbacks are the spectral reduction provided by the use of PSAs and that it requires polarization tracking schemes. In contrast, recent demonstrations of optical phase conjugation [148, 149] and [Paper D] have shown the use of DP-modulated signals without loss of spectral efficiency.

Signal regeneration is another application for which PS signal processing could be used. Similar to inline amplification, the polarization dependance of signal regenerators should be overcome for its implementation in out of lab scenarios. Regeneration of WDM signals has been recently demonstrated at the expense of a complex scheme performing an optical Fourier transform twice [142]. A disadvantage of such a scheme is that it utilizes a delay interferometer to phase-lock all the WDM channels. Thus, the data encoded on the input BPSK signal is not the same as the data encoded on the output BPSK signals. Therefore, there is need for further research on regeneration of WDM signals as well as M-QAM signals.

Regarding quadrature demultiplexing, one of the remaining challenges is the implementation of quadrature demultiplexing in a black-box operation without the need for any incoming pilot tone. This could ideally be achieved at the expense of complex optical PLL.

Due to all aforementioned issues, PS processing still faces many challenges for out of lab implementations, such as polarization dependance. Nevertheless, these techniques could find their applications in very specific scenarios or in applications outside fiber-optic communications. Regarding signal processing, the development of systems such as polarization-assisted PS processors, which are capable of operating at low nonlinear phase shifts, are quite attractive since they could be easily implemented on integrated platforms.

Chapter 4

Parametric Frequency Combs

A frequency comb is a wave whose spectrum is formed by evenly spaced frequency components which are usually phase-locked. Frequency combs can be used in many applications such as precision metrology [164], spectroscopy [165, 166], high-precision distance measurements [167, 168], waveform synthesis [169] and RF photonics [170]. In this chapter, we focus on the use of frequency combs in optical communications. First, we describe the basics of a frequency comb and which parameters of a frequency comb are important in this context. Then, we briefly discuss the different techniques for achieving frequency combs, with focus on parametric combs. Afterwards, we present the technique of comb regeneration for SH detection. Finally, the chapter is concluded by discussing and proposing further studies in the context of comb regeneration for SH superchannel detection.
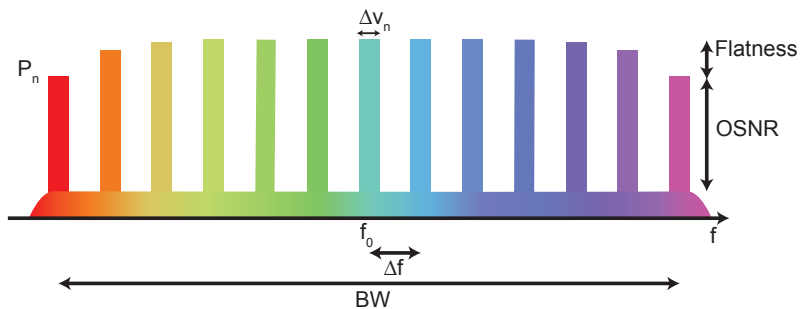

Fig. 4.1: Schematic of an optical frequency comb and those parameters of interest in the context of optical communications.

4.1 Frequency Combs in Optical Communications

The use of frequency combs in optical communications has attracted much attention since 90s. Light sources capable of generating narrow pulses were investigated in combination with optical time-division multiplexing in e.g. [171, 172]. The complexity for multiplexing and demultiplexing has however made that optical time-division multiplexing has not been implemented in commercial systems. The use of frequency combs has also received attention for replacing transmitter and local oscillator (LO) laser arrays in WDM scenarios. In 2000, the generation of 1000 WDM channels was demonstrated by broadening a mode-locked laser [173]. This and following experiments using broadening techniques in combination with mode-locked lasers [174, 175] or an electro-optic combs [176] showed the potential of using frequency combs as multi-wavelength sources. In recent years, a frequency comb was used in an experiment in which beyond 2 Pbit/s were transmitted in a 22-core fiber [177].

The comparison between a laser array and a frequency comb source should be analyzed in terms of cost, performance and energy consumption. The performance of the comb is determined by parameters such as center frequency f_0, spacing (Δf), number of carriers, phase noise ($\Delta \nu_n$) and OSNR of each carrier, total output power and the power of each carrier (P_n), i.e. flatness. These parameters are shown in Fig. 4.1. By using frequency combs based on a narrow-linewidth master laser, ideally all generated lines of the frequency comb also have narrow linewidths. Therefore, frequency combs can reduce the cost in applications in which expensive narrow-linewidth lasers are required since only a single master laser is necessary. However, the OSNR degradation and power limitation in frequency combs compared to laser arrays should also be taken into account. Accurate channel spacing, Δf, is another property provided by the use of combs. An accurate channel spacing is necessary when using narrow spacing or when using nonlinear mitigation in DSP [178]. Frequency combs can also reduce the energy consumption and cost since the number of temperature controllers and laser diode controllers is decreased. Although, all extra components that are necessary to achieve frequency combs should always be taken into account.

Beyond replacing laser arrays, frequency combs have characteristics which makes them very interesting as multi-wavelength sources for superchannel applications. Since the carriers are phase locked, one can think of exploiting the coherence between the carriers for simplifying the phase tracking algorithms in DSP [179]. Joint DSP is very interesting in metro applications when using higher-order modulation formats. When using higher-order modulation formats, complex DSP-based carrier-phase estimation and low linewidth lasers are necessary to minimize the phase-noise-induced penalty. Similar to the joint DSP, the properties of phase-locked carriers of frequency combs can be in exploited in order to perform SH detection by performing comb regeneration. This technique will be explained more in detailed in Section 4.4.

4.2 Comb Technologies

Several techniques to achieve frequency combs for optical communications have been demonstrated. These include mode-locked lasers [29], microring resonator [180], and cavity-less techniques such as electro-optic modulation [181, 182] and the use of cascaded FWM [16]. The selection of the technique depends on the requirements of the application. In addition, the combination of some of this techniques is also a feasible solution. For example, comb broadening in a nonlinear medium, i.e. parametric broadening, can be used to increase the number of carriers provided by mode-locked lasers [173–175] or electro-optic comb [176, 183, 184]. It should be highlighted that parametric effects, including comb broadening, ring structures or cascaded FWM have been used in all demonstrations of frequency combs generating beyond 100 carriers suitable for fiber-optic communications.

For the purpose of frequency comb regeneration which is in focus in this thesis, cavity-less frequency combs are preferred for the receiver side since we are aiming to replicate the transmitter comb at the receiver. However, the combination of mode-locked lasers with OIL has been suggested [29]. Both electro-optic comb [185] and parametric comb [Paper H] techniques have been proven successfully in the context of SH superchannel detection. The use of electro-optic combs can lead to a larger number of channels but also requires a PLL whose long-term stability should be investigated. An advantage of using parametric combs is that the frequency spacing can be more easily tuned and it is not limited by the electronics.

4.3 Parametric Combs

In this work, the comb technique we focus on is parametric combs. We here to a parametric comb as a frequency comb generated in a cavity-less nonlinear medium from two initial carriers. The recent demonstration of DP 64-QAM modulation over about 400 carriers generated by a parametric combs [177] has showed that parametric combs are a promising technology to be used in fiber-optic communications.

4.3.1 Parametric Comb Design

The creation of short pulses initiated from the beating of two carriers in a nonlinear medium has been investigated for decades. For example, generation of optical solitons [186–188] and low duty cycle pulses [189] are early examples.

Focusing on comb generation for multi-wavelength source, in which pulse compression is not a requirement, the combination of cascaded sections of HNLF followed by SSMF stages has been demonstrated to be capable of generating frequency combs with different frequency spacings from 25 GHz [177] to 400 GHz [17] covering in both cases the C and L band. In the following, we will explain the basics for frequency comb generation using this technique.

Intuitively, the origin of the formation of new components is cascaded FWM. If the two initial carriers are at frequencies, f_0 and f_1, new components will be generated at frequencies $2f_0 - f_1$ and $2f_1 - f_0$. If these components grow enough in power, more components will be generated. This effect effect of cascaded FWM
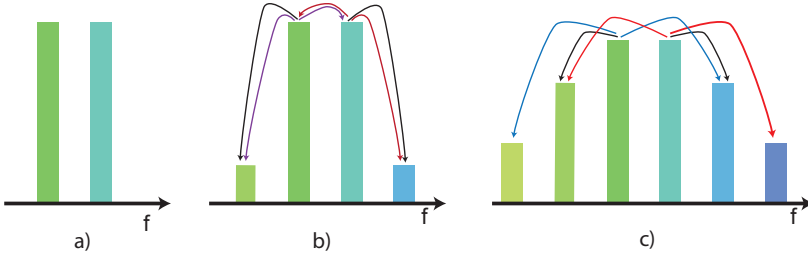
Fig. 4.2: Schematic of cascaded FWM along a HNLF when two initial carrier are launching at this input. New carriers are generated by FWM between the seed carriers. These two carriers will grow in amplitude such that new FWM products are generated. Lines with same color represent processes occurring simultaneously.

is illustrated in Fig. 4.2. When we input two carriers into a HNLF, sidebands are created by degenerate FWM [190]. Once the sidebands are created, degenerate and non-degenerate FWM contribute to the power growing of these carriers as shown in Fig. 4.2(b). Once the two sidebands have grown enough in power, many FWM terms should be considered with some of them generating new frequency terms. In Fig. 4.2(c), we decided only to plot some of these FWM terms due to the complexity of representing them all. However, the description in terms of cascaded FWM only gives a simple understanding for understanding why a frequency comb can be realized by using a nonlinear medium. More insight into the comb generation can be gained by analyzing from an SPM perspective. By modeling the optical field as a wave composed by two unmodulated carriers with equal amplitudes as

$$A_{\mathrm{a}}(t) = \sqrt{P_0}\left(e^{i\Delta\omega t/2} + e^{-i\Delta\omega t/2}\right) = 2\sqrt{P_0}\cos(\Delta\omega t/2), \tag{4.1}$$

where $\sqrt{P_0}$ is the power of each carrier, and $\Delta\omega$ is the frequency difference among the carriers, we find the intensity to be given by

$$|A_{\mathrm{a}}(t)|^2 = 2P_0(1 + \cos(\Delta\omega t)). \tag{4.2}$$

When this wave propagates through a dispersion-less nonlinear medium, the output undergoes SPM , which can be described as

$$A_{\mathrm{b}}(t) = A_{\mathrm{a}}(t)e^{iL\gamma|A_{\mathrm{a}}(t)|^2} = A_{\mathrm{a}}(t)e^{i2\gamma P_0 L(1+\cos(\Delta\omega t))}, \tag{4.3}$$

where γ is the nonlinear coefficient, L the fiber length, and we have neglected the propagation delay. Equation (4.3) can also be expressed by the Jacobi-Anger expansion as [17, 190]

$$A_{\mathrm{b}}(t) = \sqrt{P_0}\sum_{n=-\infty}^{\infty}\left(i^n J_{\mathrm{n}}(m) + i^{n+1} J_{\mathrm{n}+1}(m)\right)e^{i(n+1/2)\Delta\omega t}, \tag{4.4}$$
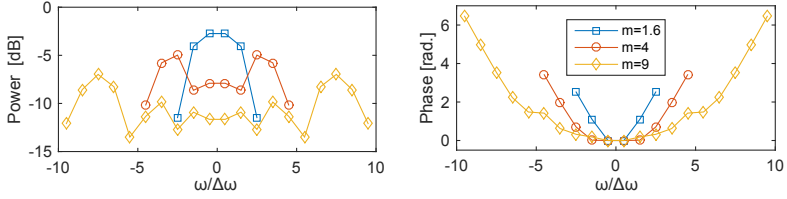
Fig. 4.3: Output spectrum for three different cases of $m = 2\gamma P_0 L$ using Eq. (4.4). The power is normalized by P_0. The phase has been normalized with respect the phase of the central carriers. Only those component with high power ($>$-15 dB) are plotted.

where $J_{\mathrm{n}}(m)$ denotes the Bessel function of the first kind with $m = 2\gamma P_0 L$. Therefore, we can see that new frequency components are generated and these new frequency components are spaced by the separation of the initial seed carriers, which is consistent with the intuitive description in terms of FWM. The spectrum is symmetric since $J_{-\mathrm{n}}(m) = (-1)^n J_{\mathrm{n}}(m)$. Based on Eq. (4.4), we show the generated spectrum for three different values of m in Fig. 4.3. We can see that the number of generated lines is approximately given by twice the nonlinear phase shift, $m = 2\gamma P_0 L$. We can then see that generating sufficient number of carriers in a single-stage HNLF is impractical since it requires very large nonlinear phase shift.

In Fig. 4.3, we can also observe that the phase follows a quasi-quadratic distribution. More understanding into the quadratic phase of the spectral components can be gained by the following derivation. Since the output is a periodic function, the spectrum can be calculated as

$$A_{\mathrm{b}}(\omega) = \Delta\omega\sqrt{P_0} \int_{-T/2}^{T/2} \cos(\Delta\omega t/2) e^{i2\gamma P_0 L(1+\cos(\Delta\omega t))} e^{-i\omega t} dt$$
$$\cdot \sum_{\mathrm{n}=-\infty}^{\mathrm{n}=\infty} \delta(\omega - n\Delta\omega/2), \qquad (4.5)$$

where $T = 4\pi/\Delta\omega$. This equation can be modified as

$$A_{\mathrm{b}}(\omega) = 2\Delta\omega\sqrt{P_0} \int_{-T/4}^{T/4} \cos(\Delta\omega t/2) e^{i2\gamma P_0 L(1+\cos(\Delta\omega t))} e^{-i\omega t} dt$$
$$\cdot \sum_{\mathrm{n}=-\infty}^{\mathrm{n}=\infty} \delta(\omega - n\Delta\omega + \Delta\omega/2). \qquad (4.6)$$

By expanding the phase term in Eq. (4.6) as a Taylor series, we have

$$e^{i2\gamma P_0 L(1+\cos(\Delta\omega t))} \approx e^{i2\gamma P_0 L(2-\Delta\omega^2 t^2/2+\dots)}, \qquad (4.7)$$

45

which means that we have a quadratic phase in the temporal domain. Note that this Taylor expansion has been made around the part of the pulse with higher energy. If we assume that $2L\gamma P_0 \gg (1/8\pi)$, the Fourier transform in Eq. (4.6) gives [191]

$$\int_{-T/4}^{T/4} \cos(\Delta\omega t)e^{i2\gamma P_0 L(2-\Delta\omega^2 t^2/2)}e^{-i\omega t}dt \propto e^{i\omega^2/(4\gamma P_0 L\Delta\omega^2)}\cos(\omega/(2P_0\gamma L\Delta\omega)),$$

(4.8)

valid for $|\omega| \leq \pi P_0 \gamma L \Delta\omega$.

The combination of Eqs. (4.6)-(4.8) shows that the phase of the spectral components is approximately quadratic in frequency, just as for chromatic dispersion. The difference between the spectrum which we have derived in Eqs. (4.6)-(4.8) compared to Eq. (4.4) is due to the the fact we have used only two Taylor terms to approximate the phase. However, the latter derivation allow us to gain more understanding into the phase of the spectral components.

In order to enhance the nonlinearities into a following nonlinear stage, the pulse should be compressed, meaning that all spectral lines should have the same phase. By noting that the frequency response of a dispersive element is given

$$E_{\text{out}}(\omega) = E_{\text{in}}(\omega)e^{i\beta_2\omega^2/2},$$

(4.9)

we can realize that a fiber with positive dispersion, e.g. an SSMF, can be used for pulse compression. The length of the SSMF, L_C, is then given by

$$L_C = -1/(2\gamma P_0 L\Delta\omega^2\beta_2),$$

(4.10)

where β_2 is the dispersion parameter of the SSMF. Neglecting nonlinearities, using a fiber with this length the chirp induced by the SSMF will compensate for the chirp induced in the HNLF.

We have now shown that after a first stage of HNLF, the pulse can be compressed by a SSMF fiber. A similar result has been achieved by calculating the chirp introduced in the HNLF [192]. In Fig. 4.4 we show the spectral and temporal shape at each stage of a parametric mixer. We can observe that after $HNLF_1$, the temporal shape is practically the same as the input temporal shape but new frequency components have been generated in this stage. After the SSMF, the pulse is compressed while the spectral shape is not affected much. The pulse compression assures to achieve the maximum broadening in the following HNLF stage. After $HNLF_2$, several more carriers are generated while the temporal pulse has evolved into a pulse with quasi-rectangular shape and we can also observe the pulse distortions at the pulse tails. This phenomena, known as optical wave breaking, [39, Ch. 4] occurs since we are operating in the normal dispersive regime. It has been shown that optical wave breaking can increase the comb flatness [193].

The number of compression stages is not limited to two. After the second broadening stage, a second compression stage consisting of SSMF could be used to compress the pulse before another broadening stage [192].
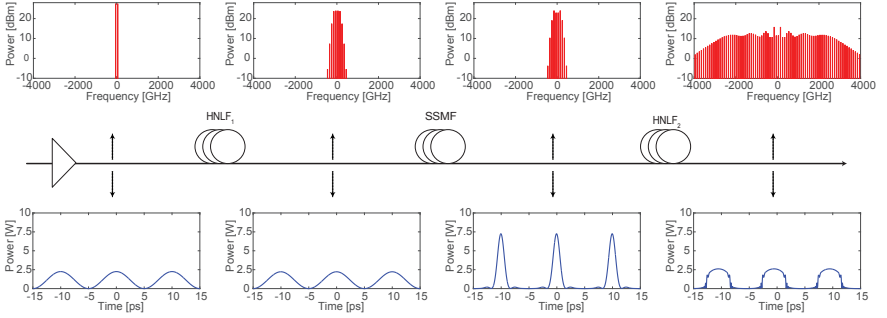
Fig. 4.4: Simulation results illustrating the generation of a parametric comb. At each point of the comb generation we show the spectrum (upper row) and the temporal pulse (lower row). The simulation consists of two initial carriers launched into three fiber sections consisting of $HNLF1_1$, SSMF and $HNLF_2$. The initial power per carrier is 27.5 dBm and the separation between carriers is 100 GHz. $HNLF_1$ and $HNLF_2$ have nonlinear coefficient of 10.7 $(W\ km)^{-1}$, dispersion of β_2=0.2 ps/(nm km), and attenuation of 0.8 dB/km. $HNLF_1$ has length of 150 m and $HNLF_2$ of 400 m. The SSMF has dispersion of β_2=-20.5 ps/(nm km), nonlinear coefficient of 1.3 $(W\ km)^{-1}$, a numerically optimized length of 88 m and attenuation of 0.2 dB/km. For simplicity, we have assumed β_3=0 ps/(nm^2 km) in both HNLFs and the SSMF.

4.3.2 Phase Noise

In the previous section, we have neglected that the phase noise of the seed carriers. In the temporal domain, this effect translates into time jitter of the pulses. In the spectral domain, we can describe the phase of the nth carrier by [194]

$$\phi_{\text{n}}(t) = n\phi_1(t) - (n-1)\phi_0(t) = \phi_0(t) + n(\phi_1(t) - \phi_0(t)), \qquad (4.11)$$

where $\phi_{0,1}(t)$ are the phases of the two central carriers, and n is the carrier number counting from the center. It is obvious that the phase noise properties are degraded as the carrier number increases when having two free running lasers as initial seeds. The carrier linewidth increases quadratically with respect to the carrier number when assuming Lorenztian shape and linearly when assuming Gaussian shape [195, Ch. 7].

The linewidth broadening has been solved by using two initial carriers which are already phase locked [196]. These two phase-locked carriers can be obtained by using electro-optic modulation, i.e. modulating the wave generated by a single free runing laser with an RF tone. In this case, the phase scaling determined by $(\phi_1(t) - \phi_0(t))$ depends on the quality of the RF oscillator. In many cases, OIL is used to select the two initial carriers and improve the OSNR of the seed carriers. In this case, any phase noise added on the OIL stage should also be considered. When using OIL, the seed carriers usually travel through two different fibers. Time alignment between the carriers is then an important aspect to consider [Paper G].

4.3.3 Dispersion and OSNR per Carrier

When using a frequency comb as a multi-wavelength source for WDM communications, the OSNR of each carrier and the power per carrier are two essential aspects. In the previous derivation, we neglected the fiber dispersion of the HNLF fiber. However, it has been shown that the fiber dispersion plays a significant role in the OSNR per carrier and the number of generated lines [192]. The use of HNLF with normal dispersion avoids modulation instability, i.e. amplification of the quantum noise, which degrades the output OSNR per carrier. However, the dispersion should be low enough to enhance the FWM processes and achieve a broad comb. Since higher-order dispersion terms should be taken into account when considering broad combs, the use of HNLF with flat dispersion in the second and beyond broadening stages is desired in this case [192]

4.3.4 Practical Considerations

In our description of parametric combs, we have considered that the parametric mixer is made of concatenation of HNLFs and SSMFs. Such a simpler scheme is only possible when using HNLFs with low loss. An important consideration to take into account is that the input power into a fiber-based parametric mixer is limited by SBS. As mentioned in Section 2.3, the use of strained fibers can reduced the power limitation by SBS. The power in the first compression stage, SSMF, can also be limited by SBS. When the frequency spacing is around 25 GHz, the first compression stage length can be in the order of several hundreds of meters which then also imposes a constraint in the power per line travelling through this compression stage. Again a gradient straining can reduce the power limitations. Characterization of both the SSMF and HNLF SBS properties can also be important in this scenario. Commonly, the Brillouin downshift frequency for the HNLF and SSMF would be different due to the different characteristics, e.g. doping, of both fibers. Avoiding overlapping of the SBS frequency bands for the SSMF and HNLF would thus be beneficial for the comb design. The limitation on power into the following broadening stages is however relaxed since after the first HNLF the total power is divided into several carriers.

In the previous discussion, we have not considered the nonlinear interaction in the compression stages. This assumption is valid for cases in which the compression stages are short. However, when using long compression stages the nonlinear interaction occurring in this stage should also be accounted for since the spectral shape will also be modified in the compression stage and not only the temporal shape. In the example shown in Fig. 4.4, a minor change in the spectral shape before and after the SSMF can be observe despite its length is of only 88 m.

The comb flatness depends on the shape of the pulse at the input of the nonlinear broadening. In our previous section, we assumed that maximum compression can be achieved by using a dispersive medium, but this was based on a first-order approximation. In Fig. 4.4, we can see that after compression the pulse shows a pedestal which is due to the neglected terms. It has been demonstrated that using a nonlinear loop mirror for shaping the pulse without those pedestals can improve
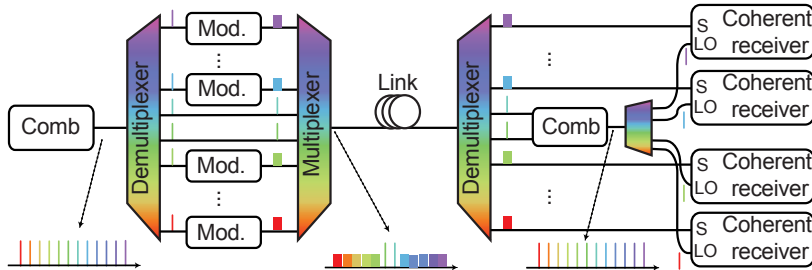
Fig. 4.5: Basic schematic of the SH superchannel based on comb regeneration.

the comb flatness [183]. The use of a programmable filter with phase control could also be used for shaping the pulse but we should take into account the loss of the programmable filter which are usually in the order of 4 dB. The comb flatness is not strictly necessary as long as the output power per line is sufficiently high since the frequency comb can be flattened at the output [177].

4.4 Self-Homodyne Superchannel Based on Comb Regeneration

Beyond using frequency combs as a multi-wavelength source, the utilization of the comb properties can be of interest in the context of optical communications. Since the carriers are phase-locked, joint DSP could be exploited. Another option to decrease the DSP complexity is frequency comb regeneration for SH superchannels [29, 197], [Paper G, H]. The schematic for SH is depicted in Fig. 4.5. As can be seen, several carriers but one or two from a frequency comb are modulated at the transmitter side. At the receiver side, a frequency comb with the same phase and frequency spacing is regenerated by using the unmodulated carriers. The regenerated comb is then used as LO for SH detection.

The two main properties which are of interest for the regenerated comb are the phase and the frequency spacing. Regarding the phase, it can be obtained by transmitting an unmodulated carrier. Since this carrier is unmodulated, the use of a narrow filtering at the receiver side is desired for mitigating the SNR penalty of SH detection. Regarding the frequency spacing, several techniques have been proposed. The work in [197] proposed the use of DSP on the modulated data to obtain the frequency spacing. Such a technique has been demonstrated for intradyne receivers in order to stabilize the frequency spacing of a frequency comb used for LOs [198]. However, different challenges are expected to arise when targeting SH detection. Another option, also proposed in [197], is the use of amplitude modulation on this pilot tone based on a reference frequency. For example, one could think to modulate this pilot tone with a 100 MHz tone used as frequency reference in the transmitter for the comb generation. This technique however implies that the regeneration of

this frequency reference at the transmitter side must be done with extremely high fidelity.

A simpler option to obtain the frequency spacing was presented in [Paper G]. By transmitting the two central carries, the frequency spacing can be easily obtained at the receiver side. The comb can be directly regenerated by using a parametric comb at the receiver side. Another approach which has also been demonstrated is the use of an electrical PLL which allows to obtain the frequency spacing more accurately [185]. As demonstrated in [Paper H], the bandwidth for the filtering of the frequency spacing determines the number of channels which can be SH detected. The number of regenerated carriers in an all-optical approach is then limited by the optical filtering bandwidth. A disadvantage of the electrical approach is that the carrier spacing is limited by the electronic bandwidth, and requires electrical PLL whose stability should be studied.

Apart from the bandwidth of the optical filtering, the number of low-phase-noise carriers can also be limited by the dispersive walk-off, which decorrelates the seed carriers. In [Paper G], we showed how the linewidth of regenerated carriers depends on the transmission distance and linewidth of the master laser. The dispersive penalty can be mitigated by using optical dispersion compensation.

4.5 Discussion

In this chapter, we have discussed the use of frequency combs in fiber-optic communications, focusing on parametric combs and the comb regeneration technique. As mentioned, many previous demonstrations have focused on frequency combs as a replacement of laser arrays. In this thesis, we have however focused on exploiting the phase coherence among the comb carriers for simplifying the DSP-based carrier recovery algorithms. Exploiting the coherence among the comb carriers, either by joint DSP or comb regeneration, is interesting to further understand of how the DSP can be simplified when using frequency combs and to know whether frequency combs can be utilized beyond multi-wavelength sources. The all-optical nature of the comb regeneration demonstrated in [Paper H] could lead towards the integration of a full SH superchannel receiver. Further analysis should aim the implementation of this system with modulation formats with very high constellation cardinality, e.g. 256-QAM. Energy saving in the DSP block should also be calculated to know whether this technique should be implemented. Further studies should also be carried out to evaluate different techniques in which the spectral overhead for SH detection can be reduced. The implementation of this technique with multicore fibers could lead to a very low overhead SH receiver.

When comparing this technique, to a conventional SH technique in which one pilot tone is transmitted per WDM channel, we should realize that the comb regeneration technique reduces the complexity at the expense of higher constraint on the filtering of the unmodulated carriers. In conventional SH detection, one polarization tracker per pilot tone, i.e. per WDM channel, is necessary. Moreover, one narrow filter per WDM channel is also necessary to mitigate the SNR penalty of SH detection [199]. Therefore, the comb regeneration technique can reduce the complexity

to achieve SH detection, since as demonstrated in [Paper H], only two narrow filters and two polarization trackers are necessary for SH detection of 24 channels.

In conclusion, the technique of SH superchannels by comb regeneration has shown promising results in two proof of principle experiments [185] and [Paper H]. However, further research should be carry out for a complete evaluation of this technique. Reducing the spectral overhead and increasing the cardinality of the constellations are two important topics which should be investigated.

Chapter 5

Outlook

In this chapter we discuss some interesting research topics for parametric processing in the future. It is important to realize that digital coherent receivers have revolutionized the field of fiber-optic communication systems. Then, parametric processing should be compatible with this scenario in which both amplitude and phase are used for encoding of data. Moreover, DP-signals are also becoming ubiquitous. Despite being the era of DSP, parametric processing could be attractive in order to reduce the complexity of DSP, e.g. by mitigation of nonlinearities and dispersion compensation provided by all-optical signal processing. The wideband capabilities of parametric processing compared to DSP should also be considered when analyzing the prospects of parametric processing. The functionalities provided by PS processing should be further explored. For example, demonstration of 16-QAM regeneration would attract much attention.

Parametric frequency combs are now commercially available and they are a promising technology for replacing laser arrays. The use of frequency combs can be extended for improved mitigation of fiber nonlinearities [178]. This technique should be analyzed in scenarios which high WDM channel number (beyond ten) and in WDM networks. The use of frequency combs for simplifying the carrier phase recovery is also attractive. Reducing the spectral overhead for achieving SH should be investigated, making the use of multicore or multimode fibers very attractive.

Apart from the mentioned research topics, we here also highlight three different topics in which further research could be of interest.

5.1 Integrated Waveguides

There have been several demonstrations of parametric processors with different integrated platforms [32, 35]. Until now, integrated waveguides cannot compete with HNLF in terms of insertion loss or gain, but large bandwidth operation has already

been demonstrated using integrated waveguides [37]. Schemes such as polarization-assisted PS processors which reduces the need for large nonlinear phase shifts, should be further investigated with integrated waveguides [200]. In scenarios in which integrated several processors are needed either in parallel or series, integrated waveguides are an ideal solution. Therefore, integrated waveguides could open the possibility of newer functionalities by combining several processors. For example, parametric processing, e.g. regeneration, of WDM channels could be achieved by parallel waveguides. In an ideal scenario, the pump laser, amplifiers and waveguide are integrated. The different ways to overcome the practical challenges to achieve such an ideal scenario should be investigated.

Microring frequency combs are an example in which integrated waveguides can be utilized [180]. Understanding the noise properties of these frequency combs is essential for their use with higher-order QAM signals, e.g. 64-QAM signals. Co-integrating the laser, microring, modulators, WDM (de)multiplexer is the ideal scheme for which further research is needed. The success of microring combs should not exclude further research in other frequency comb schemes. For example, co-intengration of a modulator with nonlinear waveguides could lead to an integrated frequency comb with widely tunable frequency spacing.

5.2 Parametric Processing in Multimode Fibers

In order to increase the fiber capacity, both multicore and mutimode fibers are emerging as a possible solution. Focusing on multimode fibers, the analysis of wether parametric processing can be utilized in this possible scenario should be carried out. When targeting for parametric amplification or wavelength conversion, a scheme capable of amplifying and/or wavelength converting several spatial modes is of great interest, so that the complexity is not to scaled by the number of modes. The design should also achieve modal independent operation since it is assumed that the data on different modes but same wavelength is mixed through transmission. Recently, the design of a multimode HNLF in which four spatial modes can be simultaneously amplified has been proposed [201]. This fiber could also be used for wavelength conversion which can be of interest in routed networks. Further analysis should be carried out in order to equalize the different gain profile of different modes. The analysis of intermodal FWM has also attracted attention in the last years [202]. Designing multimode HNLFs in which intermodal FWM can be utilized for achieving mode-independent operation should be considered in the near future. The use of PS processing in multimode fiber will be challenging, but it is worthwhile to conduct research and evaluate whether it is feasible and whether newer functionalities can be provided in this context.

The use of integrated multimode waveguides is also very interesting in this context. Phase regeneration of two modal channels using a multimode silicon waveguide has been proposed and analyzed numerically [203]. Mode demultiplexer in a silicon waveguide using FWM has also been demonstrated experimentally [204]. Thus, the development of multimode fibers opens a new area in which to explore the potential applications of parametric processing.

5.3 Low-Noise Phase-Sensitive Amplification

One of the main characteristic of PSAs is their capability to perform amplification without degrading the SNR. This ideal noiseless amplification comes at the expense of halving the spectral efficiency which contrasts with the increased use of spectral efficient modulation formats in fiber-optic communication. However, there are scenarios in which bandwidth is not the limiting factor but sensitivity, e.g. free-space optical communications. Thus, it is worth to investigate the use of PSAs in these scenarios in which sensitivity is the key figure of merit. PSAs could find its application in many diverse scenarios such imaging, sensing, and metrology, and quantum information.

Chapter 6

Summary of Papers

This thesis includes eight appended papers, which are summarized below.

Paper A: Experimental analysis of degenerate vector phase-sensitive amplification

A. Lorences-Riesgo, F. Chiarello, C. Lundström, M. Karlsson, and P. A. Andrekson, *Opt. Exp.*, vol. 22, no. 18, pp. 21889–21902, Sep. 2014.

In this paper, we characterize a degenerate vector PSA and compare it to a degenerate scalar PSA. We show that the degenerate vector PSA is affected by fiber PMD, but the pump SOPs can be optimized to mitigate such effect. Once the pump SOPs are optimized, we show that the numerical predictions agrees with the experimental results regarding the gain and PS extinction ratio curves as a function of the polarization angle between the degenerate wave and the pumps. In the comparison with the scalar case, we show that the vector scheme is less affected by pump-pump FWM and higher-order idlers.

My Contribution: I came up with the idea of the experimental setup. I built the experimental setup and performed the measurements. I made the simulations with the help of F. Chiarello and I wrote the paper.

Paper B: Phase-sensitive amplification and regeneration of dual-polarization BPSK without polarization diversity

A. Lorences-Riesgo, C. Lundström, F. Chiarello, M. Karlsson, and P. A. Andrekson, *in European Conference on Optical Communication (ECOC)*, Sep. 2014, paper Tu.1.4.3.

In this conference contribution, we demonstrate that the degenerate vector PSA can amplify both BPSK and DP-BPSK signals. A 1 dB sensitivity improvement is measured with respect to EDFA-based amplification. No penalty was observed by the presence of two polarization channels. The phase-regeneration capabilities of the vector PSA are evaluated by inputting a phase-degraded signal into the amplifier. At the output, we observe that the signal phase is regenerated and that phase fluctuations are converted into amplitude fluctuations.

My Contribution: I planned the experiment. I built the experimental setup and performed the experimental measurements. I wrote the paper and I presented it at the conference.

Paper C: Polarization-insensitive phase-sensitive amplification

A. Lorences-Riesgo, P. A. Andrekson, and M. Karlsson, *J. Lightwave Technol.*, vol. 34, no. 13, pp. 3171–3180, Jul. 2016.

Here, we describe the polarization properties of both polarization-diverse and vector PSAs. In both cases, we discuss the signal-degenerate and signal non-degenerate schemes. We introduce a graphical interpretation of the polarization properties based on the Poincaré sphere. With this graphical interpretation, the polarization properties of both polarization and vector PSA can be described by a mirror plane in the Poincaré sphere. The use of polarization trackers to achieve PS amplification of both single-polarization and DP modulated signals is analyzed. Our discussion includes the number of degree of freedom which are necessary in each case based mainly on the introduced graphical interpretation.

My Contribution: I came up with the idea of using a mirror plane for describing the polarization properties of parametric amplifiers. With the help of M. Karlsson, I analyzed the requirements of the polarization trackers for achieving polarization-independent PS amplification. I wrote the paper.

Paper D: Optical nonlinearity mitigation of 6×10 GBd polarization-division multiplexing 16QAM signals in a field-installed transmission link

J. Sun, **A. Lorences-Riesgo**, F. Parmigiani, K R. H. Bottrill, S. Yoshima, G. D. Hesketh, M. Karlsson, P. A. Andrekson, D. J. Richardson, and P. Petropoulos, *Accepted to Optical Fiber Communication Conference (OFC)*, Mar. 2017, paper Th3J.2.

In this conference contribution, we experimentally investigate the mitigation of fiber nonlinearities in an installed dispersion-managed link by using mid-span spectral inversion. By implementing two vector phase conjugators in a bidirectional HNLF, full spectral utilization is achieved. Compared to previous studies, we demonstrate that this scheme can also be implemented with DP-modulated signals and in a longer link.

Bit-error rate improvement in 6 WDM channels is demonstrated when compared with the case in which the optical phase conjugator is not included.

My Contribution: In a visit to the Univeristy of Southampton, this experimental work was performed in a joint collaboration. I collaborated on designing the DP transmitter and optimizing the optical phase-conjugator for minimizing the penalty when using DP-modulated signals. The measurements were carrier out by J. Sun and myself. I contributed in writing the paper by providing feedback.

Paper E: Quadrature demultiplexing using a degenerate vector parametric amplifier

A. Lorences-Riesgo, L. Liu, S. L. I. Olsson, R. Malik, A. Kumpera, C. Lundström, S. Radic, M. Karlsson, and P. A. Andrekson, *Opt. Exp.*, vol. 22, no. 24, pp. 29424–29434, Nov. 2014.

Here, we demonstrate quadrature decomposition of a QPSK signal into a DP-BPSK signal. The decomposition is achieved by the means of a degenerate vector amplifier operating in PI mode. The high gain of the amplifier enables the decomposition into two cross-polarized waves, which are split by a PBS. Stable decomposition is achieved by using a novel PLL scheme which minimizes the amplitude variations of the decomposed signals. Thanks to this PLL, bit-error rate curves can be measured and confirm that both quadratures can be obtained simultaneously.

My Contribution: I planned the experiment and designed the PLL scheme for quadrature demultiplexing. R. Malik and A. Kumpera built the main experimental setup following my indications. With the collaboration of L. Liu, I performed the experimental measurements. I wrote the paper.

Paper F: Quadrature decomposition of a 20 Gbaud 16-QAM signal into 2×4-PAM signals

A. Lorences-Riesgo, T. A. Eriksson, M. Mazur, P. A. Andrekson, and M. Karlsson, *in European Conference on Optical Communication (ECOC)*, Sept. 2016, paper Tu.1.E.3.

This conference contribution proposes and demonstrates the use of a polarization-assisted PS processor based on a polarization diverse implementation. For the first time, quadrature decomposition of a 16-QAM signal into its both quadratures is demonstrated. Moreover, we demonstrate that the scheme can operate at low non-linear phase shifts, which makes this scheme compatible with integrated waveguides.

My Contribution: I conceived the idea of implementing a polarization-assisted PS processor using a polarization-diverse scheme. I designed and built the experimental setup and I performed the measurements. I wrote the paper and presented the work at the conference.

Paper G: Frequency-comb regeneration for self-homodyne superchannels

A. Lorences-Riesgo, T. A. Eriksson, A. Fülöp, P. A. Andrekson and M. Karlsson, *J. Lightwave Technol.*, vol. 34, no. 8, pp. 1800-1806, Apr. 2016.

Based on a top-scored ECOC paper, we propose and study the concept of SH superchannel receiver by using comb regeneration. This idea consist on using a frequency comb at the transmitter site from which all carrier but two are modulated. At the receiver side, the frequency comb can be regenerated and the regenerated carriers can be used for LOs in a SH receiver. The proposed comb regeneration is based on using OIL and a parametric comb, leading to an all-optical comb regeneration. We theoretically asses the linewidth of the regenerated carriers for different dispersive walk-offs between the two initial carriers. The theoretical prediction are compared with the experimental results with good agreement. Moreover, we also evaluate the linewidth of the regenerated carriers when varying the OSNR of the two initial carriers.

My Contribution: In collaboration with T. A. Eriksson, we came up with the idea of comb regeneration. I performed the theoretical analysis, I and T. A. Eriksson designed and performed the main experimental measurements. I wrote the paper.

Paper H: Self-homodyne 24×32-QAM superchannel receiver enabled by all-optical comb regeneration using Brillouin amplification

A. Lorences-Riesgo, M. Mazur, T. A. Eriksson, P. A. Andrekson and M. Karlsson, *Opt. Exp.*, vol. 24, no. 26, pp. 29714-29723, Dec. 2016.

Continuing the work presented in the previous paper, we here demonstrate a SH superchannel receiver enabled by comb regeneration. To improve the high-frequency phase-noise properties of the regenerated carriers, we use Brillouin amplification for narrow filtering of the unmodulated carriers. After Brillouin amplification, the frequency comb is regenerated by cascaded FWM, i.e. a parametric frequency comb. By using the carriers from the regenerated comb as LOs, SH detection of 24 WDM channels modulated with DP 32-QAM signals is evaluated in both a back-to-back scenario and after 120 km of SSMF transmission. In the back-to-back analysis, the OSNR penalty at bit-error rate of 10^{-2} when using the regenerated comb is lower than 2.5 dB compared to an ideal SH receiver. We also show that all 24 channels can be SH detected with bit-error rate below 0.015 after 120 km transmission.

My Contribution: I conceived the idea of using Brillouin amplification for narrow filtering. I, M. Mazur and T. A. Eriksson designed the experimental setup. In collaboration with M. Mazur, I performed the measurements. I wrote the paper.

References

[1] K. C. Kao and G. A. Hockham, "Dielectric-fibre surface waveguides for optical frequencies," *Proc. Inst. Elec. Eng.*, vol. 113, no. 7, pp. 1151–1158, Jul. 1966.

[2] R. N. Hall, G. E. Fenner, J. D. Kingsley, T. J. Soltys, and R. O. Carlson, "Coherent light emission from GaAs junctions," *Phys. Rev. Lett.*, vol. 9, pp. 366–368, Nov. 1962.

[3] M. I. Nathan, W. P. Dumke, G. Burns, F. H. Dill, and G. Lasher, "Stimulated emission of radiation from GaAs p-n junctions," *Appl. Phys. Lett.*, vol. 1, no. 3, pp. 62–64, Nov. 1962.

[4] R. J. Mears, L. Reekie, I. M. Jauncey, and D. N. Payne, "Low-noise erbium-doped fibre amplifier operating at 1.54 μm," *Electron. Lett.*, vol. 23, no. 19, pp. 1026–1028, Sep. 1987.

[5] H. Sun, K.-T. Wu, and K. Roberts, "Real-time measurements of a 40 Gb/s coherent system," *Opt. Exp.*, vol. 16, no. 2, pp. 873–879, Jan. 2008.

[6] Cisco, "Cisco Visual Networking Index: Forecast and Methodology, 2015-2020," http://www.cisco.com/c/en/us/solutions/collateral/service-provider/visual-networking-index-vni/complete-white-paper-c11-481360.pdf, accessed: 28-10-2016.

[7] P. A. Andrekson, N. A. Olsson, J. R. Simpson, T. Tanbun-Ek, R. A. Logan, and M. Haner, "16 gbit/s all-optical demultiplexing using four-wave mixing," *Electron. Lett.*, vol. 27, no. 11, pp. 922–924, May 1991.

[8] P. A. Andrekson, "Picosecond optical sampling using four-wave mixing in fibre," *Electron. Lett.*, vol. 27, no. 16, pp. 1440–1441, Aug. 1991.

[9] W. Imajuku, A. Takada, and Y. Yamabayashi, "Low-noise amplification under the 3 dB noise figure in high-gain phase-sensitive fibre amplifier," *Electron. Lett.*, vol. 35, no. 22, pp. 1954–1955, Oct. 1999.

[10] R. M. Jopson, A. H. Gnauck, and R. M. Derosier, "Compensation of fibre chromatic dispersion by spectral inversion," *Electron. Lett.*, vol. 29, no. 7, pp. 576–578, Apr. 1993.

[11] S. Watanabe, T. Chikama, G. Ishikawa, T. Terahara, and H. Kuwahara, "Compensation of pulse shape distortion due to chromatic dispersion and Kerr effect by optical phase conjugation," *IEEE Photon. Technol. Lett.*, vol. 5, no. 10, pp. 1241–1243, Oct. 1993.

[12] W. Pieper, C. Kurtzke, R. Schnabel, D. Breuer, R. Ludwig, K. Petermann, and H. G. Weber, "Nonlinearity-insensitive standard-fibre transmission based on optical-phase conjugation in a semiconductor-laser amplifier," *Electron. Lett.*, vol. 30, pp. 724–726, Apr. 1994.

[13] S. Watanabe and M. Shirasaki, "Exact compensation for both chromatic dispersion and Kerr effect in a transmission fiber using optical phase conjugation," *J. Lightwave Technol.*, vol. 14, no. 3, pp. 243–248, Mar. 1996.

[14] C. Langrock, S. Kumar, J. E. McGeehan, A. E. Willner, and M. M. Fejer, "All-optical signal processing using $\chi^{(2)}$ nonlinearities in guided-wave devices," *J. Lightwave Technol.*, vol. 24, no. 7, pp. 2579–2592, Jul. 2006.

[15] M. Hirano, T. Nakanishi, T. Okuno, and M. Onishi, "Silica-based highly nonlinear fibers and their application," *IEEE J. Sel. Top. Quantum Electron.*, vol. 15, no. 1, pp. 103–113, Jan. 2009.

[16] B. P.-P. Kuo, E. Myslivets, V. Ataie, E. G. Temprana, N. Alic, and S. Radic, "Wideband parametric frequency comb as coherent optical carrier," *J. Lightwave Technol.*, vol. 31, no. 21, pp. 3414–3419, Nov. 2013.

[17] B. P.-P. Kuo, E. Myslivets, N. Alic, and S. Radic, "Wavelength multicasting via frequency comb generation in a bandwidth-enhanced fiber optical parametric mixer," *J. Lightwave Technol.*, vol. 29, no. 23, pp. 3515–3522, Dec. 2011.

[18] R. Slavík, F. Parmigiani, J. Kakande, C. Lundström, M. Sjödin, P. A. Andrekson, R. Weerasuriya, S. Sygletos, A. D. Ellis, and L. Grüner-Nielsen, "All-optical phase and amplitude regenerator for next-generation telecommunications systems," *Nature Photon.*, vol. 4, no. 10, pp. 690–695, Sep. 2010.

[19] J. Kakande, R. Slavík, F. Parmigiani, A. Bogris, D. Syvridis, L. Grüner-Nielsen, R. Phelan, P. Petropoulos, and D. J. Richardson, "Multilevel quantization of optical phase in a novel coherent parametric mixer architecture," *Nature Photon.*, vol. 5, no. 12, pp. 748–752, Oct. 2011.

[20] Z. Tong, C. Lundström, P. A. Andrekson, C. J. McKinstrie, M. Karlsson, D. J. Blessing, E. Tipsuwannakul, B. J. Puttnam, H. Toda, and L. Grüner-Nielsen, "Towards ultrasensitive optical links enabled by low-noise phase-sensitive amplifiers," *Nature Photon.*, vol. 5, no. 7, pp. 430–436, Jun. 2011.

[21] E. Palushani, H. C. H. Mulvad, M. Galili, H. Hu, L. K. Oxenløwe, A. T. Clausen, and P. Jeppesen, "OTDM-to-WDM conversion based on time-to-frequency mapping by time-domain optical Fourier transformation," *IEEE Journal of Selected Topics in Quantum Electronics*, vol. 18, no. 2, pp. 681–688, Mar. 2012.

[22] R. P. Webb, J. M. Dailey, R. J. Manning, and A. D. Ellis, "Phase discrimination and simultaneous frequency conversion of the orthogonal components of an optical signal by four-wave mixing in an SOA," *Opt. Exp.*, vol. 19, no. 21, pp. 20 015–20 022, Oct. 2011.

[23] Z. Zheng, L. An, Z. Li, X. Zhao, and X. Liu, "All-optical regeneration of DQPSK/QPSK signals based on phase-sensitive amplification," *Opt. Commun.*, vol. 281, no. 10, pp. 2755 – 2759, May 2008.

[24] F. Da Ros, K. Dalgaard, L. Lei, J. Xu, and C. Peucheret, "QPSK-to-2×BPSK wavelength and modulation format conversion through phase-sensitive four-wave mixing in a highly nonlinear optical fiber," *Opt. Exp.*, vol. 21, no. 23, pp. 28 743–28 750, Nov. 2013.

[25] M. Gao, T. Kurosu, T. Inoue, and S. Namiki, "Low-penalty phase demultiplexing of QPSK signal by dual-pump phase sensitive amplifiers," in *European Conference on Optical Communication (ECOC)*, Sep. 2013, paper We.3.A.5.

[26] T. Miyazaki and F. Kubota, "PSK self-homodyne detection using a pilot carrier for multibit/symbol transmission with inverse-RZ signal," *IEEE Photon. Technol. Lett.*, vol. 17, no. 6, pp. 1334–1336, Jun. 2005.

[27] T. Miyazaki, "Linewidth-tolerant QPSK homodyne transmission using a polarization-multiplexed pilot carrier," *IEEE Photon. Technol. Lett.*, vol. 18, no. 2, pp. 388–390, Jan. 2006.

[28] S. Beppu, K. Kasai, M. Yoshida, and M. Nakazawa, "2048 QAM (66 Gbit/s) single-carrier coherent optical transmission over 150 km with a potential SE of 15.3 bit/s/Hz," *Opt. Exp.*, vol. 23, no. 4, pp. 4960–4969, Feb. 2015.

[29] P. J. Delfyett, S. Gee, M.-T. Choi, H. Izadpanah, W. Lee, S. Ozharar, F. Quinlan, and T. Yilmaz, "Optical frequency combs from semiconductor lasers and applications in ultrawideband signal processing and communications," *J. Lightwave Technol.*, vol. 24, no. 7, pp. 2701–2719, Jul. 2006.

[30] J. A. Levenson, I. Abram, T. Rivera, and P. Grangier, "Reduction of quantum noise in optical parametric amplification," *J. Opt. Soc. Am. B*, vol. 10, no. 11, pp. 2233–2238, Nov. 1993.

[31] J. A. Levenson, I. Abram, T. Rivera, P. Fayolle, J. C. Garreau, and P. Grangier, "Quantum optical cloning amplifier," *Phys. Rev. Lett.*, vol. 70, pp. 267–270, Jan. 1993.

[32] M. A. Foster, A. C. Turner, J. E. Sharping, B. S. Schmidt, M. Lipson, and A. L. Gaeta, "Broad-band optical parametric gain on a silicon photonic chip," *Nature*, vol. 441, no. 7096, pp. 960–963, Jun. 2006.

[33] B. J. Eggleton, B. Luther-Davies, and K. Richardson, "Chalcogenide photonics," *Nature photonics*, vol. 5, no. 3, pp. 141–148, 2011.

[34] K. Hammani, M. A. Ettabib, A. Bogris, A. Kapsalis, D. Syvridis, M. Brun, P. Labeye, S. Nicoletti, D. J. Richardson, and P. Petropoulos, "Optical properties of silicon germanium waveguides at telecommunication wavelengths," *Opt. Exp.*, vol. 21, no. 14, pp. 16 690–16 701, Jul. 2013.

[35] D. J. Moss, R. Morandotti, A. L. Gaeta, and M. Lipson, "New CMOS-compatible platforms based on silicon nitride and hydex for nonlinear optics," *Nature Photon.*, vol. 7, no. 8, pp. 597–607, Aug. 2013.

[36] K. Croussore and G. Li, "Phase and amplitude regeneration of differential phase-shift keyed signals using phase-sensitive amplification," *IEEE J. Sel. Top. Quantum Electron.*, vol. 14, no. 3, pp. 648–658, May 2008.

[37] M. Pu, H. Hu, L. Ottaviano, E. Semenova, D. Vukovic, L. K. Oxenløwe, and K. Yvind, "AlGaAs-on-insulator nanowire with 750 nm FWM bandwidth, -9 dB CW conversion efficiency, and ultrafast operation enabling record Tbaud wavelength conversion," in *Optical Fiber Communication Conference (OFC)*, Mar. 2015, paper Th5A.3.

[38] M. Hirano, T. Haruna, Y. Tamura, T. Kawano, S. Ohnuki, Y. Yamamoto, Y. Koyano, and T. Sasaki, "Record low loss, record high FOM optical fiber with manufacturable process," in *Optical Fiber Communication Conference (OFC)*, Mar. 2013, paper PDP5A.7.

[39] G. Agrawal, *Nonlinear Fiber Optics*, 5th ed., ser. Optics and Photonics. Elsevier Science, 2013.

[40] M. Karlsson, "Four-wave mixing in fibers with randomly varying zero-dispersion wavelength," *J. Opt. Soc. Am. B*, vol. 15, no. 8, pp. 2269–2275, Aug. 1998.

[41] F. Yaman, Q. Lin, S. Radic, and G. P. Agrawal, "Impact of dispersion fluctuations on dual-pump fiber-optic parametric amplifiers," *IEEE Photon. Technol. Lett.*, vol. 16, no. 5, pp. 1292–1294, May 2004.

[42] P. Velanas, A. Bogris, and D. Syvridis, "Impact of dispersion fluctuations on the noise properties of fiber optic parametric amplifiers," *J. Lightwave Technol.*, vol. 24, no. 5, pp. 2171–2178, May 2006.

[43] C. D. Poole and R. E. Wagner, "Phenomenological approach to polarisation dispersion in long single-mode fibres," *Electron. Lett.*, vol. 22, no. 19, pp. 1029–1030, Sep. 1986.

[44] P. O. Hedekvist, M. Karlsson, and P. A. Andrekson, "Polarization dependence and efficiency in a fiber four-wave mixing phase conjugator with orthogonal pump waves," *IEEE Photon. Technol. Lett.*, vol. 8, no. 6, pp. 776–778, Jun. 1996.

[45] S. Radic and C. J. McKinstrie, "Two-pump fiber parametric amplifiers," *Opt. Fiber Tech.*, vol. 9, no. 1, pp. 7 – 23, Jan. 2003.

[46] P. Kylemark, J. Ren, S. Radic, C. J. McKinstrie, M. Karlsson, and P. A. Andrekson, "Noise in orthogonally pumped fiber-optical parametric amplifiers," *IEEE Photon. Technol. Lett.*, vol. 19, no. 2, pp. 88–90, Jan. 2007.

[47] R. W. Boyd, *Nonlinear Optics*, ser. Nonlinear Optics Series. Elsevier Science, 2008.

[48] C. J. McKinstrie and H. Kogelnik, "Nonlinear wave propagation in a rapidly-spun fiber," *Opt. Exp.*, vol. 14, no. 18, pp. 8072–8087, Sep. 2006.

[49] C. J. McKinstrie, H. Kogelnik, and L. Schenato, "Four-wave mixing in a rapidly-spun fiber," *Opt. Exp.*, vol. 14, no. 19, pp. 8516–8534, Sep. 2006.

[50] P. K. A. Wai and C. R. Menyuk, "Polarization mode dispersion, decorrelation, and diffusion in optical fibers with randomly varying birefringence," *J. Lightwave Technol.*, vol. 14, no. 2, pp. 148–157, Feb. 1996.

[51] D. Marcuse, C. R. Menyuk, and P. K. A. Wai, "Application of the Manakov-PMD equation to studies of signal propagation in optical fibers with randomly varying birefringence," *J. Lightwave Technol.*, vol. 15, no. 9, pp. 1735–1746, Sep. 1997.

[52] C. J. McKinstrie, H. Kogelnik, R. Jopson, S. Radic, and A. Kanaev, "Four-wave mixing in fibers with random birefringence," *Opt. Exp.*, vol. 12, no. 10, pp. 2033–2055, May 2004.

[53] A. Hasegawa and F. Tappert, "Transmission of stationary nonlinear optical pulses in dispersive dielectric fibers. I. Anomalous dispersion," *Appl. Phys. Lett.*, vol. 23, no. 3, pp. 142–144, Aug. 1973.

[54] L. F. Mollenauer, R. H. Stolen, and J. P. Gordon, "Experimental observation of picosecond pulse narrowing and solitons in optical fibers," *Phys. Rev. Lett.*, vol. 45, pp. 1095–1098, Sep. 1980.

[55] M. Karlsson, "Transmission systems with low noise phase-sensitive parametric amplifiers," *J. Lightwave Technol.*, vol. 34, no. 5, pp. 1411–1423, Mar. 2016.

[56] R. Engelbrecht, "Analysis of SBS gain shaping and threshold increase by arbitrary strain distributions," *J. Lightwave Technol.*, vol. 32, no. 9, pp. 1689–1700, May 2014.

[57] T. Nakanishi, M. Tanak, T. Hasegawa, M. Hirano, T. Okuno, and O. M., "Al_2O_3-SiO_2 core highly nonlinear dispersion-shifted fiber with Brillouin gain suppression improved by 6.1 dB," in *European Conference on Optical Communication (ECOC)*, Sep. 2006, paper Th.4.2.2.

[58] Y. Takushima and T. Okoshi, "Suppression of stimulated Brillouin scattering using optical isolators," *Electron. Lett.*, vol. 28, no. 12, pp. 1155–1157, Jun. 1992.

[59] D. Cotter, "Suppression of stimulated Brillouin scattering during transmission of high-power narrowband laser light in monomode fibre," *Electron. Lett.*, vol. 18, no. 15, pp. 638–640, Jul. 1982.

[60] J. Hansryd and P. A. Andrekson, "Broad-band continuous-wave-pumped fiber optical parametric amplifier with 49-dB gain and wavelength-conversion efficiency," *IEEE Photon. Technol. Lett.*, vol. 13, no. 3, pp. 194–196, Mar. 2001.

[61] A. Mussot, M. L. Parquier, and P. Szriftgiser, "Thermal noise for SBS suppression in fiber optical parametric amplifiers," *Opt. Commun.*, vol. 283, no. 12, pp. 2607 – 2610, 2010.

[62] M.-C. Ho, M. E. Marhic, K. Y. K. Wong, and L. G. Kazovsky, "Narrow-linewidth idler generation in fiber four-wave mixing and parametric amplification by dithering two pumps in opposition of phase," *J. Lightwave Technol.*, vol. 20, no. 3, pp. 469–476, Mar. 2002.

[63] J. Hansryd, F. Dross, M. Westlund, P. A. Andrekson, and S. N. Knudsen, "Increase of the SBS threshold in a short highly nonlinear fiber by applying a temperature distribution," *J. Lightwave Technol.*, vol. 19, no. 11, pp. 1691–1697, Nov. 2001.

[64] M. R. Lorenzen, D. Noordegraaf, C. V. Nielsen, O. Odgaard, L. Grüner-Nielsen, and K. Rottwitt, "Suppression of Brillouin scattering in fibre-optical parametric amplifier by applying temperature control and phase modulation," *Electron. Lett.*, vol. 45, no. 2, pp. 125–126, Jan. 2009.

[65] N. Yoshizawa and T. Imai, "Stimulated Brillouin scattering suppression by means of applying strain distribution to fiber with cabling," *J. Lightwave Technol.*, vol. 11, no. 10, pp. 1518–1522, Oct. 1993.

[66] J. M. C. Boggio, J. D. Marconi, and H. L. Fragnito, "Experimental and numerical investigation of the SBS-threshold increase in an optical fiber by applying strain distributions," *J. Lightwave Technol.*, vol. 23, no. 11, pp. 3808–3814, Nov. 2005.

[67] M. Takahashi, M. Tadakuma, and T. Yagi, "Dispersion and Brillouin managed HNLFs by strain control techniques," *J. Lightwave Technol.*, vol. 28, no. 1, pp. 59–64, Jan. 2010.

[68] E. Myslivets, C. Lundström, J. M. Aparicio, S. Moro, A. O. J. Wiberg, C.-S. Brès, N. Alic, P. A. Andrekson, and S. Radic, "Spatial equalization of zero-dispersion wavelength profiles in nonlinear fibers," *IEEE Photon. Technol. Lett.*, vol. 21, no. 24, pp. 1807–1809, Dec. 2009.

[69] L. Grüner-Nielsen, S. Herstrøm, S. Dasgupta, D. J. Richardson, D. Jakobsen, C. Lundström, P. A. Andrekson, M. E. V. Pedersen, and B. Palsdottir, "Silica-based highly nonlinear fibers with a high SBS threshold," in *IEEE Winter Topicals Meetings (WTM)*, Jan. 2011, paper MD4.2.

[70] B. P.-P. Kuo, J. M. Fini, L. Grüner-Nielsen, and S. Radic, "Dispersion-stabilized highly-nonlinear fiber for wideband parametric mixer synthesis," *Opt. Exp.*, vol. 20, no. 17, pp. 18 611–18 619, Aug. 2012.

[71] C. Lundström, R. Malik, L. Gruner-Nielsen, B. Corcoran, S. L. I. Olsson, M. Karlsson, and P. A. Andrekson, "Fiber optic parametric amplifier with 10-dB net gain without pump dithering," *IEEE Photon. Technol. Lett.*, vol. 25, no. 3, pp. 234–237, Feb. 2013.

[72] E. Mateo, F. Yaman, and G. Li, "Control of four-wave mixing phase-matching condition using the Brillouin slow-light effect in fibers," *Opt. Lett.*, vol. 33, no. 5, pp. 488–490, Mar. 2008.

[73] L. Wang and C. Shu, "Dynamic control of gain profile in fiber-optical parametric amplifier by gain-transparent SBS," *IEEE Photon. Technol. Lett.*, vol. 25, no. 20, pp. 1996–1999, Oct. 2013.

[74] ——, "Dynamic control of phase matching in four-wave mixing wavelength conversion of amplitude- and phase- modulated signals," *J. Lightwave Technol.*, vol. 31, no. 9, pp. 1468–1474, May 2013.

[75] C. Huang, X. Guo, X. Fu, L. Wang, and C. Shu, "Active control of gain saturation in fiber-optical parametric amplifier using stimulated Brillouin scattering," *Opt. Lett.*, vol. 39, no. 19, pp. 5713–5716, Oct. 2014.

[76] A. Almaiman, Y. Cao, M. Ziyadi, A. Mohajerin-Ariaei, P. Liao, C. Bao, F. Alishahi, A. Fallahpour, B. Shamee, N. Ahmed, A. J. Willner, Y. Akasaka, T. Ikeuchi, S. Takasaka, R. Sugizaki, S. Wilkinson, J. D. Touch, M. Tur, and A. E. Willner, "Experimental demonstration of phase-sensitive regeneration of a binary phase-shift keying channel without a phase-locked loop using Brillouin amplification," *Opt. Lett.*, vol. 41, no. 23, pp. 5434–5437, Dec. 2016.

[77] A. Almainman, Y. Cao, M. Ziyadi, A. Mohajerin-Ariaei, P. Liao, C. Bao, F. Alishahi, A. Fallahpour, B. Shamee, J. Touch, Y. Akasaka, T. Ikeuchi, S. Wilkinson, M. Tur, and A. Willner, "Experimental demonstration of phase-sensitive regeneration of a 20-40 Gb/s QPSK channel without phase-locked loop using Brillouin amplification," in *European Conference on Optical Communication (ECOC)*, Sep. 2016, paper W.3.C.4.

[78] Y. Cao, A. Almaiman, M. Ziyadi, P. Liao, A. M. Ariaei, F. Alishah, C. Bao, A. Fallahpour, B. Shamee, A. Willner, A. Youichi, T. Ikeuchi, S. Wilkinson, J. Touch, M. Tur, and A. Willner, "Demonstration of automatically phase-locked self-homodyne detection with a low-power pilot tone based on Brillouin amplification and optical frequency combs," in *Optical Fiber Communication Conference (OFC)*, Mar. 2016, paper M2A.6.

[79] M.-C. Ho, K. Uesaka, M. E. Marhic, Y. Akasaka, and L. G. Kazovsky, "200-nm-bandwidth fiber optical amplifier combining parametric and Raman gain," *J. Lightwave Technol.*, vol. 19, no. 7, pp. 977–981, Jul. 2001.

[80] M. F. C. Stephens, I. D. Phillips, P. Rosa, P. Harper, and N. J. Doran, "Improved WDM performance of a fibre optical parametric amplifier using Raman-assisted pumping," *Opt. Exp.*, vol. 23, no. 2, pp. 902–911, Jan. 2015.

[81] P. L. Voss, K. G. Köprülü, and P. Kumar, "Raman-noise-induced quantum limits for $\chi^{(3)}$ nondegenerate phase-sensitive amplification and quadrature squeezing," *J. Opt. Soc. Am. B*, vol. 23, no. 4, pp. 598–610, Apr. 2006.

[82] Z. Tong, A. Bogris, M. Karlsson, and P. A. Andrekson, "Full characterization of the signal and idler noise figure spectra in single-pumped fiber optical parametric amplifiers," *Opt. Exp.*, vol. 18, no. 3, pp. 2884–2893, Feb. 2010.

[83] C. J. McKinstrie and S. Radic, "Phase-sensitive amplification in a fiber," *Opt. Exp.*, vol. 12, no. 20, pp. 4973–4979, Oct. 2004.

[84] C. J. McKinstrie, S. Radic, and M. Raymer, "Quantum noise properties of parametric amplifiers driven by two pump waves," *Opt. Exp.*, vol. 12, no. 21, pp. 5037–5066, Oct. 2004.

[85] C. J. McKinstrie, S. Radic, and A. R. Chraplyvy, "Parametric amplifiers driven by two pump waves," *IEEE J. Sel. Top. Quantum Electron.*, vol. 8, no. 3, pp. 538–547, May 2002.

[86] Y. Chen and A. W. Snyder, "Four-photon parametric mixing in optical fibers: effect of pump depletion," *Opt. Lett.*, vol. 14, no. 1, pp. 87–89, Jan. 1989.

[87] M. Vasilyev, "Distributed phase-sensitive amplification," *Opt. Exp.*, vol. 13, no. 19, pp. 7563–7571, Sep. 2005.

[88] J. Hansryd, P. A. Andrekson, M. Westlund, J. Li, and P. Hedekvist, "Fiber-based optical parametric amplifiers and their applications," *IEEE J. Sel. Top. Quantum Electron.*, vol. 8, no. 3, pp. 506–520, May 2002.

[89] M. E. Marhic, *Fiber optical parametric amplifiers, oscillators and related devices.* Cambridge University press, 2008.

[90] C. J. McKinstrie, M. Yu, M. G. Raymer, and S. Radic, "Quantum noise properties of parametric processes," *Opt. Exp.*, vol. 13, no. 13, pp. 4986–5012, Jun. 2005.

[91] Z. Tong, C. J. McKinstrie, C. Lundström, M. Karlsson, and P. A. Andrekson, "Noise performance of optical fiber transmission links that use non-degenerate cascaded phase-sensitive amplifiers," *Opt. Exp.*, vol. 18, no. 15, pp. 15 426–15 439, Jul. 2010.

[92] M. E. Marhic, C. H. Hsia, and J.-M. Jeong, "Optical amplification in a nonlinear fibre interferometer," *Electron. Lett.*, vol. 27, no. 3, pp. 210–211, Jan. 1991.

[93] W. Imajuku, A. Takada, and Y. Yamabayashi, "Inline coherent optical amplifier with noise figure lower than 3 dB quantum limit," *Electron. Lett.*, vol. 36, no. 1, pp. 63–64, Jan. 2000.

[94] M. E. Marhic and C.-H. Hsia, "Optical amplification and squeezed-light generation in fibre interferometers performing degenerate four-wave mixing," *Quantum Optics*, vol. 3, no. 6, p. 341, Dec. 1991.

[95] R. Tang, J. Lasri, P. S. Devgan, V. Grigoryan, P. Kumar, and M. Vasilyev, "Gain characteristics of a frequency nondegenerate phase-sensitive fiber-optic parametric amplifier with phase self-stabilized input," *Opt. Exp.*, vol. 13, no. 26, pp. 10 483–10 493, Dec. 2005.

[96] J. Kakande, F. Parmigiani, M. Ibsen, P. Petropoulos, and D. J. Richardson, "Wide bandwidth experimental study of nondegenerate phase-sensitive amplifiers in single- and dual-pump configurations," *IEEE Photon. Technol. Lett.*, vol. 22, no. 24, pp. 1781–1783, Dec. 2010.

[97] T. Umeki, T. Kazama, O. Tadanaga, K. Enbutsu, M. Asobe, Y. Miyamoto, and H. Takenouchi, "PDM signal amplification using PPLN-based polarization-independent phase-sensitive amplifier," *J. Lightwave Technol.*, vol. 33, no. 7, pp. 1326–1332, Apr. 2015.

[98] A. Lorences-Riesgo, T. A. Eriksson, C. Lundström, M. Karlsson, and P. A. Andrekson, "Phase-sensitive amplification of 28 Gbaud DP-QPSK signal," in *Optical Fiber Communication Conference (OFC)*, Mar. 2013, paper W4C.4.

[99] T. Richter, B. Corcoran, S. L. I. Olsson, C. Lundström, M. Karlsson, C. Schubert, and P. A. Andrekson, "Experimental characterization of a phase-sensitive four-mode fiber-optic parametric amplifier," in *European Conference on Optical Communication (ECOC)*, Sep. 2012, paper Th.1.F.1.

[100] C. Lundström, Z. Tong, M. Karlsson, and P. A. Andrekson, "Phase-to-phase and phase-to-amplitude transfer characteristics of a nondegenerate-idler phase-sensitive amplifier," *Opt. Lett.*, vol. 36, no. 22, pp. 4356–4358, Nov. 2011.

[101] C. Lundström, B. Corcoran, M. Karlsson, and P. A. Andrekson, "Phase and amplitude characteristics of a phase-sensitive amplifier operating in gain saturation," *Opt. Exp.*, vol. 20, no. 19, pp. 21 400–21 412, Sep. 2012.

[102] Y. Dai and C. Shu, "Bit-rate variable DPSK demodulation based on cascaded four-wave mixing," *Opt. Exp.*, vol. 19, no. 4, pp. 2952–2958, Feb. 2011.

[103] X. Fu, Y. Dai, G. Lei, and C. Shu, "Bit-rate flexible demodulation of DPSK signals based on phase sensitive gain in cascaded four-wave mixing," *IEEE Photon. Technol. Lett.*, vol. 24, no. 12, pp. 994–996, Jun. 2012.

[104] B. Corcoran, S. L. I. Olsson, C. Lundström, M. Karlsson, and P. A. Andrekson, "Phase-sensitive optical pre-amplifier implemented in an 80km DQPSK link," in *Optical Fiber Communication Conference (OFC)*, Mar. 2012, paper PDP5A.4.

[105] S. L. I. Olsson, B. Corcoran, C. Lundström, T. A. Eriksson, M. Karlsson, and P. A. Andrekson, "Phase-sensitive amplified transmission links for improved sensitivity and nonlinearity tolerance," *J. Lightwave Technol.*, vol. 33, no. 3, pp. 710–721, Feb. 2015.

[106] R. Tang, P. S. Devgan, V. S. Grigoryan, P. Kumar, and M. Vasilyev, "In-line phase-sensitive amplification of multi-channel CW signals based on frequency nondegenerate four-wave-mixing in fiber," *Opt. Exp.*, vol. 16, no. 12, pp. 9046–9053, Jun. 2008.

[107] F. Parmigiani, R. Slavík, J. Kakande, C. Lundström, M. Sjödin, P. A. Andrekson, R. Weerasuriya, S. Sygletos, A. D. Ellis, L. Grüner-Nielsen, D. Jakobsen, S. Herstrm, R. Phelan, J. O'Gorman, A. Bogris, D. Syvridis, S. Dasgupta, P. Petropoulos, and D. J. Richardson, "All-optical phase regeneration of 40Gbit/s DPSK signals in a black-box phase sensitive amplifier," in *Optical Fiber Communication Conference (OFC)*, Mar. 2010, paper PDPC3.

[108] M. Ziyadi, A. Mohajerin-Ariaei, J. yuan Yang, Y. Akasaka, M. Chitgarha, S. Khaleghi, A. Almaiman, A. Abouzaid, J. Touch, and M. Sekiya, "Experimental demonstration of optical regeneration of DP-BPSK/QPSK using polarization-diversity PSA," in *Conference on Lasers and Electro-Optics (CLEO)*, Jun. 2014, paper STu2J.3.

[109] R. Malik, A. Kumpera, A. Lorences-Riesgo, P. A. Andrekson, and M. Karlsson, "Frequency-resolved noise figure measurements of phase (in)sensitive fiber optical parametric amplifiers," *Opt. Exp.*, vol. 22, no. 23, pp. 27 821–27 832, Nov. 2014.

[110] F. Parmigiani, G. Hesketh, R. Slavík, P. Horak, P. Petropoulos, and D. J. Richardson, "Polarization-assisted phase-sensitive processor," *J. Lightwave Technol.*, vol. 33, no. 6, pp. 1166–1174, Mar. 2015.

[111] T. Umeki, O. Tadanaga, M. Asobe, Y. Miyamoto, and H. Takenouchi, "First demonstration of high-order QAM signal amplification in PPLN-based phase sensitive amplifier," *Opt. Exp.*, vol. 22, no. 3, pp. 2473–2482, Feb. 2014.

[112] T. Hasegawa, K. Inoue, and K. Oda, "Polarization independent frequency conversion by fiber four-wave mixing with a polarization diversity technique," *IEEE Photon. Technol. Lett.*, vol. 5, no. 8, pp. 947–949, Aug. 1993.

[113] K. K.-Y. Wong, M. E. Marhic, K. Uesaka, and L. G. Kazovsky, "Polarization-independent one-pump fiber-optical parametric amplifier," *IEEE Photon. Technol. Lett.*, vol. 14, no. 11, pp. 1506–1508, Nov. 2002.

[114] H. Hu, E. Palushani, M. Galili, H. C. H. Mulvad, A. Clausen, L. K. Oxenløwe, and P. Jeppesen, "640 Gbit/s and 1.28 Tbit/s polarisation insensitive all optical wavelength conversion," *Opt. Exp.*, vol. 18, no. 10, pp. 9961–9966, May 2010.

[115] T. Richter, R. Elschner, A. Gandhe, K. Petermann, and C. Schubert, "Parametric amplification and wavelength conversion of single- and dual-polarization DQPSK signals," *IEEE J. Sel. Top. Quantum Electron.*, vol. 18, no. 2, pp. 988–995, Mar. 2012.

[116] G. K. P. Lei and M. E. Marhic, "Amplification of DWDM channels at 1.28 Tb/s in a bidirectional fiber optical parametric amplifier," *Opt. Exp.*, vol. 22, no. 7, pp. 8726–8733, Apr. 2014.

[117] S. Takasaka and R. Sugizaki, "Polarization insensitive fiber optical parametric amplifier using a SBS suppressed diversity loop," in *Optical Fiber Communication Conference (OFC)*, 2016, paper M3D.4.

[118] M. E. Marhic, "Polarization independence and phase-sensitive parametric amplification," *J. Opt. Soc. Am. B*, vol. 28, no. 11, pp. 2685–2689, Nov. 2011.

[119] M. E. Marhic, G. Kalogerakis, and L. G. Kazovsky, "Gain reciprocity in fibre optical parametric amplifiers," *Electron. Lett.*, vol. 42, no. 9, pp. 519–520, Apr. 2006.

[120] C. J. McKinstrie, S. Radic, and C. Xie, "Phase conjugation driven by orthogonal pum pwaves in birefringent fibers," *J. Opt. Soc. Am. B*, vol. 20, no. 7, pp. 1437–1446, Jul. 2003.

[121] B. P.-P. Kuo, E. Myslivets, A. O. J. Wiberg, S. Zlatanovic, C.-S. Brès, S. Moro, F. Gholami, A. Peric, N. Alic, and S. Radic, "Transmission of 640-Gb/s RZ-OOK channel over 100-km SSMF by wavelength-transparent conjugation," *J. Lightwave Technol.*, vol. 29, no. 4, pp. 516–523, Feb. 2011.

[122] F. Parmigiani, G. Hesketh, R. Slavík, P. Horak, P. Petropoulos, and D. J. Richardson, "Optical phase quantizer based on phase sensitive four wave mixing at low nonlinear phase shifts," *IEEE Photon. Technol. Lett.*, vol. 26, no. 21, pp. 2146–2149, Nov. 2014.

[123] P. Kylemark, P.-O. Hedekvist, H. Sunnerud, M. Karlsson, and P. A. Andrekson, "Noise characteristics of fiber optical parametric amplifiers," *J. Lightwave Technol.*, vol. 22, no. 2, pp. 409–416, Feb. 2004.

[124] Z. Tong, A. Bogris, C. Lundström, C. J. McKinstrie, M. Vasilyev, M. Karlsson, and P. A. Andrekson, "Modeling and measurement of the noise figure of a cascaded non-degenerate phase-sensitive parametric amplifier," *Opt. Exp.*, vol. 18, no. 14, pp. 14 820–14 835, Jul. 2010.

[125] Z. Tong, C. Lundström, M. Karlsson, M. Vasilyev, and P. A. Andrekson, "Noise performance of a frequency nondegenerate phase-sensitive amplifier with unequalized inputs," *Opt. Lett.*, vol. 36, no. 5, pp. 722–724, Mar. 2011.

[126] C. J. McKinstrie, M. G. Raymer, S. Radic, and M. V. Vasilyev, "Quantum mechanics of phase-sensitive amplification in a fiber," *Opt. Commun.*, vol. 257, no. 1, pp. 146–163, 2006.

REFERENCES

[127] C. M. Caves, "Quantum limits on noise in linear amplifiers," *Phys. Rev. B*, vol. 26, pp. 1817–1839, Oct. 1982.

[128] Z. Tong, C. Lundström, E. Tipsuwannakul, M. Karlsson, and P. Andrekson, "Phase-sensitive amplified DWDM DQPSK signals using free-running lasers with 6-dB link SNR improvement over EDFA-based systems," in *European Conference on Optical Communication (ECOC)*, Sep. 2010, paper PDP1.3.

[129] S. L. I. Olsson, B. Corcoran, C. Lundström, E. Tipsuwannakul, S. Sygletos, A. D. Ellis, Z. Tong, M. Karlsson, and P. A. Andrekson, "Injection locking-based pump recovery for phase-sensitive amplified links," *Opt. Exp.*, vol. 21, no. 12, pp. 14 512–14 529, Jun. 2013.

[130] S. L. I. Olsson, C. Lundström, M. Karlsson, and P. A. Andrekson, "Long-haul (3465 km) transmission of a 10 GBd QPSK signal with low noise phase-sensitive in-line amplification," in *European Conference on Optical Communication (ECOC)*, Sep. 2014, paper PD.2.2.

[131] B. Corcoran, S. L. I. Olsson, C. Lundström, M. Karlsson, and P. A. Andrekson, "Mitigation of nonlinear impairments on QPSK data in phase-sensitive amplified links," in *European Conference on Optical Communication (ECOC)*, Sep. 2013, paper We.3.A.1.

[132] M. Abe, T. Kazama, T. Umeki, K. Enbutsu, Y. Miyamoto, and H. Takenouchi, "PDM-QPSK WDM signal amplification using PPLN-based polarization-independent in-line phase-sensitive amplifier," in *European Conference on Optical Communication (ECOC)*, Sep. 2016.

[133] R. Slavík, A. Bogris, J. Kakande, F. Parmigiani, L. Grüner-Nielsen, R. Phelan, J. Vojtech, P. Petropoulos, D. Syvridis, and D. J. Richardson, "Field-trial of an all-optical PSK regenerator/multicaster in a 40 Gbit/s, 38 channel DWDM transmission experiment," *J. Lightwave Technol.*, vol. 30, no. 4, pp. 512–520, Feb. 2012.

[134] R. Slavík, A. Bogris, F. Parmigiani, J. Kakande, M. Westlund, M. Skoöld, L. Grüner-Nielsen, R. Phelan, D. Syvridis, P. Petropoulos, and D. J. Richardson, "Coherent all-optical phase and amplitude regenerator of binary phase-encoded signals," *IEEE J. Sel. Top. Quantum Electron.*, vol. 18, no. 2, pp. 859–869, Mar. 2012.

[135] J. Kakande, A. Bogris, R. Slavík, F. Parmigiani, D. Syvridis, P. Petropoulos, and D. J. Richardson, "First demonstration of all-optical QPSK signal regeneration in a novel multi-format phase sensitive amplifier," in *European Conference on Optical Communication (ECOC)*, Sep. 2010, paper PD 3.3.

[136] J. Kakande, A. Bogris, R. Slavík, F. Parmigiani, D. Syvridis, M. Sköld, M. Westlund, P. Petropoulos, and D. J. Richardson, "QPSK phase and amplitude regeneration at 56 Gbaud in a novel idler-free non-degenerate phase sensitive amplifier," in *Optical Fiber Communication Conference (OFC)*, Mar. 2011, paper OMT4.

[137] T. Richter, R. Elschner, and C. Schubert, "QAM phase-regeneration in a phase-sensitive fiber-amplifier," in *European Conference on Optical Communication (ECOC)*, Sep. 2013, paper We.3.A.2.

[138] A. Bogris, "All-optical demultiplexing of 16-QAM signals into QPSK tributaries using four-level optical phase quantizers," *Opt. Lett.*, vol. 39, no. 7, pp. 1775–1778, Apr. 2014.

[139] L. Li and M. Vasilyev, "All-optical 2R regenerator of 16-QAM signals," *Proc. SPIE*, vol. 9009, pp. 900 908–1–900 908–6, 2013.

[140] Y. Cao, M. Ziyadi, Y. Akasaka, A. Mohajerin-Ariaei, J. yuan Yang, A. Almaiman, P. Liao, F. Alishahi, N. Ahmed, A. J. Willner, S. Takasaka, R. Sugizaki, J. Touch, M. Sekiya, M. Tur, and A. E. Willner, "All optical signal level swapping and multilevel amplitude noise mitigation based on different regions of optical parametric amplification," *Opt. Lett.*, vol. 41, no. 4, pp. 677–680, Feb. 2016.

[141] M. Sorokina, S. Sygletos, A. Ellis, and S. Turitsyn, "Regenerative Fourier transformation for dual-quadrature regeneration of multilevel rectangular QAM," *Opt. Lett.*, vol. 40, no. 13, pp. 3117–3120, Jul. 2015.

[142] P. Guan, M. L. F. Da Ros, H. Hu, K. Røge, M. Galili, T. Morioka, and L. Oxenløwe, "Channel WDM regeneration in a single phase-sensitive amplifier through optical Fourier transformation," in *European Conference on Optical Communication (ECOC)*, Sep. 2006.

[143] J.-Y. Yang, M. Ziyadi, Y. Akasaka, S. Khaleghi, M. R. Chitgarha, J. Touch, and M. Sekiya, "Investigation of polarization-insensitive phase regeneration using polarization-diversity phase-sensitive amplifier," in *European Conference on Optical Communication (ECOC)*, Sep. 2013, paper P.3.9.

[144] R. A. Fisher, B. R. Suydam, and D. Yevick, "Optical phase conjugation for time-domain undoing of dispersive self-phase-modulation effects," *Opt. Lett.*, vol. 8, no. 12, pp. 611–613, Dec. 1983.

[145] H. Hu, R. M. Jopson, A. H. Gnauck, M. Dinu, S. Chandrasekhar, X. Liu, C. Xie, M. Montoliu, S. Randel, and C. J. McKinstrie, "Fiber nonlinearity compensation of an 8-channel WDM PDM-QPSK signal using multiple phase conjugations," in *Optical Fiber Communication Conference (OFC)*, Mar. 2014, paper M3C.2.

[146] A. D. Ellis, M. E. McCarthy, M. A. Z. Al-Khateeb, and S. Sygletos, "Capacity limits of systems employing multiple optical phase conjugators," *Opt. Exp.*, vol. 23, no. 16, pp. 20 381–20 393, Aug. 2015.

[147] M. E. McCarthy, M. A. Z. A. Kahteeb, F. M. Ferreira, and A. D. Ellis, "PMD tolerant nonlinear compensation using in-line phase conjugation," *Opt. Exp.*, vol. 24, no. 4, pp. 3385–3392, Feb. 2016.

[148] A. D. Ellis, M. Tan, M. A. Iqbal, M. A. Z. Al-Khateeb, V. Gordienko, G. S. Mondaca, S. Fabbri, M. F. C. Stephens, M. E. McCarthy, A. Perentos, I. D. Phillips, D. Lavery, G. Liga, R. Maher, P. Harper, N. Doran, S. K. Turitsyn, S. Sygletos, and P. Bayvel, "4 Tb/s transmission reach enhancement using 10×400 Gb/s super-channels and polarization insensitive dual band optical phase conjugation," *J. Lightwave Technol.*, vol. 34, no. 8, pp. 1717–1723, Apr. 2016.

[149] T. Umeki, T. Kazama, A. Sano, K. Shibahara, K. Suzuki, M. Abe, H. Takenouchi, and Y. Miyamoto, "Simultaneous nonlinearity mitigation in 92×180-Gbit/s PDM-16QAM transmission over 3840 km using PPLN-based guard-band-less optical phase conjugation," *Opt. Exp.*, vol. 24, no. 15, pp. 16 945–16 951, Jul. 2016.

[150] S. Yoshima, Y. Sun, K. R. H. Bottrill, F. Parmigiani, P. Petropoulos, and D. J. Richardson, "Nonlinearity mitigation through optical phase conjugation in a deployed fibre link with full bandwidth utilization," in *European Conference on Optical Communication (ECOC)*, Sep. 2015, paper ID0682.

[151] S. Yoshima, Z. Liu, Y. Sun, K. R. Bottrill, F. Parmigiani, P. Petropoulos, and D. J. Richardson, "Nonlinearity mitigation for multi-channel 64-QAM signals in a deployed fiber link through optical phase conjugation," in *Optical Fiber Communication Conference (OFC)*, Mar. 2016, paper Th4F.4.

[152] X. Liu, A. R. Chraplyvy, P. J. Winzer, R. W. Tkach, and S. Chandrasekhar, "Phase-conjugated twin waves for communication beyond the Kerr nonlinearity limit," *Nature Photon.*, vol. 7, no. 7, pp. 560–568, May 2013.

[153] H. Eliasson, S. L. I. Olsson, M. Karlsson, and P. A. Andrekson, "Mitigation of nonlinear distortion in hybrid Raman/phase-sensitive amplifier links," *Opt. Exp.*, vol. 24, no. 2, pp. 888–900, Jan. 2016.

[154] G. W. Lu, E. Tipsuwannakul, T. Miyazaki, C. Lundstrom, M. Karlsson, and P. A. Andrekson, "Format conversion of optical multilevel signals using FWM-based optical phase erasure," *J. Lightwave Technol.*, vol. 29, no. 16, pp. 2460–2466, Aug. 2011.

[155] M. Karlsson, "Four-dimensional rotations in coherent optical communications," *J. Lightwave Technol.*, vol. 32, no. 6, pp. 1246–1257, Mar. 2014.

[156] G. Björk, K. Stensson, and M. Karlsson, "Proposed implementation of "non-physical" four-dimensional polarization rotations," *J. Lightwave Technol.*, vol. 34, no. 14, pp. 3317–3322, Jul. 2016.

[157] N. K. Kjøller, M. Galili, K. Dalgaard, H. C. H. Mulvad, K. M. Roge, and L. K. Oxenløwe, "Quadrature decomposition by phase conjugation and projection in a polarizing beam splitter," in *European Conference on Optical Communication (ECOC)*, Sep. 2014, paper P.3.8.

[158] G. W. Lu, K. S. Abedin, and T. Miyazaki, "All-optical RZ-DPSK WDM to RZ-DQPSK phase multiplexing using four-wave mixing in highly nonlinear fiber," *IEEE Photon. Technol. Lett.*, vol. 19, no. 21, pp. 1699–1701, Nov. 2007.

[159] M. R. Chitgarha, S. Khaleghi, Z. Bakhtiari, M. Ziyadi, O. Gerstel, L. Paraschis, C. Langrock, M. M. Fejer, and A. E. Willner, "Demonstration of reconfigurable optical generation of higher-order modulation formats up to 64 QAM using optical nonlinearity," *Opt. Lett.*, vol. 38, no. 17, pp. 3350–3353, Sep. 2013.

[160] F. Yaman, Q. Lin, and G. Agrawal, "Effects of polarization-mode dispersion in dual-pump fiber-optic parametric amplifiers," *IEEE Photon. Technol. Lett.*, vol. 16, no. 2, pp. 431–433, Feb. 2004.

[161] S. J. B. Yoo, "Wavelength conversion technologies for WDM network applications," *J. Lightwave Technol.*, vol. 14, no. 6, pp. 955–966, Jun. 1996.

[162] G. Kalogerakis, M. E. Marhic, K. K.-Y. Wong, and L. G. Kazovsky, "Transmission of optical communication signals by distributed parametric amplification," *J. Lightwave Technol.*, vol. 23, no. 10, p. 2945, Oct. 2005.

[163] X. Xu, C. Zhang, T. I. Yuk, and K. K. Y. Wong, "Distributed parametric amplifier for RZ-DPSK signal transmission system," *Opt. Exp.*, vol. 20, no. 17, pp. 19 271–19 278, Aug. 2012.

[164] T. Udem, R. Holzwarth, and T. W. Hänsch, "Optical frequency metrology," *Nature*, vol. 416, no. 6877, pp. 233–237, Mar. 2002.

[165] R. Holzwarth, T. Udem, T. W. Hänsch, J. C. Knight, W. J. Wadsworth, and P. S. J. Russell, "Optical frequency synthesizer for precision spectroscopy," *Phys. Rev. Lett.*, vol. 85, pp. 2264–2267, Sep. 2000.

[166] A. Cingöz, D. C. Yost, T. K. Allison, A. Ruehl, M. E. Fermann, I. Hartl, and J. Ye, "Direct frequency comb spectroscopy in the extreme ultraviolet," *Nature*, vol. 482, no. 7383, pp. 68–71, Sep. 2012.

[167] I. Coddington, W. C. Swann, L. Nenadovic, and N. R. Newbury, "Rapid and precise absolute distance measurements at long range," *Nature Photon.*, vol. 3, no. 6, pp. 351–356, Jun. 2009.

[168] J. Lee, Y.-J. Kim, K. Lee, S. Lee, and S.-W. Kim, "Time-of-flight measurement with femtosecond light pulses," *Nature Photon.*, vol. 4, no. 10, pp. 716–720, Mar. 2010.

[169] Z. Jiang, C.-B. Huang, D. E. Leaird, and A. M. Weiner, "Optical arbitrary waveform processing of more than 100 spectral comb lines," *Nature Photon.*, vol. 1, no. 8, pp. 463–467, Aug. 2007.

[170] V. Torres-Company and A. M. Weiner, "Optical frequency comb technology for ultra-broadband radio-frequency photonics," *Laser & Phot. Rev.*, vol. 8, no. 3, pp. 368–393, Dec. 2014.

[171] D. M. Spirit, A. D. Ellis, and P. E. Barnsley, "Optical time division multiplexing: systems and networks," *IEEE Commun. Mag.*, vol. 32, no. 12, pp. 56–62, Dec. 1994.

[172] S. Kawanishi, "Ultrahigh-speed optical time-division-multiplexed transmission technology based on optical signal processing," *IEEE J. Quantum Electron.*, vol. 34, no. 11, pp. 2064–2079, Nov. 1998.

[173] H. Takara, T. Ohara, K. Mori, K. Sato, E. Yamada, Y. Inoue, T. Shibata, M. Abe, T. Morioka, and K. I. Sato, "More than 1000 channel optical frequency chain generation from single supercontinuum source with 12.5 GHz channel spacing," *Electronics Letters*, vol. 36, no. 25, pp. 2089–2090, Dec. 2000.

[174] K. Mori, K. Sato, H. Takara, and T. Ohara, "Supercontinuum lightwave source generating 50 GHz spaced optical ITU grid seamlessly over S-, C- and L-bands," *Electron. Lett.*, vol. 39, no. 6, pp. 544–546, Mar. 2003.

[175] H. Takara, H. Masuda, K. Mori, K. Sato, Y. Inoue, T. Ohara, A. Mori, M. Kohtoku, Y. Miyamoto, T. Morioka, and K. S., "124 nm seamless bandwidth, 313×10 Gbit/s DWDM transmission," *Electron. Lett.*, vol. 39, no. 4, pp. 382–383, Feb. 2003.

[176] T. Ohara, H. Takara, T. Yamamoto, H. Masuda, T. Morioka, M. Abe, and H. Takahashi, "Over-1000-channel ultradense WDM transmission with supercontinuum multicarrier source," *J. Lightwave Technol.*, vol. 24, no. 6, pp. 2311–2317, Jun. 2006.

[177] B. J. Puttnam, R. S. Luís, W. Klaus, J. Sakaguchi, J.-M. D. Mendinueta, Y. Awaji, N. Wada, Y. Tamura, T. Hayashi, M. Hirano, and J. Marciante, "2.15 Pb/s transmission using a 22 core homogeneous single-mode multi-core fiber and wideband optical comb," in *European Conference on Optical Communication (ECOC)*, Sep. 2015, paper PD3.1.

[178] E. Temprana, E. Myslivets, B. P.-P. Kuo, L. Liu, V. Ataie, N. Alic, and S. Radic, "Overcoming Kerr-induced capacity limit in optical fiber transmission," *Science*, vol. 348, no. 6242, pp. 1445–1448, Jun. 2015.

[179] C. Liu, J. Pan, T. Detwiler, A. Stark, Y.-T. Hsueh, G.-K. Chang, and S. E. Ralph, "Joint digital signal processing for superchannel coherent optical communication systems," *Opt. Exp.*, vol. 21, no. 7, pp. 8342–8356, Apr. 2013.

[180] J. Pfeifle, V. Brasch, M. Lauermann, Y. Yu, D. Wegner, T. Herr, K. Hartinger, P. Schindler, J. Li, D. Hillerkuss, R. Schmogrow, C. Weimann, R. Holzwarth, W. Freude, J. Leuthold, T. J. Kippenberg, and C. Koos, "Coherent terabit communications with microresonator Kerr frequency combs," *Nature Photon.*, vol. 8, no. 4, pp. 375–380, May 2014.

[181] M. Fujiwara, J. Kani, H. Suzuki, K. Araya, and M. Teshima, "Flattened optical multicarrier generation of 12.5 GHz spaced 256 channels based on sinusoidal

amplitude and phase hybrid modulation," *Electron. Lett.*, vol. 37, no. 15, pp. 967–968, Jul. 2001.

[182] W. Mao, P. A. Andrekson, and J. Toulouse, "Investigation of a spectrally flat multi-wavelength DWDM source based on optical phase- and intensity-modulation," in *Optical Fiber Communication Conference (OFC)*, Mar. 2004, paper MF78.

[183] V. Ataie, E. Myslivets, B. P.-P. Kuo, N. Alic, and S. Radic, "Spectrally equalized frequency comb generation in multistage parametric mixer with nonlinear pulse shaping," *J. Lightwave Technol.*, vol. 32, no. 4, pp. 840–846, Feb. 2014.

[184] V. Ataie, E. Temprana, L. Liu, E. Myslivets, B. P.-P. Kuo, N. Alic, and S. Radic, "Ultrahigh count coherent WDM channels transmission using optical parametric comb-based frequency synthesizer," *J. Lightwave Technol.*, vol. 33, no. 3, pp. 694–699, Sep. 2015.

[185] M. Mazur, A. Lorences-Riesgo, M. Karlsson, and P. A. Andrekson, "10 Tb/s self-homodyne 64-QAM superchannel transmission with 4% spectral overhead," in *Accepted to Optical Fiber Communication Conference (OFC)*, Mar. 2017, paper Th3F.4.

[186] K. Tai, A. Tomita, J. L. Jewell, and A. Hasegawa, "Generation of subpicosecond solitonlike optical pulses at 0.3 THz repetition rate by induced modulational instability," *Appl. Phys. Lett.*, vol. 49, no. 5, pp. 236–238, Aug. 1986.

[187] P. V. Mamyshev, S. V. Chernikov, and E. M. Dianov, "Generation of fundamental soliton trains for high-bit-rate optical fiber communication lines," *IEEE J. Quantum Electron.*, vol. 27, no. 10, pp. 2347–2355, Oct. 1991.

[188] S. V. Chernikov, R. Kashyap, and J. R. Taylor, "Comblike dispersion-profiled fiber for soliton pulse train generation," *Opt. Lett.*, vol. 19, no. 8, pp. 539–541, Apr. 1994.

[189] C. Finot, J. Fatome, S. Pitois, and G. Millot, "All-fibered high-quality low duty-cycle 20-GHz and 40-GHz picosecond pulse sources," *IEEE Photon. Technol. Lett.*, vol. 19, no. 21, pp. 1711–1713, Nov. 2007.

[190] C. J. McKinstrie and M. G. Raymer, "Four-wave-mixing cascades near the zero-dispersion frequency," *Opt. Exp.*, vol. 14, no. 21, pp. 9600–9610, Oct. 2006.

[191] J. Azaña, N. K. Berger, B. Levit, and B. Fischer, "Spectro-temporal imaging of optical pulses with a single time lens," *IEEE Photon. Technol. Lett.*, vol. 16, no. 3, pp. 882–884, Mar. 2004.

[192] E. Myslivets, B. P.-P. Kuo, N. Alic, and S. Radic, "Generation of wideband frequency combs by continuous-wave seeding of multistage mixers with synthesized dispersion," *Opt. Exp.*, vol. 20, no. 3, pp. 3331–3344, Jan. 2012.

[193] C. Finot, B. Kibler, L. Provost, and S. Wabnitz, "Beneficial impact of wave-breaking for coherent continuum formation in normally dispersive nonlinear fibers," *J. Opt. Soc. Am. B*, vol. 25, no. 11, pp. 1938–1948, Nov. 2008.

[194] F. C. Cruz, "Optical frequency combs generated by four-wave mixing in optical fibers for astrophysical spectrometer calibration and metrology," *Opt. Exp.*, vol. 16, no. 17, pp. 13 267–13 275, Aug. 2008.

[195] K. Petermann, *Laser diode modulation and noise.* Kluwer Academic, 1998.

[196] Z. Tong, A. O. J. Wiberg, E. Myslivets, B. P.-P. Kuo, N. Alic, and S. Radic, "Spectral linewidth preservation in parametric frequency combs seeded by dual pumps," *Opt. Exp.*, vol. 20, no. 16, pp. 17 610–17 619, Jul. 2012.

[197] A. C. Bordonalli, M. J. Fice, and A. J. Seeds, "Optical injection locking to optical frequency combs for superchannel coherent detection," *Opt. Exp.*, vol. 23, no. 2, pp. 1547–1557, Jan. 2015.

[198] J. N. Kemal, J. Pfeifle, P. Marin-Palomo, M. D. G. Pascual, S. Wolf, F. Smyth, W. Freude, and C. Koos, "Multi-wavelength coherent transmission using an optical frequency comb as a local oscillator," *Opt. Exp.*, vol. 24, no. 22, pp. 25 432–25 445, Oct. 2016.

[199] M. Sjödin, P. Johannisson, M. Karlsson, Z. Tong, and P. A. Andrekson, "OSNR requirements for self-homodyne coherent systems," *IEEE Photon. Technol. Lett.*, vol. 22, no. 2, pp. 91–93, Jan. 2010.

[200] M. A. Ettabib, K. Bottrill, F. Parmigiani, A. Kapsalis, A. Bogris, M. Brun, P. Labeye, S. Nicoletti, K. Hammani, D. Syvridis, D. J. Richardson, and P. Petropoulos, "All-optical phase regeneration with record PSA extinction ratio in a low-birefringence silicon germanium waveguide," *J. Lightwave Technol.*, vol. 34, no. 17, pp. 3993–3998, Sep. 2016.

[201] E. Nazemosadat, A. Lorences-Riesgo, M. Karlsson, and P. A. Andrekson, "Highly nonlinear few-mode fiber for optical parametric amplification," in *European Conference on Optical Communication (ECOC)*, Sep. 2016, paper W.4.P1.SC1.7.

[202] Y. Xiao, R.-J. Essiambre, M. Desgroseilliers, A. M. Tulino, R. Ryf, S. Mumtaz, and G. P. Agrawal, "Theory of intermodal four-wave mixing with random linear mode coupling in few-mode fibers," *Opt. Exp.*, vol. 22, no. 26, pp. 32 039–32 059, Dec. 2014.

[203] W. Yang, Y. Yu, L. Chen, G. Chen, M. Ye, and X. Zhang, "Simultaneous phase regeneration of MDM signals utilizing a multimode silicon waveguide," *J. Lightwave Technol.*, vol. 34, no. 11, pp. 2702–2709, Jun. 2016.

[204] Y. Ding, J. Xu, F. Da Ros, B. Huang, H. Ou, and C. Peucheret, "On-chip two-mode division multiplexing using tapered directional coupler-based mode multiplexer and demultiplexer," *Opt. Exp.*, vol. 21, no. 8, pp. 10 376–10 382, Apr. 2013.

Appendix A

Gain in Degenerate Phase-Sensitive Amplifiers

Polarization-Diverse PSA

A generic signal can be decomposed in two orthogonal polarizations according to

$$J_{\text{S,in}} = \sqrt{P_\text{S}}\frac{e^{i\phi_\text{S}}}{\sqrt{2}} \left(e^{i\varphi}\cos(\alpha/2) \begin{bmatrix} 1 \\ ie^{i\psi} \end{bmatrix} + e^{-i\varphi}\sin(\alpha/2) \begin{bmatrix} 1 \\ -ie^{i\psi} \end{bmatrix} \right), \qquad \text{(A.1)}$$

where α is the polarization angle (Stokes space) between the signal and the vector $[1 \ ie^{i\psi}]^T/\sqrt{2}$, φ is the relative phase between the two signal components, and ϕ_S is the global input phase. The signal power is denoted by P_S. The Jones vector $[1 \ ie^{i\psi}]^T/\sqrt{2}$ corresponds to a Stokes vector given by $[0 \ -\sin(\psi) \ \cos(\psi)]$, i.e., the Stokes vector normal to the mirror plane.

Using Eqs. (3.28), (A.1), the output of a polarization-diverse one-mode PSA is

$$J_{\text{S,out}} = \frac{\sqrt{P_\text{S}}}{\sqrt{2}}(\mu\cos(\alpha/2)e^{i\phi_\text{S}} + \nu\sin(\alpha/2)e^{-i\phi_\text{S}})e^{i\varphi} \begin{bmatrix} 1 \\ ie^{i\psi} \end{bmatrix}$$
$$+ \frac{\sqrt{P_\text{S}}}{\sqrt{2}}(\mu\sin(\alpha/2)e^{i\phi_\text{S}} + \nu\cos(\alpha/2)e^{-i\phi_\text{S}})e^{-i\varphi} \begin{bmatrix} 1 \\ -ie^{i\psi} \end{bmatrix}. \qquad \text{(A.2)}$$

By calculating the ratio between the output and input powers, we obtain Eq. (3.29).

Vector PSA

In this case we decompose the signal along the two orthogonal pump polarizations according to

$$J_{\text{S,in}} = P_\text{S}e^{i\phi_\text{S}} \left(e^{i\varphi}\cos(\alpha/2)J_{\text{P1}} + e^{-i\varphi}\sin(\alpha/2)J_{\text{P2}} \right), \qquad \text{(A.3)}$$

where α is the polarization angle (Stokes space) among the signal and $P1$. Using Eqs. (3.35), (A.3), the output of a vector PSA is

$$J_{S,out} = \sqrt{P_S}(\mu\cos(\alpha/2)e^{i\phi_S} + \nu\sin(\alpha/2)e^{-i\phi_S})e^{i\varphi}J_{P1}$$

$$+ \frac{\sqrt{P_S}}{\sqrt{2}}(\mu\sin(\alpha/2)e^{i\phi_S} + \nu\cos(\alpha/2)e^{-i\phi_S})e^{-i\varphi}J_{P2}. \qquad (A.4)$$

By calculating the ratio between the output and input powers, we obtain Eq. (3.36).